MAGNETOM Flash

The Magazine of MR

Issue Number 4/2010
Special Edition for the USA

SIEMENS

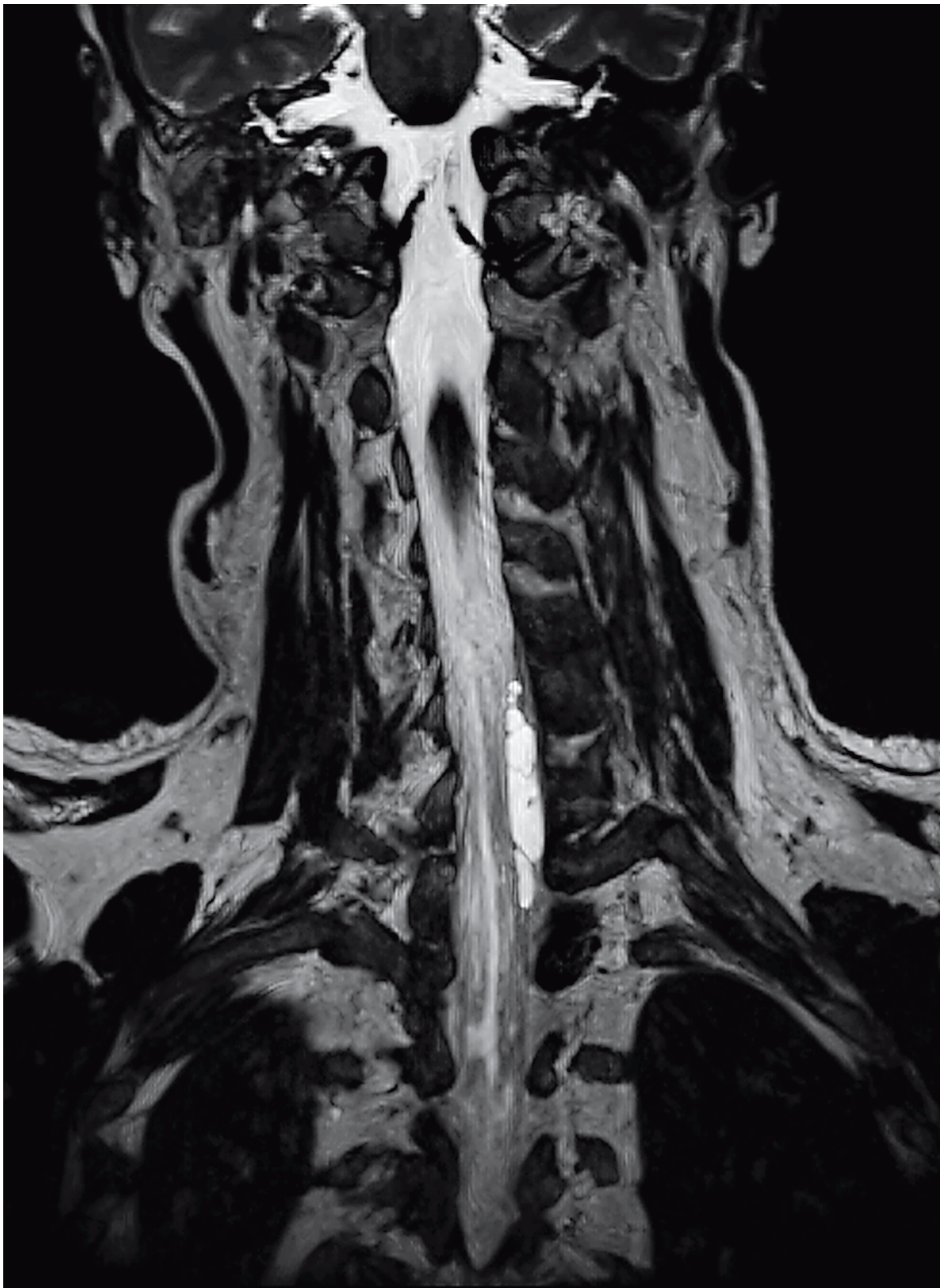

Clinical

How I do it

USA

Matthias Lichy, M.D.

Dear MAGNETOM user,

At the recent annual meeting of the ISMRM, the radiological community heard about the latest steps in MR technology and how Siemens is a leader in contributing to the innovations of these developments. A central theme was how new technologies can help us improve our day-to-day patient care and productivity. Future steps in MR technology were also a focal point, including ultra high field imaging, parallel transmission and compressed MR image acquisition.

The Siemens user community was also able to participate in another remarkable event: the MAGNETOM World Summit, held in Shenzhen, China. More than 500 participants from all corners of the globe exchanged ideas on how to use innovative imaging techniques such as *syngo* TimCT or *syngo* Tissue4D in daily routine. This exchange of knowledge lies at the heart of what every MAGNETOM World Summit organized by Siemens Healthcare MR is all about.

MAGNETOM Flash magazine and our internet platform, MAGNETOM World (**www.siemens.com/magnetom-world**), also support this sharing of knowledge. Those who attended these meetings received their own copies of the two latest MAGNETOM Flash issues including clinical and research highlights from world-wide known and honored researchers and clinicians from the United States of America. For those who could not attend either meeting, the editorial team of MAGNETOM Flash has selected articles from the two latest international versions. We hope they will provide you with new ideas and understanding.

We hope you will enjoy reading this special U.S. issue of MAGNETOM Flash!

Matthias Lichy, M.D.

The Editorial Team

We appreciate your comments.
Please contact us at magnetomworld.med@siemens.com

Antje Hellwich
Associate Editor

Okan Ekinci, M.D.
Center of Clinical Competence –
Cardiology, Erlangen, Germany

Peter Kreisler, Ph.D.
Collaborations & Applications,
Erlangen, Germany

Heike Weh,
Clinical Data Manager,
Erlangen, Germany

Bernhard Baden,
Clinical Data Manager,
Erlangen, Germany

Ignacio Vallines, Ph.D.,
Applications Manager,
Erlangen, Germany

Wellesley Were
MR Business Development
Manager
Australia and New Zealand

Milind Dhamankar, M.D.
Sr. Director, MR Product
Marketing, Malvern, USA

Michelle Kessler, US
Installed Base Manager,
Malvern, PA, USA

Gary R. McNeal, MS (BME)
Advanced Application Specialist,
Cardiovascular MR Imaging
Hoffman Estates, USA

Dr. Sunil Kumar S.L.
Senior Manager Applications,
Canada

Content

Content

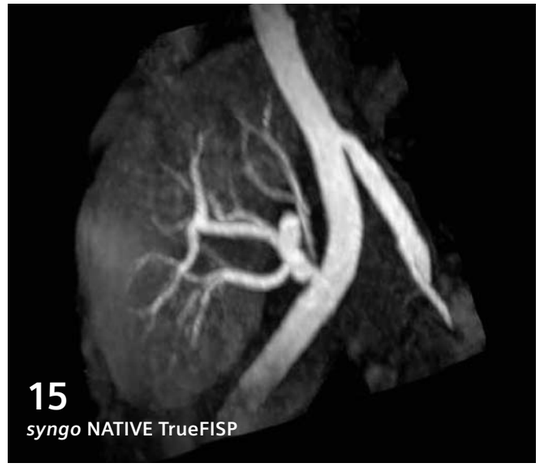

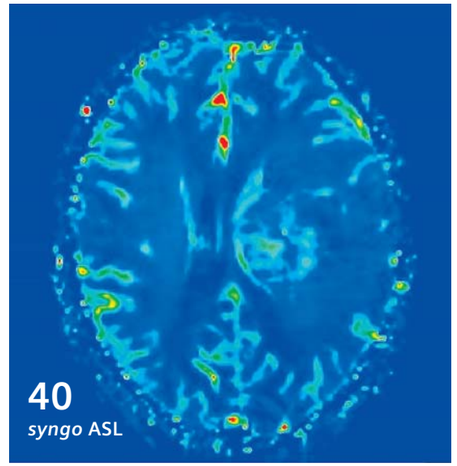

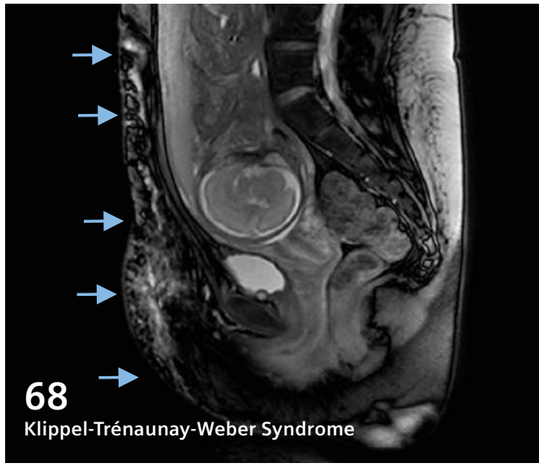

Further clinical information

Visit the MAGNETOM World Internet pages at **www.siemens.com/magnetom-world** for further clinical information and talks by international experts.

Diagnostic Relevant Reduction of Motion Artifacts in the Posterior Fossa by *syngo* BLADE Imaging

T. von Kalle[1]; B. Blank[2]; C. Fabig-Moritz[1]; P. Müller-Abt[1]; M. Zieger[1]; K. Wohlfarth[3]; P. Winkler[1]

[1]*Department of Pediatric Radiology, Olgahospital Klinikum Stuttgart, Germany*
[2]*Department of Pediatric Oncology, Hematology and Immunology, Olgahospital Klinikum Stuttgart, Germany*
[3]*Siemens Healthcare, Erlangen, Germany*

1

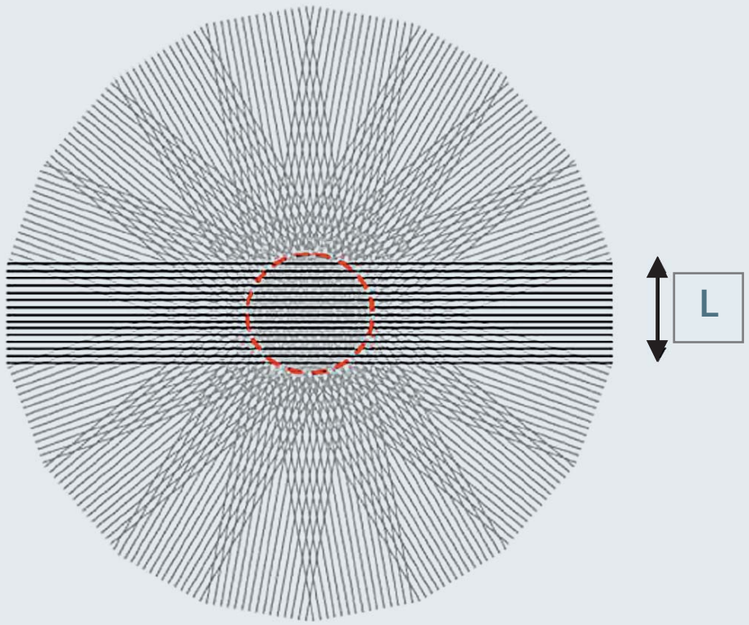

1 k-space trajectory in BLADE imaging. The k-space is covered by a series of blades each of which consists of the lowest phase encoding lines. The centre of the k-space (red circle) with diameter L is resampled for every blade. Data are then combined to a high resolution image.

Although movement and pulsation artifacts are a frequent problem in daily routine [1–4] especially in the diagnostics of pediatric patients, only few articles on this topic can be found in the literature. According to our experience mainly MR images of the posterior fossa, the cerebellum and the brain stem, may be significantly impaired by artifacts from pulsatile flow of blood or cerebrospinal fluid even without patient head movement [5, 6]. Sedation or general anesthesia rarely influence these pulsation or flow artifacts. However, accurate assessment of small brain lesions is essential in many pediatric patients, especially in those with malignant brain tumors.
MR imaging with "rotating blade-like k-space covering" (BLADE) and "Periodically Rotated Overlapping Parallel Lines with Enhanced Reconstruction" (PROPELLER) have been shown to effectively reduce artifacts in healthy volunteers and adult patients [7, 8, 9], as well as in pediatric patients [4, 10] and therefore have the potential to reduce the frequency of anesthesia in children. As these MR techniques reduce motion artifacts by fast segmental image acquisition combined with mathematical algorithms, we assumed that it might at the same time reduce the visibility of small brain lesions. We therefore compared the image quality of two T2-weighted fluid attenuated inversion recovery (T2w FLAIR) sequences with different k-space trajectories (conventional Cartesian and BLADE) with respect to artifacts and depiction of small hyperintense brain lesions [5].

Imaging techniques

We used a 1.5T scanner (MAGNETOM Avanto, Siemens Healthcare, Erlangen, Germany) and the Siemens 12-channel head matrix coil.
For each patient we compared two sequences with transverse 4 mm sections (gap 10%) that were applied in identical slice positions:
1. The T2w FLAIR standard sequence, a spin-echo sequence with conventional rectilinear Cartesian k-space trajectories (image parameters: TI 2500 ms, TR 9000 ms, TE 100 ms, BW 150 Hz/pixel, turbo factor 19, TA160 s, FOV 230 x 230 mm, matrix 256 x 256).
2. The BLADE FLAIR sequence with rotating blade-like k-space trajectories (image parameters: TI 2500 ms, TR 9000 ms, TE 107 ms, BW 250 Hz/pixel, turbo factor 29, TA 260 s, BLADE-Coverage 130 %, FOV 230 x 230 mm, matrix 256 x 256).
During the acquisition of both sequences children were encouraged not to move their head. They were offered video films or audio programs during the examination.

BLADE technique

syngo BLADE is the product name of the motion insensitive Siemens turbo-spin-echo sequence which utilizes the PROPELLER k-space trajectory [11].
The technique is approved for diagnostic MR examinations of patients. It consists of blade-like rotating k-space coverage. During each echo train of a BLADE sequence the lowest phase encoding lines of a conventional rectilinear k-space are acquired. The number of lines, which depends on the length of the echo train, determines the resolution of the image. During the acquisition process the direction of this "blade" is rotated around the k-space centre such that the complete series covers the whole k-space (Fig. 1). Images can be displayed with or without an additional motion correction algorithm.

2

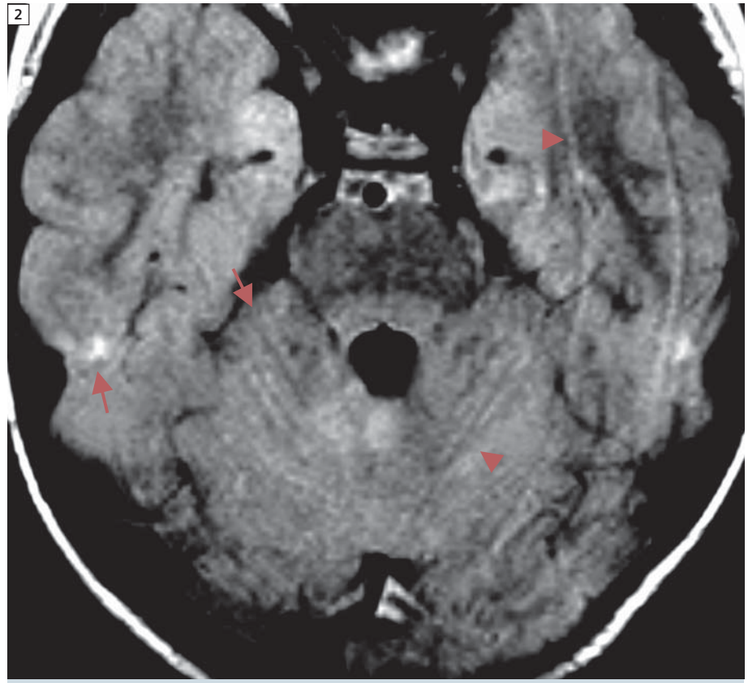

2 Movement artifacts caused by head movements (arrowheads) and pulsation artifacts caused by pulsatile flow (arrows). T2w FLAIR sequence with conventional rectilinear k-space trajectories.

Patients

The typical hyperintense white matter abnormalities in the cerebellum of patients with neurofibromatosis type 1 (NF 1) [12] served the purpose of our study to assess and compare the visibility of small and low contrast lesions.
We re-evaluated images of children with NF 1, who had been routinely scanned for optic pathway gliomas and who had been examined with T2w FLAIR sequences of both techniques. 26 patients, 10 girls and 16 boys from 2 years 7 months to 17 years (median age 8 years 5 months) were included in the study.

Image evaluation

Four experienced pediatric radiologists independently assessed unlabeled images of both FLAIR sequences of each patient. Structures of the posterior fossa, cerebellum and brain stem, were evaluated according to the presence of movement artifacts (caused by head movements) or pulsation artifacts (caused by pulsatile flow of blood and/or cerebrospinal fluid) (Fig. 2), their differentiation from lesions, and their delineation from the surrounding tissue by contrast (difference in signal intensities) and edge definition (clearly or poorly defined margins) as has been described elsewhere

Table 1: Scores for movement and pulsation artifacts, and the differentiation of artifacts and lesions in the posterior fossa.

	Conventional		*syngo* BLADE	
	yes	**no**	**yes**	**no**
Movement	29	75	4	100
Pulsation	99	5	25	79
Differentiation lesion/artefacts	53	30	81	2

Yes = artifacts present, lesions and artifacts distinguishable. No = artifacts not present, lesions and artifact not distinguishable. Maximum score for each sequence = 104. Last line. Patients with neither artifacts nor lesions were excluded. Results of statistical tests cf Table 2.

[5] The transverse diameters of the largest and smallest lesions were measured in both sequences of each patient. Signal intensities of a representative lesion and the adjacent normal brain tissue were measured. [5]

Discussion

Techniques with rotating blade-like k-space covering (BLADE) [9], with periodically rotated overlapping parallel lines with enhanced reconstruction (PROPELLER) [8,10], and with k-space alignment similar to a trellis [13] have been shown to effectively reduce artifacts in T1- and T2-weighted images. Studies on pediatric [4] and adult patients [7] found a comparable detectability of lesions in contrast-enhanced T1-weighted images of FLAIR BLADE sequences and conventional spin-echo sequences. However, image quality and delineation of small or poorly delineated lesions in MR images in T2-weighted FLAIR acquired with these techniques have not been systematically studied.

In our study, all observers found more pulsation artifacts than movement artifacts in images of both the conventional and the *syngo* BLADE sequence (Table 1). Artifacts were reported significantly less often in images acquired with BLADE technique than in images with rectilinear k-space trajectory (Table 1 and 2). These results confirm that artifacts caused by pulsation, flow and motion are significantly reduced by the BLADE technique in comparison to the standard sequence with conventional

Table 2: Posterior fossa. Comparison of conventional vs. BLADE images. McNemar's test. p-values for each observer. Cohen's kappa for interobserver agreement.

	Presence of movement artifacts	Presence of pulsation artifacts	Differentiation of lesions and artifacts	Delineation of lesions	
				Edge definition	Contrast
Observer 1	0.03	0.02	0.04	> 0.05	> 0.05
Observer 2	0.02	0.00002	0.002	0.0027	0.0009
Observer 3	0.041	0.000007	0.001	> 0.05	> 0.05
Observer 4	0.013	0.00002	0.013	> 0.05	> 0.05
Cohen's kappa	0.34	0.37	0.72	0.11	0.01

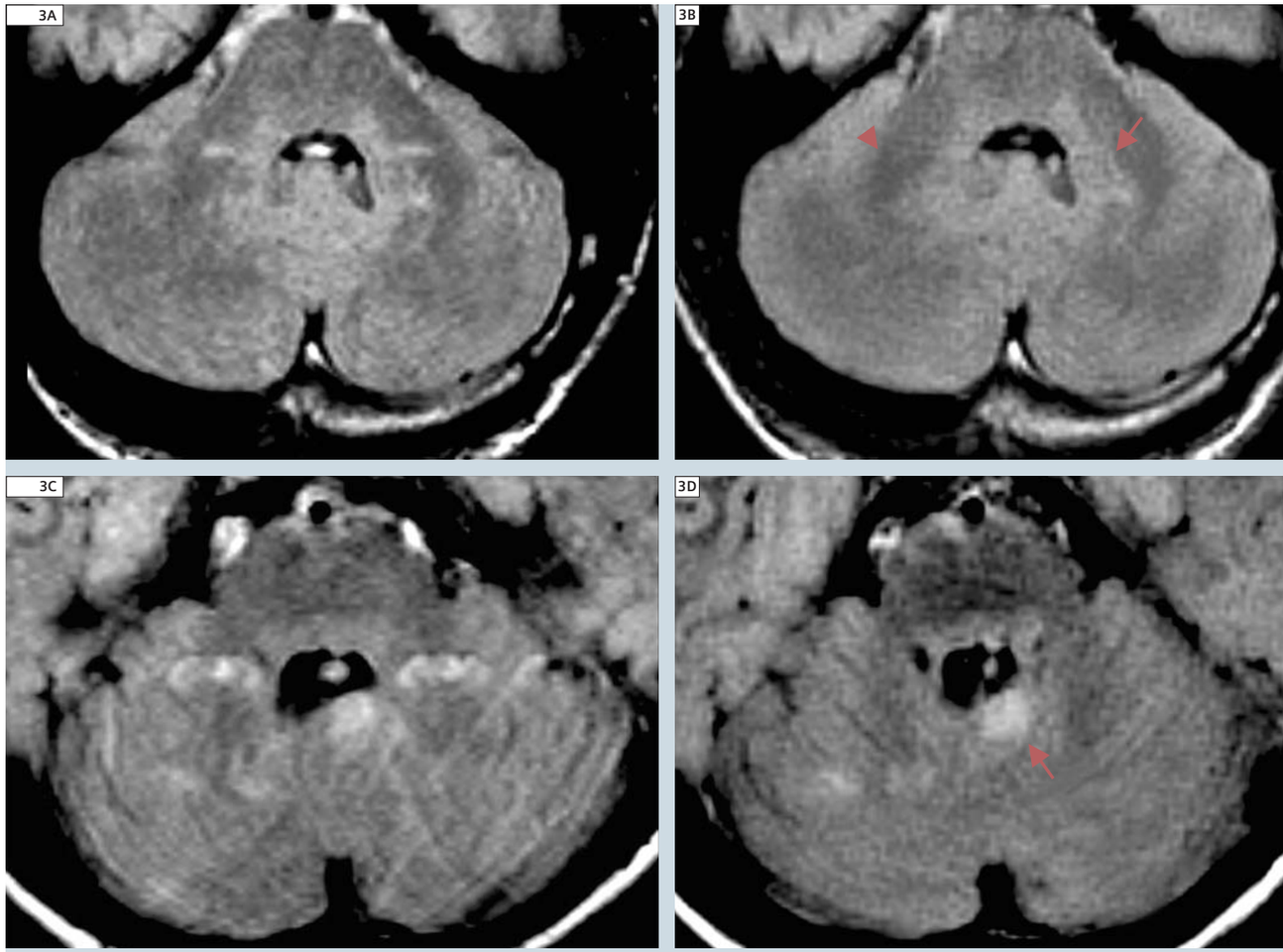

3 T2w FLAIR images of the posterior fossa of two different patients. Rectilinear k-space coverage (left), BLADE (right). Lesions typical of neurofibromatosis type 1: low contrast confluent (arrowhead), high contrast round (arrow). Artifacts and lesions not reliably distinguishable in conventional images (left).

rectilinear k-space covering. As the children were encouraged not to move during the examination, there were only moderate to minor movement artifacts even in conventional T2w FLAIR images. Pulsation artifacts were more frequent and more severe in conventional images and sometimes also present in BLADE images. Ratings of subtle movement artifacts in conventional images and subtle pulsation artifacts in BLADE images led to an only fair interobserver agreement (Cohen's kappa < 0.4, Table 2). These artifacts did not disturb the depiction of lesions.

There was good observer agreement (Cohen's kappa 0.74, Table 2) that artifacts compromised the assessment of lesions more often and more severely in conventional T2w FLAIR images than in BLADE images. In 6 of all 26 patients (23%) observers agreed that in conventional T2w FLAIR images they could not differentiate lesions from artifacts in the posterior fossa, rendering nearly a fourth of the examinations with conventional k-space trajectory inadequate for a reliable diagnosis. In none of the BLADE sequences more than one observer considered artifacts and lesions to be indistinguishable (Fig. 3).

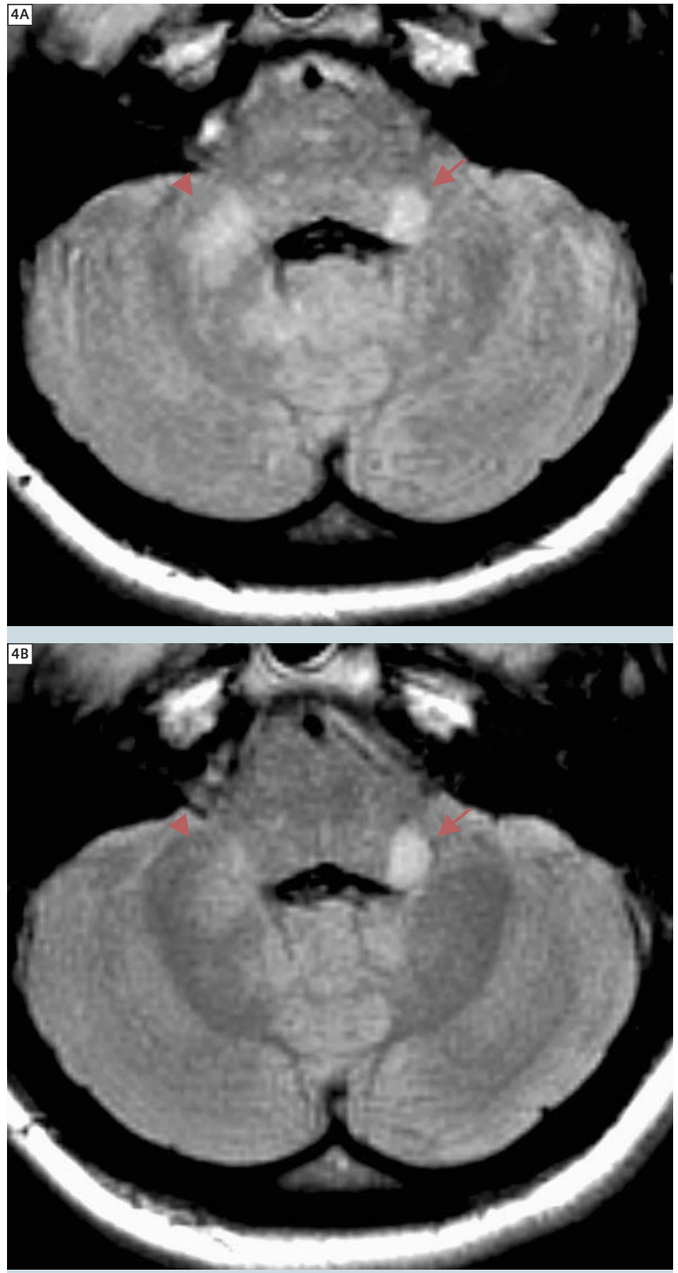

4 Absence of major artifacts and comparable visibility of lesions in images of both techniques (T2w FLAIR: rectilinear k-space top, BLADE bottom), low contrast confluent (arrowhead), high contrast round (arrow).

As Gill et al. reported for their sample [12], most hyperintense lesions in the thalami, brain stem and cerebellum were confluent or diffuse with poorly defined edges. A smaller number of lesions were well circumscribed with edges that were distinct from the adjacent normal tissue. Mean ratios of signal intensities were only slightly lower in the posterior fossa than in cerebrum and midbrain.

If lesions were not obscured by artifacts, visibility of lesions with both clearly and poorly defined edges appeared to be comparable in images of both techniques (Fig. 4). Observers' comparisons of both imaging techniques according to contrast and edge definition did not reveal consistently significant differences for lesions of the posterior fossa (Table 2). There only was a tendency to better edge definition in BLADE images. Visibility of lesions also was independent of size. Even the smallest lesions of our sample (2–3 mm) were equally depicted by both techniques.

BLADE technique is based on standard image acquisition techniques and therefore has the advantage of providing image characteristics equal to standard sequences. As an alternative to *syngo* BLADE imaging, pulsation artifacts may be identified by a second data acquisition after changing the phase encoding direction [1] or the slice orientation, with the disadvantage of a longer examination time and the higher risk of movement artifacts. Reduction of motion artifacts in non-sedated children can also be achieved by rapid sequences (e.g. single shot techniques) which, in neuroimaging, have the disadvantages of a poorer differentiation of gray and white matter [3, 10,14] and a lower spatial resolution [15].

Observers of our study had the subjective impression that the appearance of FLAIR BLADE images differed slightly from that of conventional images which did not impair image quality and lesion detectability (Figs. 3 and 4). These subtle differences have already been reported for PROPELLER technique [2]. BLADE images might therefore be identified by experienced radiologists despite "blinding". We have, however, not identified bias due to this fact in our study.

In our study, data acquisition time and image reconstruction time together were approximately 2–3 minutes longer for *syngo* BLADE sequences than for conventional FLAIR sequences. The advantage of artifact reduction by the BLADE technique clearly outweighed the prolonged duration.

There are limitations of our retrospective study: We were not able to measure the degree of patients' movements. Therefore, like other investigators [2, 4, 9], we can only assume that these parameters were similar in statistical mean throughout the examination. As both sequences were performed successively, pulsation and flow artifacts were also assumed as unchanged for both acquisitions. For our retrospective analysis we had to accept that in addition to the k-space trajectory some of the parameters of both sequences were not identical. As the BLADE technique benefits from long echo trains, a turbo factor had been chosen that was larger than that of our routine T2w FLAIR sequence. However, a change of these parameters would have had only minor influence on motion artefacts, and presumably would not have changed the quality of results. Prospective studies of a larger patient group could avoid these shortcomings.

Conclusion

BLADE technique reduces movement and pulsation artifacts in T2w FLAIR images without relevant loss of image quality. It therefore markedly improves depiction of small and low contrast brain lesions in children in the posterior fossa of pediatric patients. This can be crucial especially in patients after surgery of malignant brain tumors. In the absence of major artifacts lesions of all sizes were depicted in comparable quality by both techniques.

References

1 Böck JC, Neumann K, Sander B, Schmidt D, Schörner W (1991) Prepontine artifacts due to pulsation of cerebrospinal fluid in T_2-weighted coronal MRI. Clinical relevance, incidence and a technique for efficient artefact suppression. RoeFo 154: 202-205.
2 Forbes KP, Pipe JG, Bird CR, Heiserman JE (2001) PROPELLER MRI: Clinical testing of a novel technique for quantification and compensation of head motion. J Magn Reson Imaging 14: 215-222.
3 Penzkofer AK, Pfluger T, Pochmann Y, Meissner O, Leisinger G (2002) MR imaging of the brain in pediatric patients: Diagnostic value of HASTE sequences. AJR 179: 509-514.
4 Alibek S, Adamietz B, Cavallaro A, Stemmer A, Anders K, Kramer M, Bautz W, Staatz G (2008) Contrast-enhanced T1-weighted fluid-attenuated inversion-recovery BLADE Magnetic Resonance Imaging of the brain: An alternative to spin-echo technique for detection of brain lesions in the unsedated pediatric patient? Acad Radiol 15: 986-995.
5 Von Kalle T, Blank B, Fabig-Moritz C, Müller-Abt P, Zieger M, Wohlfarth K, Winkler P (2009) reduced artefacts and improved assessment of hyperintense brain lesions with BLADE MR imaging in patients with neurofibromatosis type 1. Pediatr Radiol 39: 1216-1222.
Kallmes DF, Hui FK, Mugler JP III (2001) Suppression of cerebrospinal fluid and blood flow artifacts in FLAIR MR imaging with a single-slab three-dimensional pulse sequence: Initial experience. Radiographics 221: 251-255.
6 Naganawa S, Satake H, Iwano S, Kawai H, Kubota S, Komada T, Kawamura M, Sakurai Y, Fukatsu H (2008) Contrast-enhanced MR imaging of the brain using T1-weighted FLAIR with BLADE compared with a conventional spin-echo sequence. Eur Radiol 18: 337-342.
7 Forbes KP, Pipe JG, Karis JP, Heiserman JE (2002) Improved image quality and detection of acute cerebral infarction with PROPELLER diffusion-weighted MR imaging. Radiology 225:551-555.
8 Wintersperger BJ, Runge VM, Biswas J, Nelson CB, Stemmer A, Simonetta AB, Reiser MF, Naul LG, Schoenberg SO (2006) Brain magnetic resonance imaging at 3 Tesla using BLADE compared with standard rectilinear data sampling. Invest Radio 41: 586-592.
9 Forbes KP, Pipe JG, Karis JP, Farthing V, Heiserman JE (2003) Brain imaging in the unsedated pediatric patient: Comparison of periodically rotated overlapping parallel lines with enhanced reconstruction and single-shot fast spin-echo sequences. AJNR 24: 794-798.
10 Pipe JG (1999) Motion correction with PROPELLER MRI: Application to head motion and free-breathing cardiac imaging. Magn Reson Med 42: 963-969.
11 Gill DS, Hyman SL, Steinberg A, North KN (2006): Age-related findings on MRI in neurofibromatosis type 1. Pediatr Radiol 36: 1048-1056.
12 Maclaren JR, Bones PJ, Millane RP, Watts R (2008) MRI with TRELLIS: a novel approach to motion correction. Magn Res Imaging 26: 474-483.
13 Iskandar BJ, Sansone JM, Medow J, Rowley HA (2004) The use of quick-brain magnetic resonance imaging in the evaluation of shunt-treated hydrocephalus. J Neurosurg (Pediatrics 2) 101: 147-151.
14 Ba-Ssalamah A, Schick S, Heimberger K, Linnau KF, Schibany N, Prokesch R, Trattnig S (2000) Ultrafast magnetic resonance imaging of the brain. Magn Reson Imaging 18: 237-43.

Contact
Thekla v. Kalle, M.D.
Department of Pediatric Radiology
Olgahospital Klinikum Stuttgart
Bismarckstr. 8
70176 Stuttgart
Germany
Phone: +49 (0) 711/ 278-04
t.vonkalle@klinikum-stuttgart.de
www.klinikum-stuttgart.de

3D High Resolution MRI of the Knee at 3T Using a Moderately T2-weighted 3D-TSE-fs (*syngo* SPACE) sequence – Useful or Not?

A. Horng[1], M. Notohamiprodjo[1], J. Raya[1], J. Park[1], W. Horger[2], A. Crispin[1], M. F. Reiser[1], C. Glaser[1]

[1]Department of Clinical Radiology, University of Munich – Grosshadern Campus, Munich, Germany
[2]Siemens Healthcare, Erlangen, Germany

Background

Magnetic resonance imaging (MRI) of the knee is justifiably one of the most commonly performed MRI examinations, as it offers excellent direct depiction of cartilage, ligaments, menisci and periarticular soft tissue. This can be achieved by standard application of fat-saturated moderately T2-weighted 2D Turbo Spin Echo (TSE)-sequences in three orientations [1, 2]. However, conventional TSE-sequences are not isotropic, hence structures and signal alterations / lesions with a size less than the usual slice thickness of 3 to 6 mm, i.e. meniscal roots, may not be completely detected. A slice thickness below 3 mm is rarely acquired because of its reduced signal-to-noise ratio (SNR) and contrast-to-noise ratio (CNR) and because of the prolonged acquisition time for complete joint coverage. Furthermore post-processing options for 2D-sequences for the assessment of structures, which are captured in an oblique course through several slices, like the anterior cruciate ligament or the femoral trochlear cartilage [3] are limited.
In this setting the introduction of a highly resolved 3D moderately T2-weighted (3D-T2w-TSE) sequence may be useful. In the literature time efficient 3D-T2w-TSE sequences have already been evaluated for the central nervous system [4] and recently for the body trunk [5, 6]. They enable data acquisition with high isotropic spatial resolution and allow for an interactive 3-dimensional visualization. Such post-processing after an initial isotropic data acquisition has been proven successful in many other MR and CT-based applications.

Technical considerations for *syngo* SPACE

Recently a 3D-TSE-sequence with moderate T2-weighting called "Sampling Perfection with Application optimized Contrasts using different flip angle Evolutions" (*syngo* SPACE), was developed for 3T systems. A restore pulse and variable flip angle distribution enable extremely large turbo factors. The variable flip angles provide a particular evolution of the signal during the echo train resulting in a "pseudo steady-state" with constant signal level neglecting relaxation [7]. Additionally, SAR is reduced by this acquisition scheme. The usage of this technique on a high field 3T system allows integration of parallel imaging with excellent SNR and CNR at reasonable acquisition times [8, 9].
The application of *syngo* SPACE at 3T might establish a new approach to MRI of the knee. Parallel imaging facilitates blockwise 3D-data acquisition with isotropic spatial resolution for evaluation of the whole knee in a reasonable time window. The acquisition time should be either less or at least comparable to acquisition times of conventional 2D TSE datasets in three planes. The advantage of an isotropic 3D-dataset is the possibility of 3-dimensional multiplanar reformatting (MPR), which may enhance the evaluation of small delicate or oblique structures like meniscal roots or the fascicles of the anterior cruciate ligament. Disadvantages might be slightly decreased in-plane resolution as compared to conventional 2D-TSE-fs-sequences and some additionally required time for the 3D reconstructions.
Recently our research group evaluated *syngo* SPACE for isotropic highly resolved MRI of the knee at 3T (MAGNETOM Trio, Siemens Healthcare, Erlangen, Germany) with consecutive 3-dimensional-MPR in comparison to conventional 2D-TSE-fs-sequences in three planes (coronal, sagittal, axial) [10].
Sequence parameters for *syngo* SPACE and for the moderately T2w-2D-TSE-fs-sequence are given in table 1. Fat saturation in *syngo* SPACE was performed with the SPectral selection Attenuated Inversion Recovery (SPAIR) technique. Parallel imaging was performed with the k-space based technique *syngo* GRAPPA with an acceleration factor R = 2. For signal reception, a dedicated multichannel knee coil with 8 independent RF-channels was used. Reformation of the datasets was performed on a *syngo* MultiModality Workstation (Leonardo, software version VB15A, Siemens Healthcare, Erlangen, Germany).
Analysis of axial, sagittal and coronal reformations (MPR) of 0.5 mm, 1 mm and 2 mm slice thickness suggest a slice thickness for MPR of 1 mm ($SPACE_{1mm}$) to be optimal for the visualization of anatomical structures (Fig. 1). This slice thickness provides significantly higher SNR for ligaments, subchondral bone and menisci and at least equal SNR for cartilage, bone marrow, muscle and fat of *syngo* SPACE as compared to conventional 2D-TSE-fs. Though identification of anatomical structures was comparable for *syngo* SPACE and 2D-TSE-fs, the $SPACE_{1mm}$ showed significantly better visualization of menisci in axial sections and meniscal roots in coronal sections despite slightly inferior CNR (joint fluid/cartilage, joint fluid/menisci, fat/ligaments and bone marrow/subchondral bone) as compared to 2D-TSE-fs.

Clinical application

The reconstruction time for one *syngo* SPACE dataset was below 30 s, the data acquisition time was 10 min 35 sec with *syngo* SPACE versus 12 min 48 sec with 2D TSE in three planes (table 1). Thus the overall acquisition time for *syngo* SPACE was comparable to the acquisition of the 2D-TSE-fs datasets in three

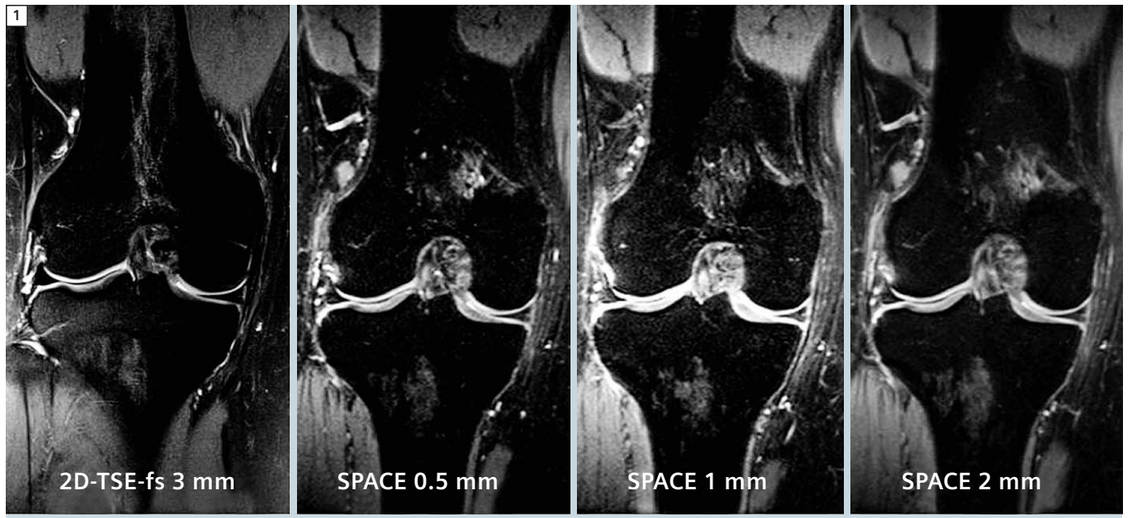

1 Coronal *syngo* SPACE reconstructions in 0.5 mm, 1 mm and 2 mm show a good homogeneity throughout the image as compared to the T2w-2D-TSE-fs.

Table 1: Sequence parameters for the *syngo* SPACE and the T2w-2D-TSE-fs-sequences.

	TR [ms]	TE [ms]	FA [°]	Resolution [mm³]	FOV [cm]	Matrix	Parallel Imaging	T_{akqis}
***syngo* SPACE**	1200	30	120	0.5	16	320 x 320	GRAPPA r=2	10'35"
T2w-2D-TSE-fs	3200	30	180	0.36 x 0.36 x 3	16	448 x 448	GRAPPA r=2	12'34"

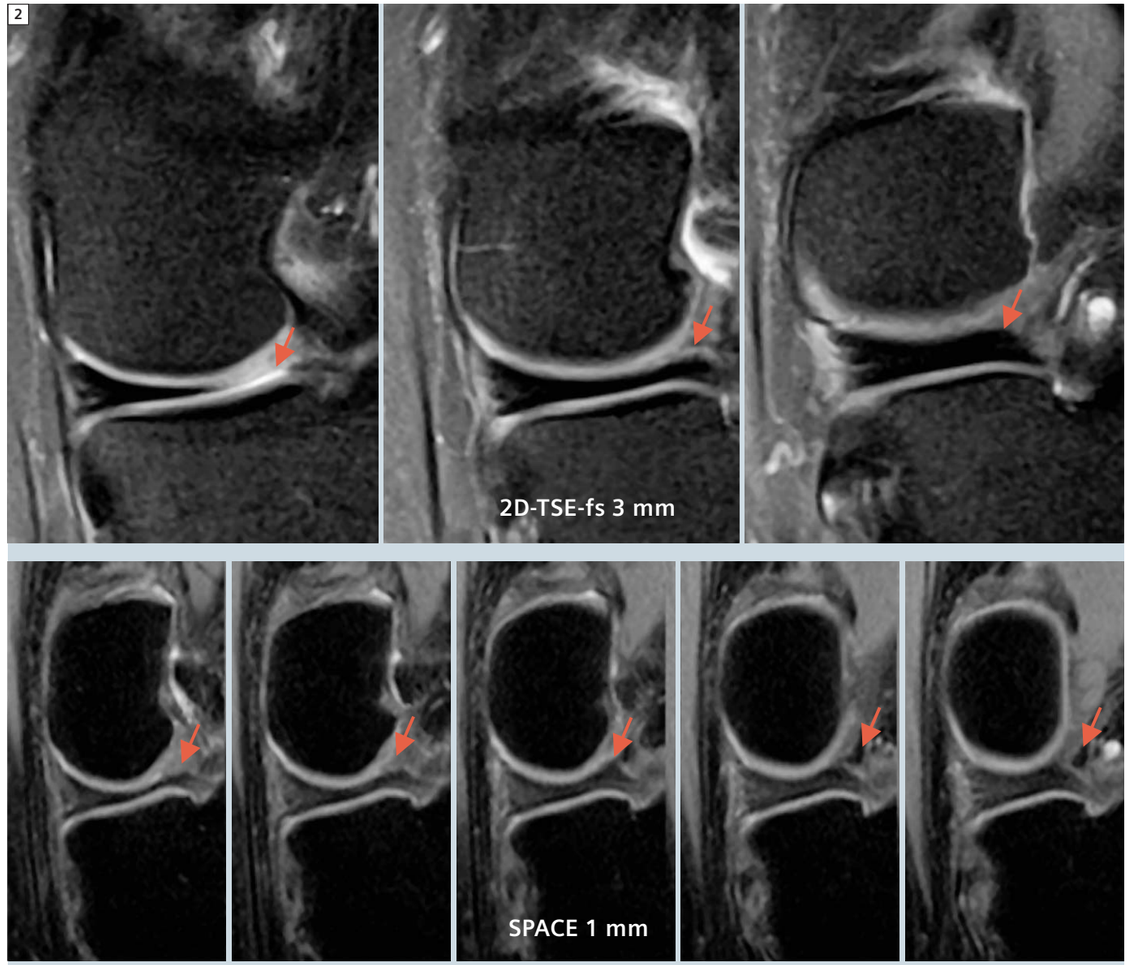

2 Coronal reconstructed *syngo* SPACE$_{1mm}$ and 2D-TSE-fs of a healthy volunteer. SPACE provides better visualization of the posterior medial meniscal root as compared to T2w-2D-TSE-fs, where the insertion of the root is blurred because of larger partial volume effects.

planes suggesting that the technique is feasible for daily clinical use.
The advantage of *syngo* SPACE over 2D-TSE-fs is the possibility of free multiplanar isotropic reconstructions at comparable SNR resulting in a slightly improved detection and differentiation of relevant small ligamenteous (Fig. 2) and meniscal structures (Figs. 3, 4). Clinical relevance thus might be better visualization of small avulsive ligamenteous lesions, e.g. of meniscal roots and of radial or complex meniscal tears whose configuration is challenging to interpret on conventional angulated thick sagittal or coronal sections (Fig. 5). The signal / image characteristics of *syngo* SPACE appear more similar to TSE image characteristics than to GRE and therefore are unlikely to require a big adjustment of the radiologist's reading and interpretation habits to the new sequence.
Usage of the free 3D-reformation according to the course of oblique anatomical structures as seen for femoral trochlear cartilage (Fig. 6) and the anterior cruciate ligament (Fig. 7) may aid in the evaluation of primarily difficult anatomical sites or a complicated situation after injury.

Conclusion

Blockwise acquired *syngo* SPACE is a new approach to MRI of the knee at 3T. It allows highly-resolved isotropic true 3-dimensional acquisition and subsequent reconstruction. Overall acquisition time is shorter than that of three separate 2-dimensional datasets and SNR for 1 mm reconstructions is similar to con-

Continued on page 90

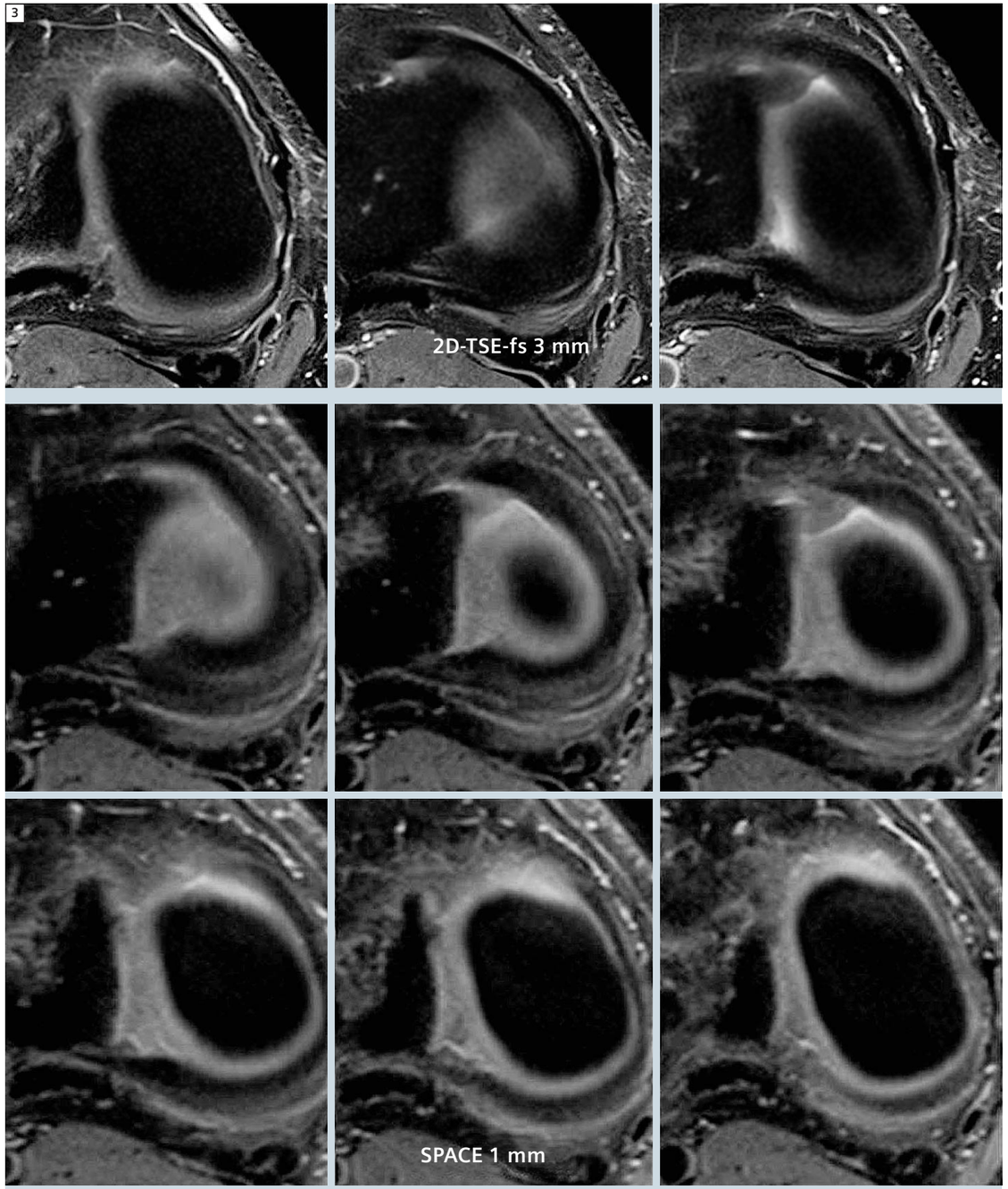

3 Axial sections of the medial meniscus of a healthy individual. *syngo* SPACE provides more detailed depiction of the meniscus throughout a higher number of slices as compared to 2D-TSE-fs. Both the meniscal body and its attachments (meniscal roots) are clearly visualized in SPACE while in 2D-TSE-fs parts of those are masked by partial volume effects.

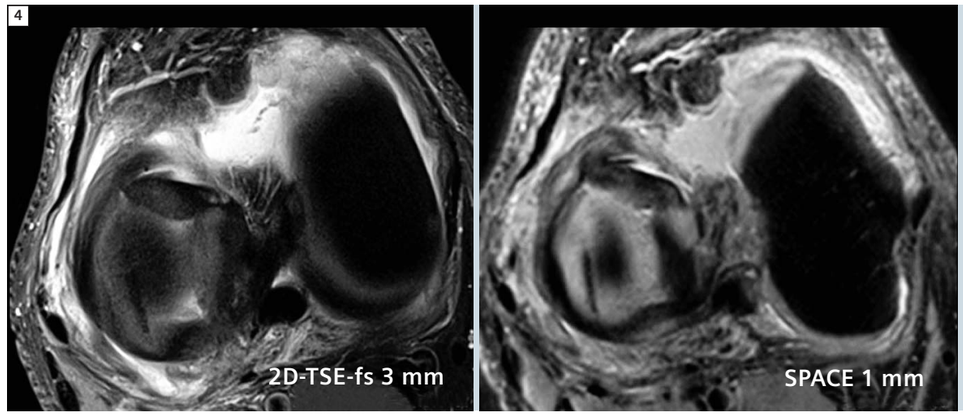

4 Axial reconstructed *syngo* SPACE$_{1mm}$ and 2D-TSE-fs of a patient with a bucket handle tear. SPACE provides better visualization of the configuration of the bucket handle tear as compared to T2w-2D-TSE-fs, in which delineation is impaired due to partial volume effects.

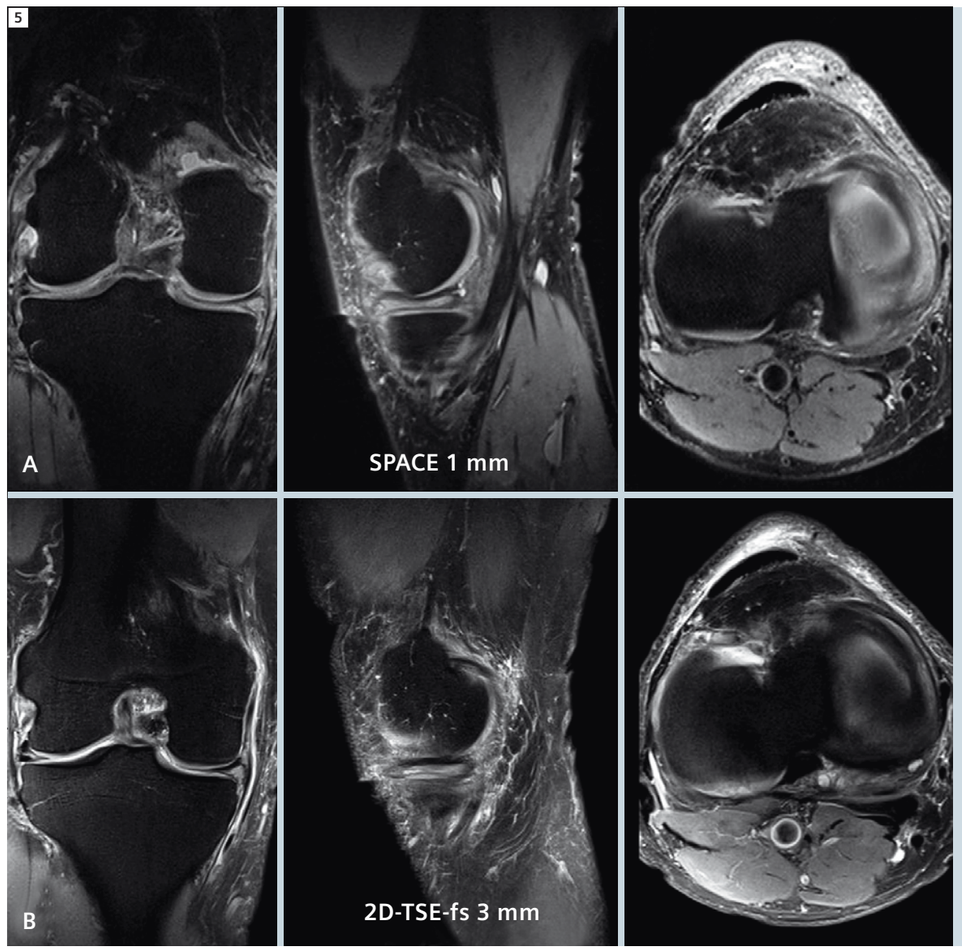

5 Coronal, sagittal and axial reconstructed *syngo* SPACE$_{1mm}$ images (row A) show a good delineation of a horizontal tear within the medial meniscus which approach the quality of the T2w-2D-TSE-fs sequence (row B) and provide an even clearer depiction of the lesion's borders and its extent.

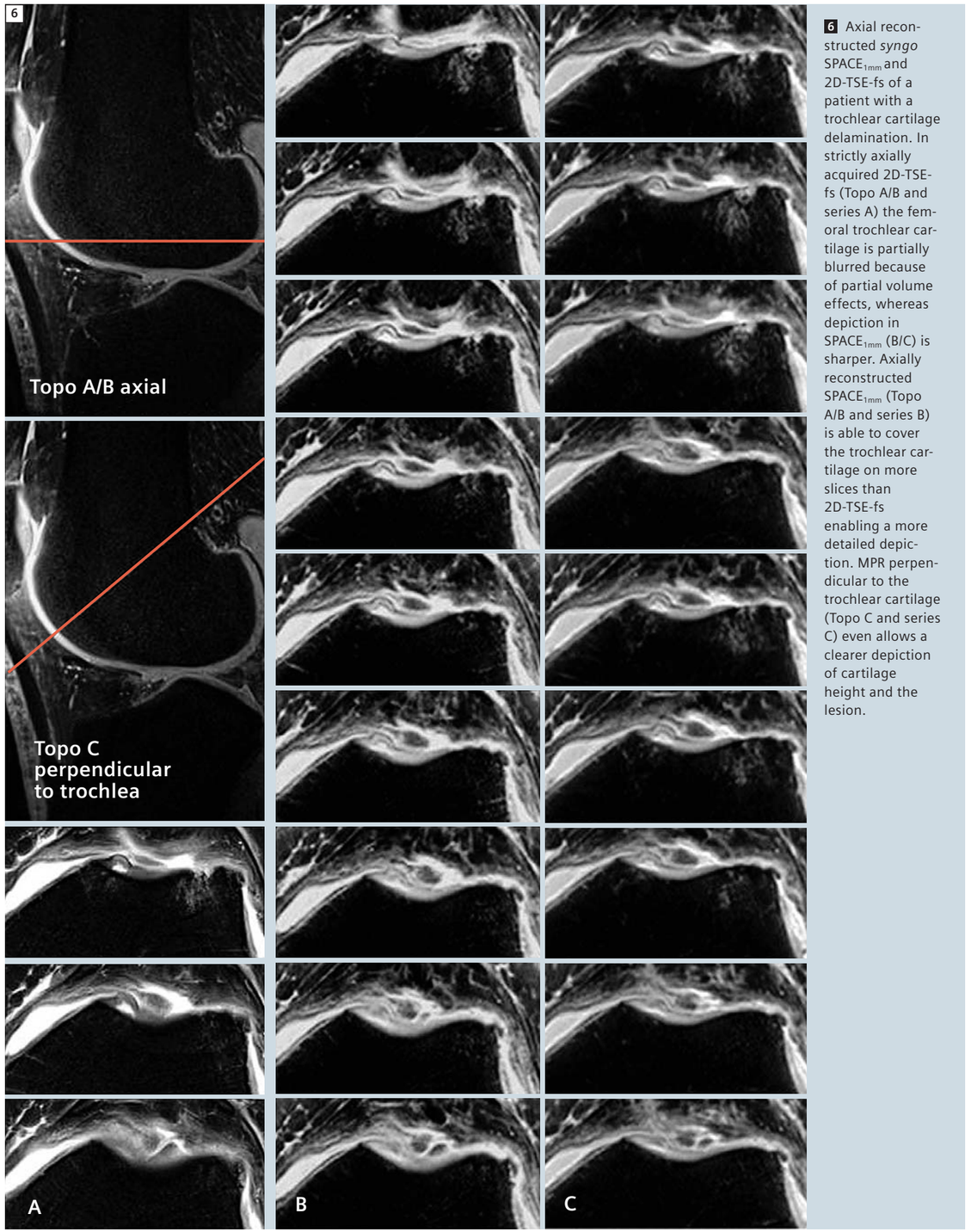

6 Axial reconstructed *syngo* SPACE$_{1mm}$ and 2D-TSE-fs of a patient with a trochlear cartilage delamination. In strictly axially acquired 2D-TSE-fs (Topo A/B and series A) the femoral trochlear cartilage is partially blurred because of partial volume effects, whereas depiction in SPACE$_{1mm}$ (B/C) is sharper. Axially reconstructed SPACE$_{1mm}$ (Topo A/B and series B) is able to cover the trochlear cartilage on more slices than 2D-TSE-fs enabling a more detailed depiction. MPR perpendicular to the trochlear cartilage (Topo C and series C) even allows a clearer depiction of cartilage height and the lesion.

Continued from page 86

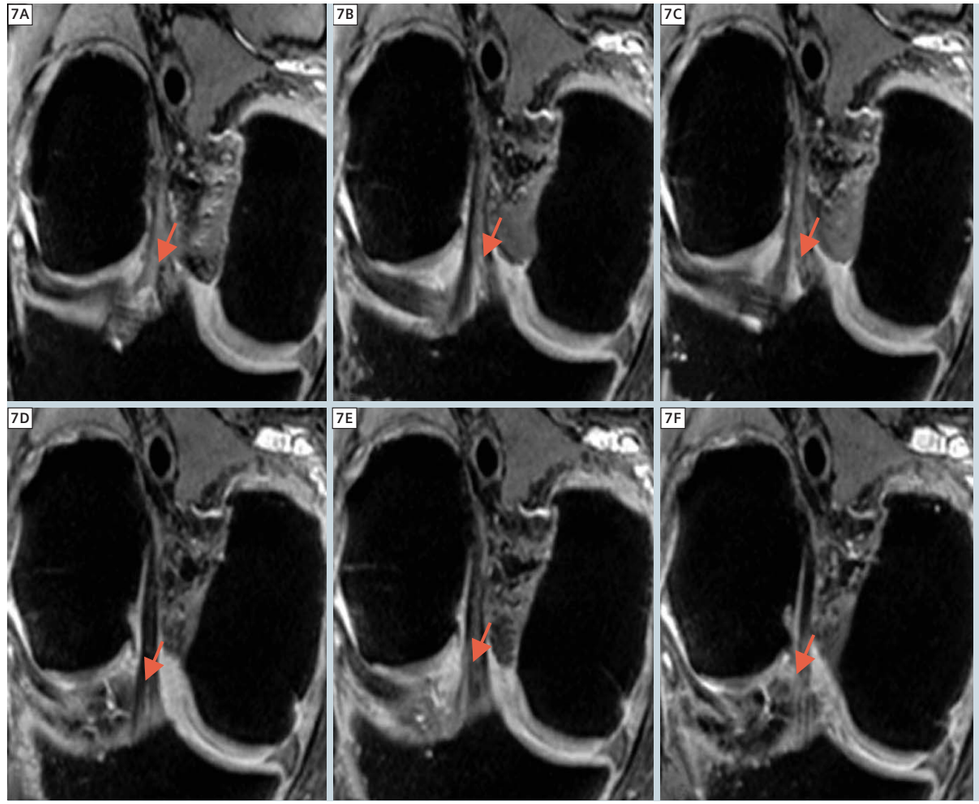

7 Anterior cruciate ligament of a healthy volunteer (sequence A–F). *syngo* SPACE$_{1mm}$ tilted to the course of the anterior cruciate ligament allows excellent traceability of the two bundles.

ventional 2D-TSE-fs. The identification of anatomical structures at least equals the conventional sequence and allows superior discrimination of relevant small ligamentous structures.
These data suggest that a protocol comprising 1 mm *syngo* SPACE reconstructions in three orientations would be useful for clinical evaluation. The additional possibility of free 3-dimensional reconstruction depending on the specific clinical need may become useful for the diagnosis of difficult anatomical situations and presurgical planning, i.e. for traumatic ligamenteous lesions or complex meniscal tears.

References
1 Glaser, C., et al., [Meniscus and ligament injuries]. Radiologe, 2006. 46(1): p. 26-35.
2 Protocols for MRI examinations of joints and the spine as recommended by the AG MSK of the Deutsche Röntgengesellschaft. Rofo, 2006. 178(12): p. 128-130.
3 Mosher, T.J., Musculoskeletal imaging at 3T: current techniques and future applications. Magn Reson Imaging Clin N Am, 2006. 14(1): p. 63-76.
4 Mugler, J.P., 3rd, et al., Optimized single-slab three-dimensional spin-echo MR imaging of the brain. Radiology, 2000. 216(3): p. 891-9.
5 Lichy, M.P., et al., Magnetic resonance imaging of the body trunk using a single-slab, 3-dimensional, T2-weighted turbo-spin-echo sequence with high sampling efficiency (SPACE) for high spatial resolution imaging: initial clinical experiences. Invest Radiol, 2005. 40(12): p. 754-60.
6 Isoda, H., et al., MRCP imaging at 3.0 T vs. 1.5 T: preliminary experience in healthy volunteers. J Magn Reson Imaging, 2007. 25(5): p. 1000-6.
7 Alsop, D.C., The sensitivity of low flip angle RARE imaging. Magn Reson Med, 1997. 37(2): p. 176–84.
8 Masi, J.N., et al., Cartilage MR imaging at 3.0 versus that at 1.5 T: preliminary results in a porcine model. Radiology, 2005. 236(1): p. 140-50.
9 Link, T.M., et al., 3.0 vs 1.5 T MRI in the detection of focal cartilage pathology--ROC analysis in an experimental model. Osteoarthritis Cartilage, 2006. 14(1): p. 63-70.
10 Notohamiprodjo, M., et al., A New Approach for High Resolution MRI of the Knee at 3T – Evaluation of a Moderately T2-Weighted 3D-TSE-Fs (SPACE) Sequence, Investigative Radiology, 2009 44(9): p.585-597.

Contact
Annie Horng, M.D.
Department of Clinical Radiology
University Hospitals Munich –
Campus Grosshadern
Marchioninistrasse 15
81377 Munich
Germany
Phone: +49 89 7095 3620
annie.horng@med.uni-muenchen.de

Case Reports: Musculoskeletal MRI in Sports Medicine

Heinz-Peter Schlemmer[1,3]; Tina Holder[1]; T. Nägele[1,2]; Claus D. Claussen[1,2]

[1]Radiologie SpOrt Stuttgart, Germany
[2]University Hospital of Tuebingen, Germany
[3]German Cancer Research Center, Heidelberg, Germany

Background

In contrast to its role in oncology, for example, MR imaging in sports medicine deals primarily with healthy and young individuals. This imaging technique is an invaluable tool in sports medicine, not only because of its excellent soft tissue contrast but also because of its non-invasive and non-ionizing nature. While imaging in recreational sports is mainly limited to an evaluation of the effects of severe traumatic events, such as a skiing accident, the role of musculoskeletal MRI in case of competitive sports is much more extensive. For example, following an injury, MRI is also used to assist in the detailed evaluation of the degree of performance impairment of the athlete – with direct impact on treatment / training actions taken for effective fast and full recovery. This implies that time-to-diagnosis and the easy access and availability of MRI scan time (also for follow-up exams) is important for these athletes. One should also take into account that the pattern and severity of injuries can differ between recreational and competitive sports. This has a direct impact on the indication to MRI and the required knowledge of technologists and radiologists. But also non-traumatic pain and limitation of mobility, and as a consequence insufficient training and competitive performances, of athletes can have various causes and are one of the main indications for MRI. Because of the importance of the results of such MR exams to the athlete, the interdisciplinary approach is one of the key elements for optimal and responsible treatment and support. Consequently, all cases shown in this article were examined at and treated by an association of different facilities including the Department of Sports Medicine at Tuebingen University and the Olympic Training Center Stuttgart.

In this article, we present a selection of cases. Whilst not being a representative selection, they do reflect very well the variety and range of musculoskeletal imaging in sports medicine: in cases 1 and 2, MRI was used to support the clinical diagnoses of ligamental tear / rupture. Cases 3 through 5 show typical patterns of muscular tears and haematoma after trauma. In these patients, MRI was used to evaluate the involvement and extension of the different muscles to evaluate and quantify the degree of performance impairment and to provide information for further rehabilitation training. And finally, in cases 6 and 7, the images of two young athletes with pain at training but without corresponding trauma are shown.

All MRI exams shown in this article were performed at 1.5 Tesla (MAGNETOM Avanto).

Case 1

22-year-old male soccer player with severe knee pain after traumatic knee injury.

An extensive effusion is obvious. Already suspected by clinical signs, oedema and tear of the anterior cruciate ligament supports the diagnosis of a complete rupture of the ligament (arrowhead in Fig. 1A). In addition, a horizontally shaped oedema within the dorsal medial meniscus supports the suspicion of a horizontal (smaller) meniscal tear (arrow in Fig. 1B).

Images were acquired with the dedicated CP extremity coil. Sequence parameters for the shown images were:

- Sagittal PDw TSE with spectral fat suppression: TR / TE = 3754 / 37 ms, SL 1.5 mm, FOV 140 x 140 mm, Matrix 269 x 384 px
- Coronal PDw TSE with spectral fat suppression: TR / TE = 3754 / 37 ms, SL 1.5 mm, FOV 140 x 140 mm, Matrix 269 x 384 px

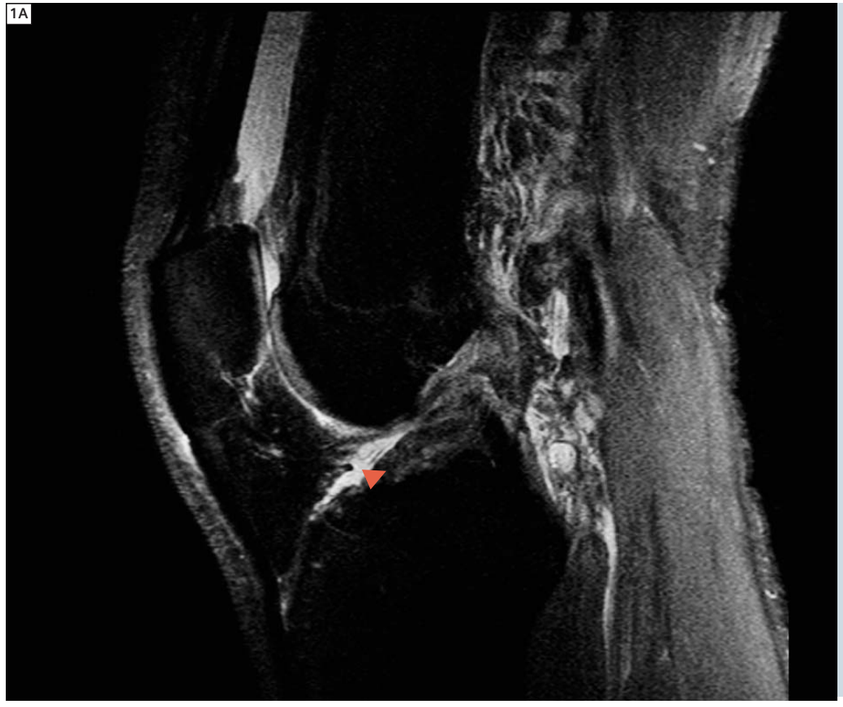

1A Sagittal PDw STIR.

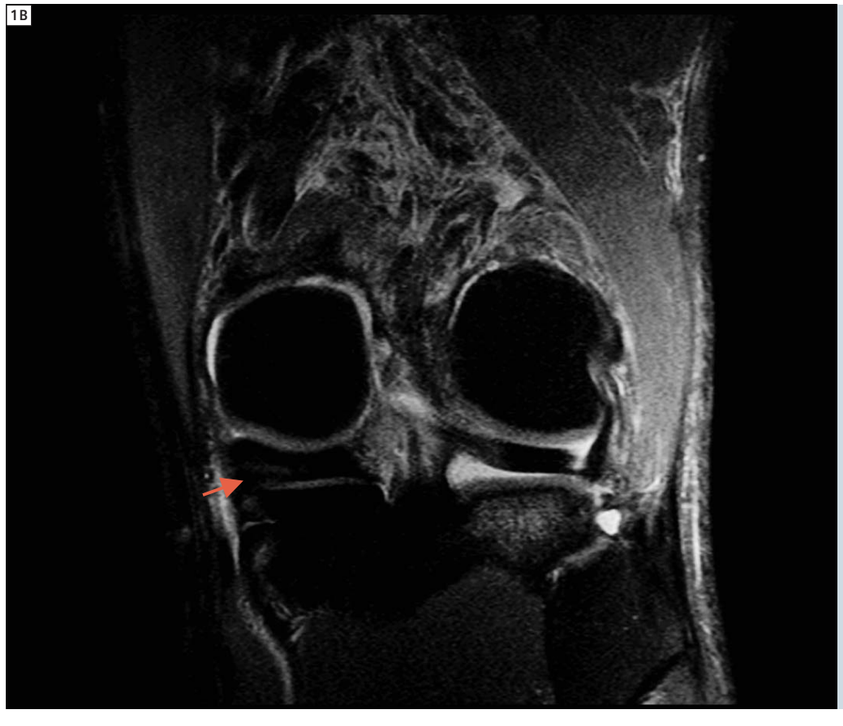

1B Coronal PDw STIR

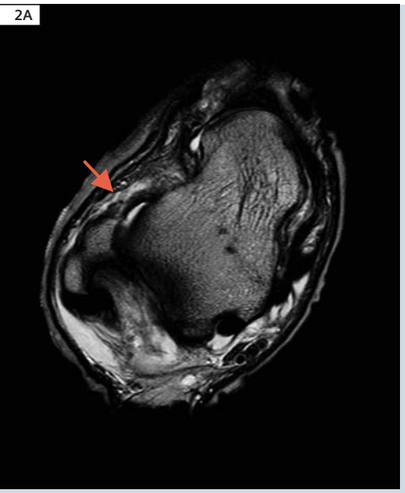

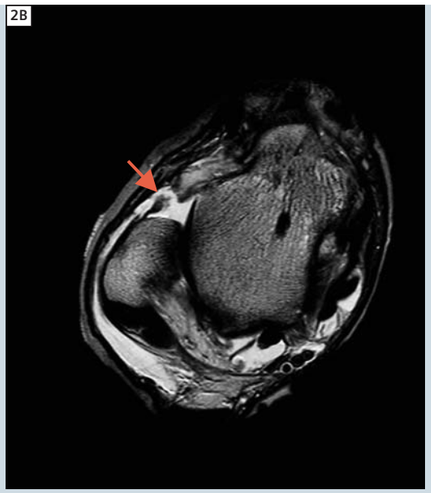

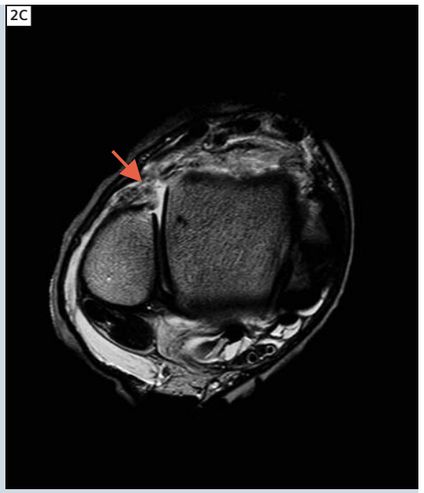

2A–C 1st trauma: transversal T2w TSE.

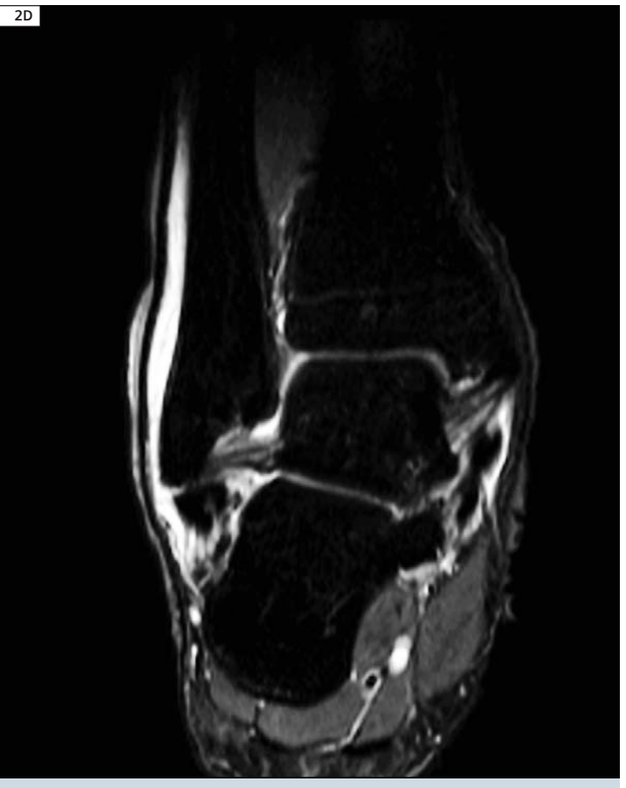

2D 1st trauma: coronal PDw STIR.

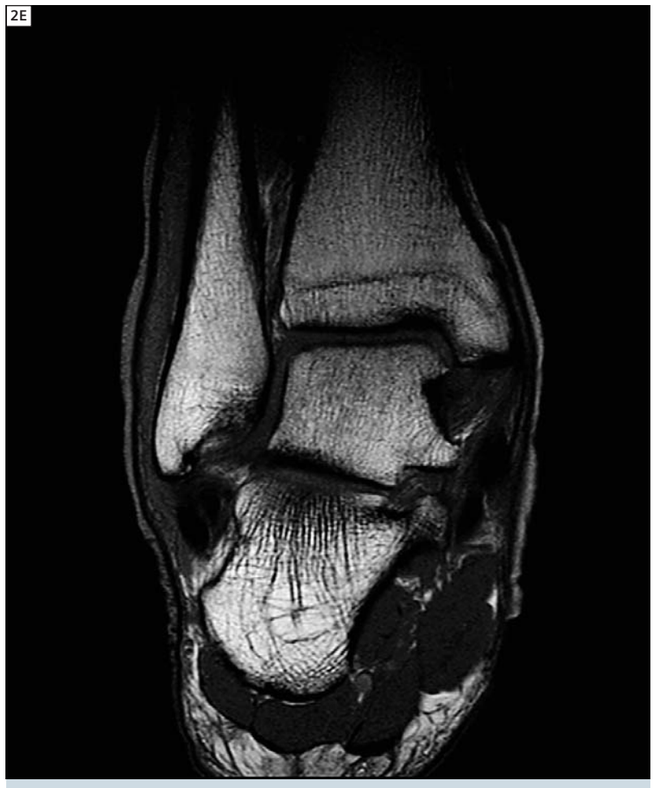

2E 1st trauma: coronal T1w TSE.

Case 2

23-year-old male soccer player after traumatic ankle injury.
MRI demonstrates a complete rupture of the anterior fibulotalar ligament (arrow in Figs. 2A–C). In addition, a partial rupture of the anterior syndesmosis ligament is present and an extensive oedema and haemorrhage of the surrounding soft tissue can also be observed (Figs. 2D and E). 7 months after the initial traumatic event, another trauma of similar type occurred. Follow-up MRI showed a thickened but now continuous fibulotalar ligament and ventral syndesmosis (arrowheads in Figs. 2D–F); no re-rupture was found.
Images were acquired with the 4-channel flex coil. Sequence parameters for the shown images were:

- Transversal T2w TSE: TR / TE = 5259 / 85 ms, SL 3 mm, FOV 140 x 140 mm, Matrix 269 x 448 px
- Coronal PDw STIR: TR / TE / TI = 6500 / 29 / 160 ms, SL 3 mm, FOV 160 x 160 mm, Matrix 169 x 256 px
- Coronal T1w TSE: TR / TE = 537 / 9.5 ms, SL 3 mm, FOV 111 x 160 mm, Matrix 250 x 448 px, TA
- Follow-up MRI transversal T2w TSE: TR / TE = 4110 / 105 ms, SL 3 mm, FOV 110 x 110 mm, Matrix 512 x 512 px

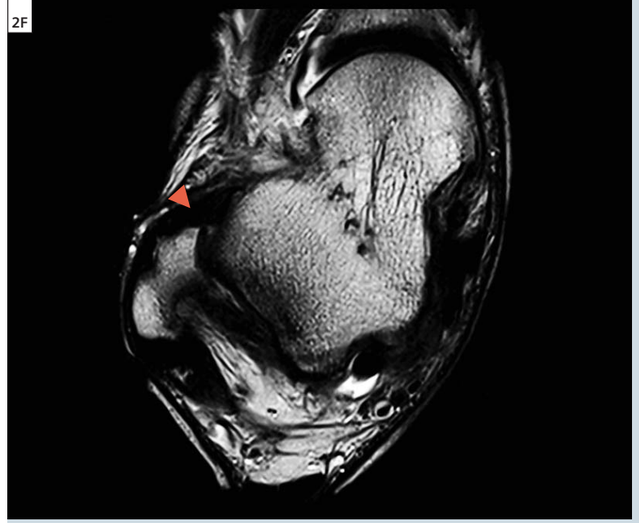

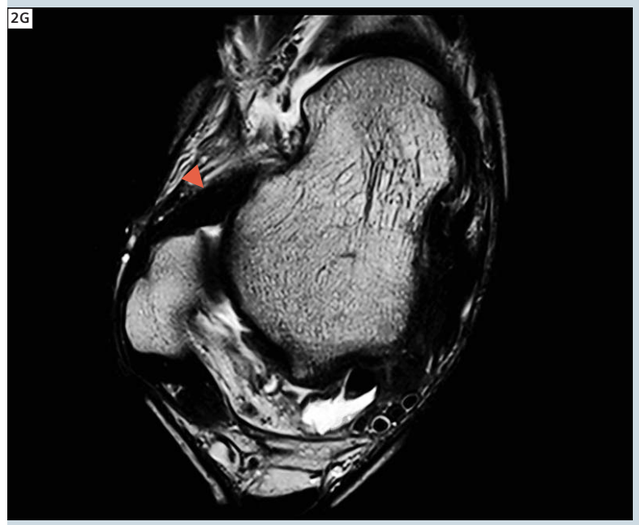

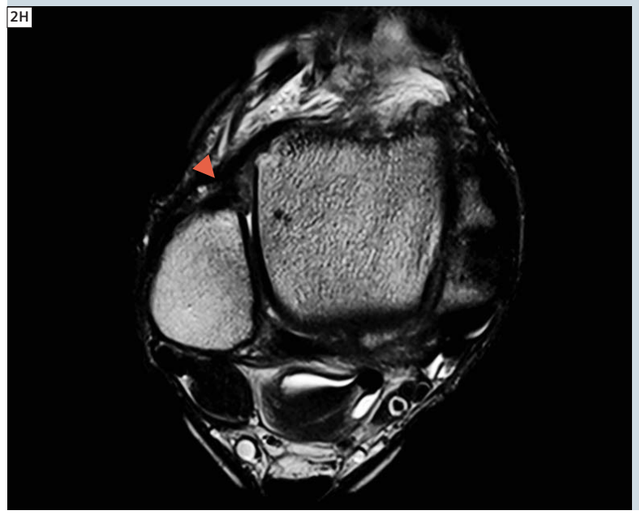

2F–H 2nd trauma: transversal T2w TSE.

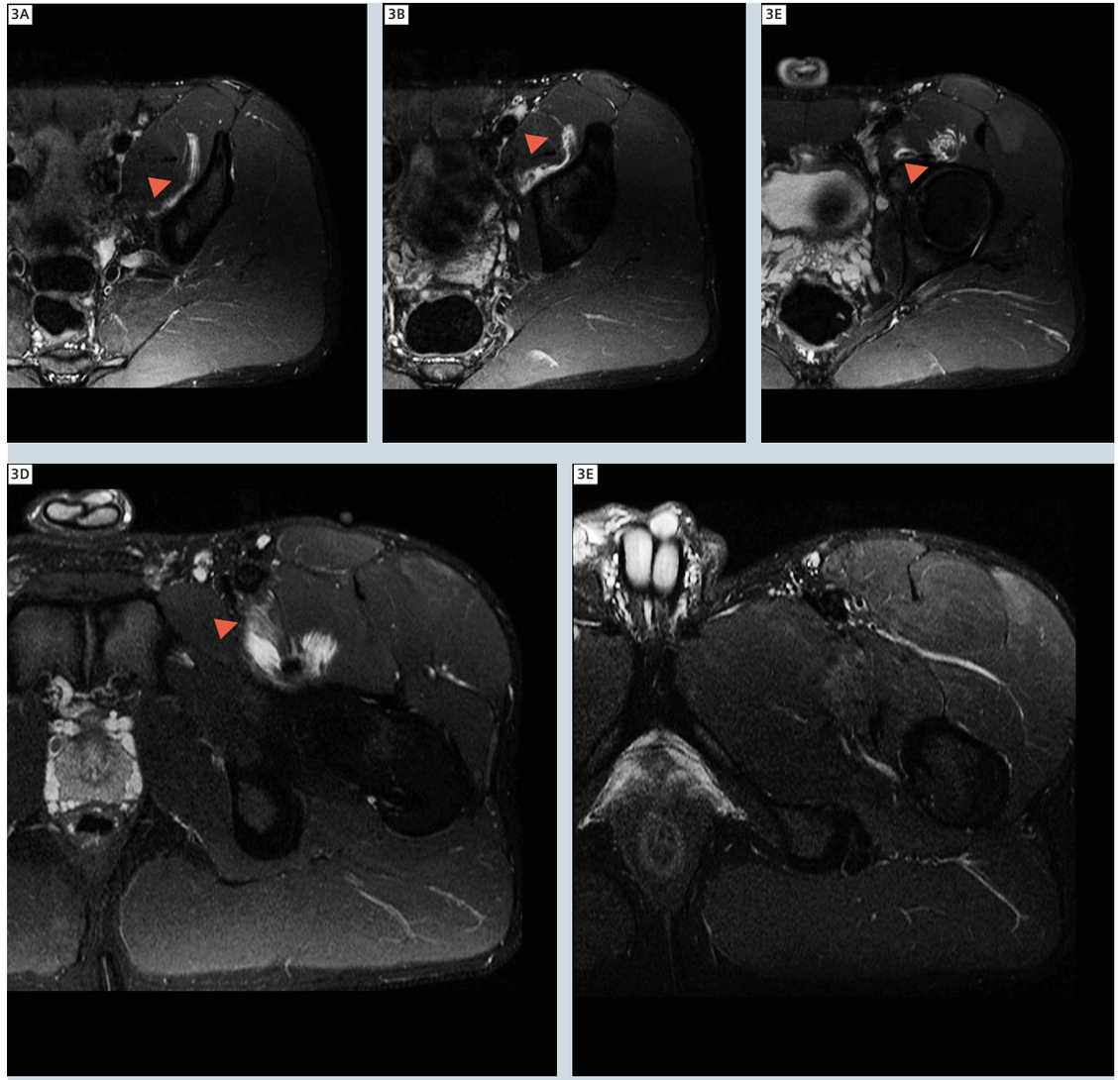

3A–E Transversal PDw STIR.

Case 3

22-year-old male soccer player after trauma of the left upper leg.
Tear of the fascia of the left iliac muscle at the ventral border of the acetabulum and less prominent tear of the iliac muscle itself (arrowheads in Fig. 3).
Images were acquired with the Spine and Body Matrix coil. Sequence parameters for the shown images were:

- Transversal PDw STIR: TR / TE / TI = 5390 / 29 / 160 ms, SL 4 mm, FOV 220 x 200 mm, Matrix 224 x 320 px
- Oblique coronal PDw TSE with spectral fat saturation: TR / TE = 4340 / 13 ms, SL 3 mm, FOV 250 x 250 mm, Matrix 240 x 320 px, TA
- Obliques sagittal PDw STIR: TR / TE / TI = 7540 / 29 / 160 ms, SL 4 mm, FOV 189 x 270 mm, Matrix 157 x 320 px

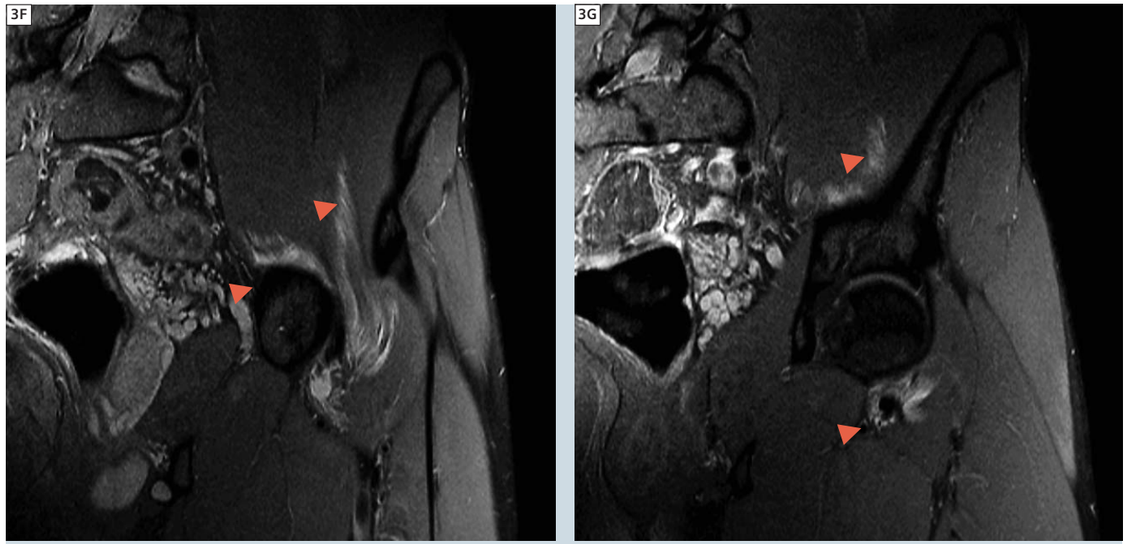

3F–G Oblique coronal PDw STIR.

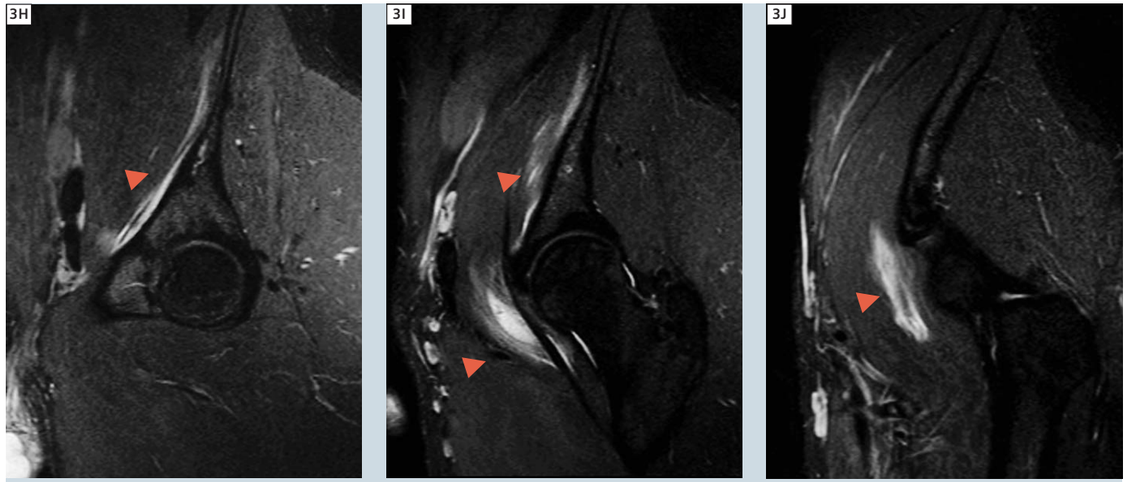

3H–J Oblique sagittal PDw STIR.

→ **Visit**
www.siemens.com/magnetom-world
to check out the protocols of the MSK Advisory Board.

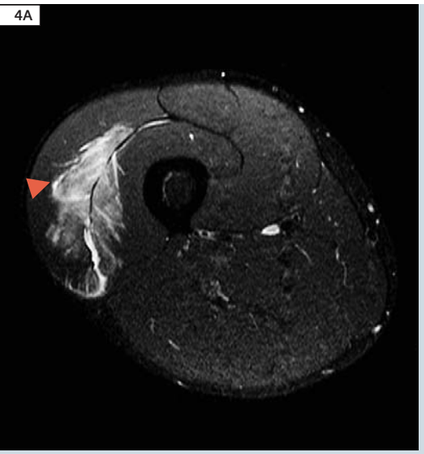

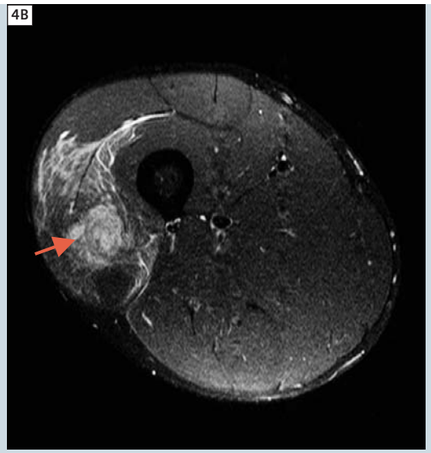

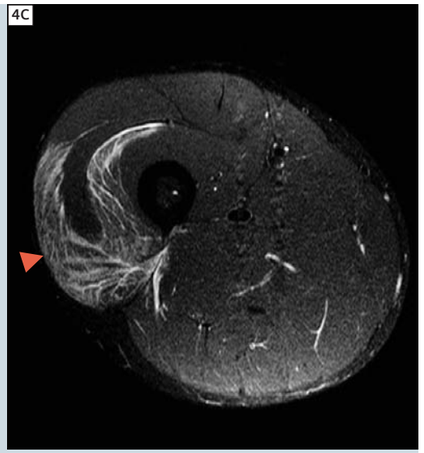

4A–C Transversal PDw STIR.

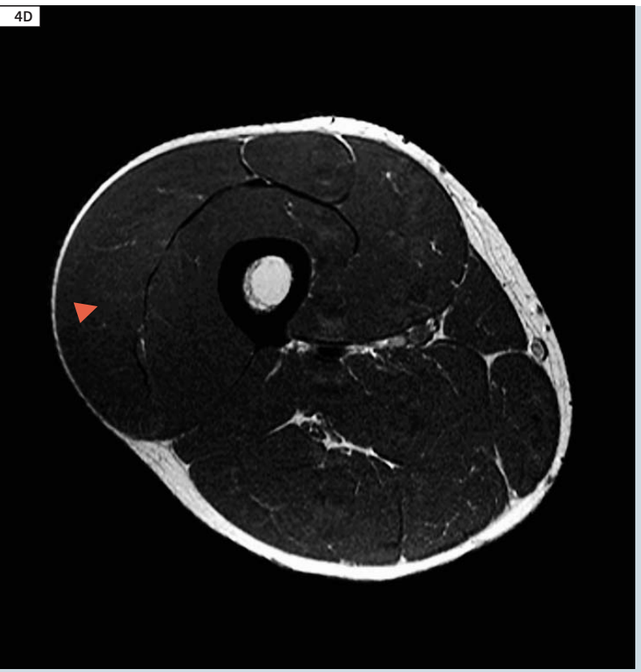

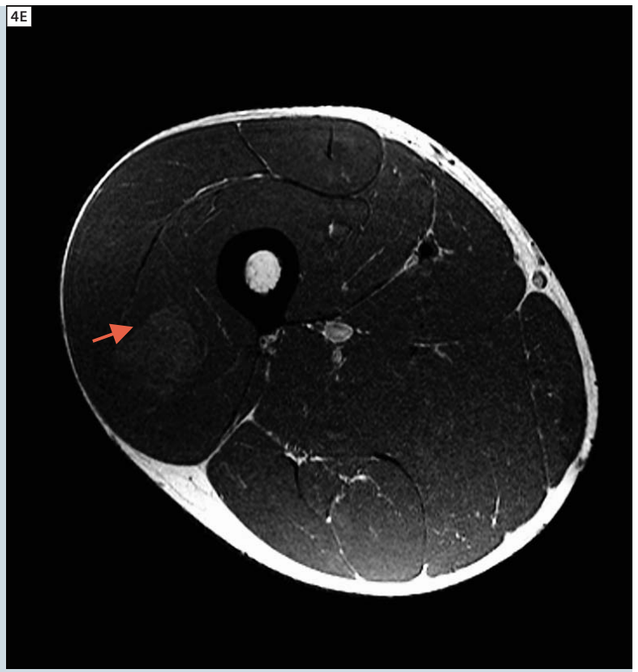

4D–E Transversal T1w TSE.

Case 4

24-year-old male soccer player after direct trauma (pound on right upper leg). On T2w images, a space occupying lesion within the lateral vastus muscle (arrow) and slight increased signal intensities on T1w images was seen, representing an extensive haematoma. Also a surrounding haemorrhage (arrowheads) was obvious. There were no clear signs of a tear in the muscles. The femur showed neither a fracture nor abnormalities of the signal intensities of the bone marrow.
Images were acquired using the Spine and Body Matrix coil. Sequence parameters for the shown images were:

- Transversal PDw STIR: TR / TE / TI = 8073 / 29 / 160 ms, SL 4 mm, FOV 220 x 220 mm, Matrix 224 x 320 px
- Transversal T1w TSE: TR / TE = 580 / 13 ms, SL 4 mm, FOV 200 x 200 mm, Matrix 256 x 320 px
- Sagittal PDw STIR: TR / TE / TI = 4580 / 29 / 160 ms, SL 4 mm, FOV 280 x 400 mm, Matrix 157 x 320 px
- Coronal T2w TSE: TR / TE = 7130 / 86 ms, SL 4 mm, FOV 281 x 399 mm, Matrix 216 x 384 px

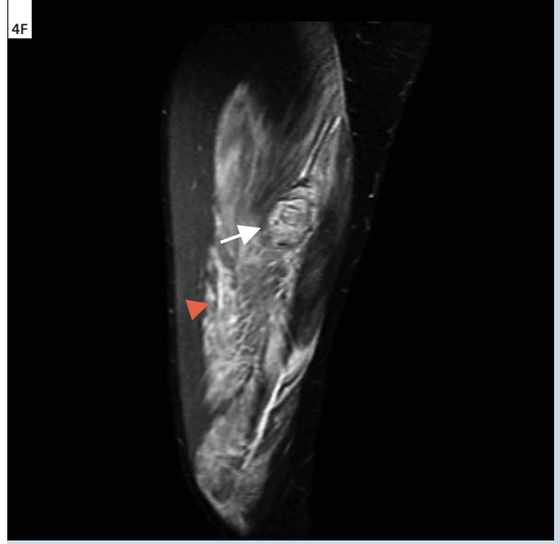

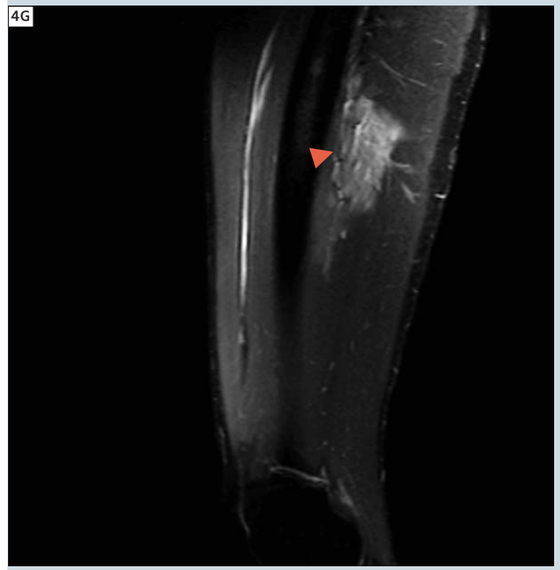

4F–G Sagittal PDw STIR.

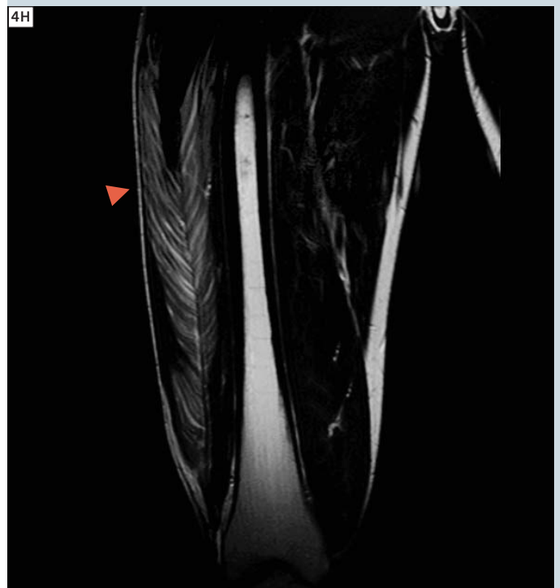

4H Coronal T2w TSE.

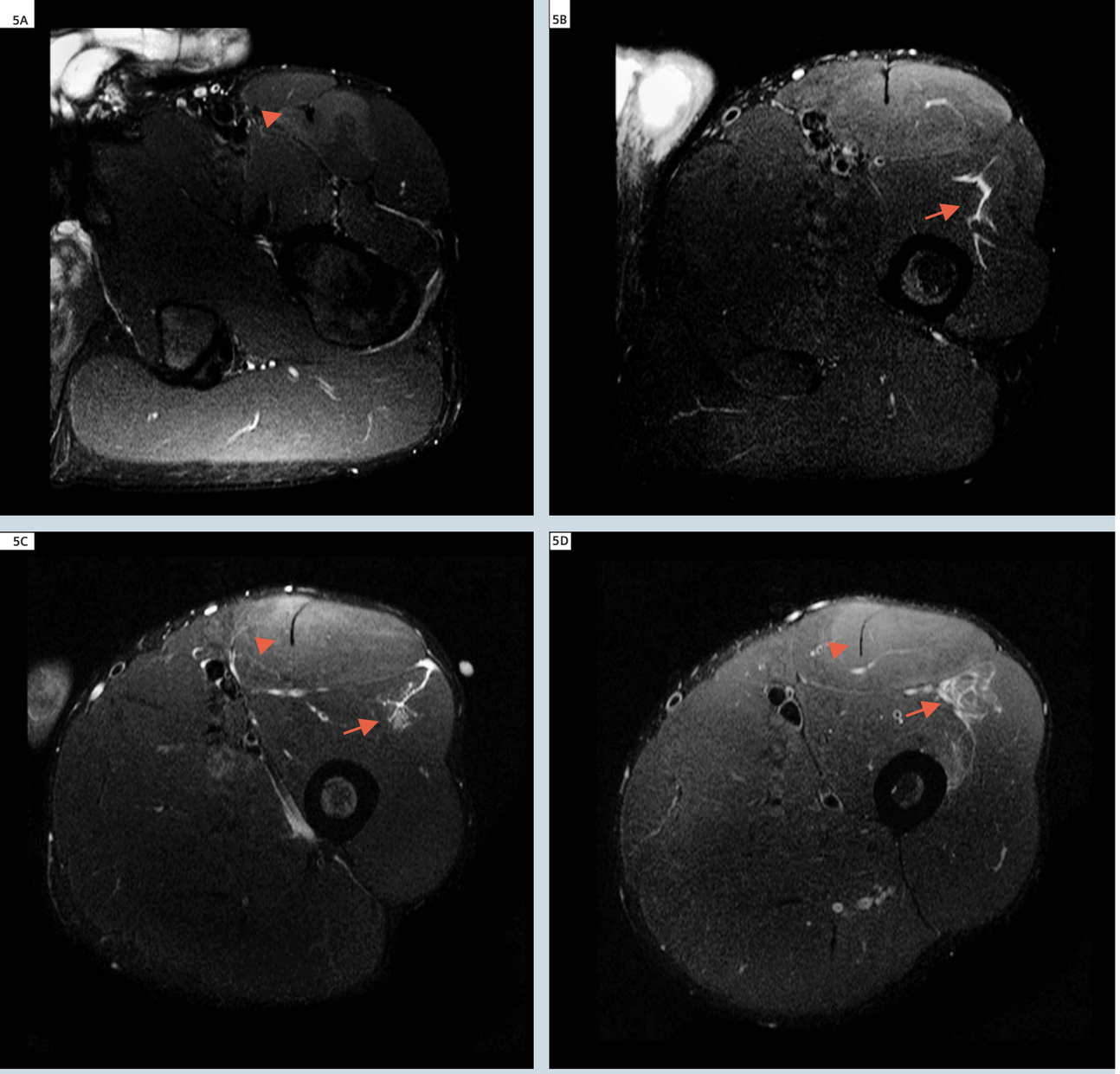

5A–D Transversal PDw STIR.

Case 5

24-year-old male soccer player after trauma.
In contrast to case 4, an approximate 15 mm long acute tear of the lateral vastus muscle (arrow) was seen in this patient but there were no signs of a dehiscence of the muscles. Slight increase of the signal intensities on PDw images within the vastus intermedius and rectus femoris muscles were rated as a strain.
The patient was positioned feet first and the images were acquired with the Spine and Body Matrix coil. Sequence parameters for the shown images were:

- Transversal PDw STIR: TR / TE / TI = 5390 / 29 / 160 ms, SL 4 mm, FOV 220 x 220 mm, Matrix 224 x 320 px

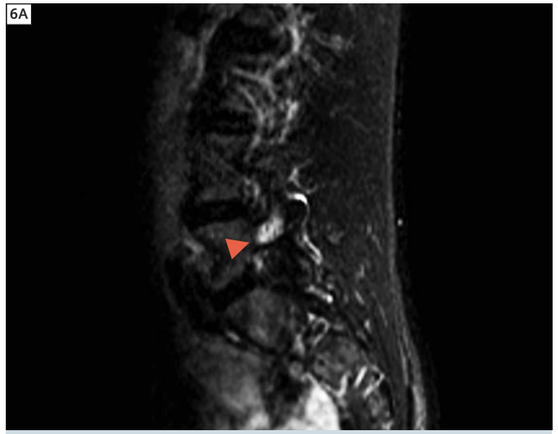

6A Sagittal T2w STIR.

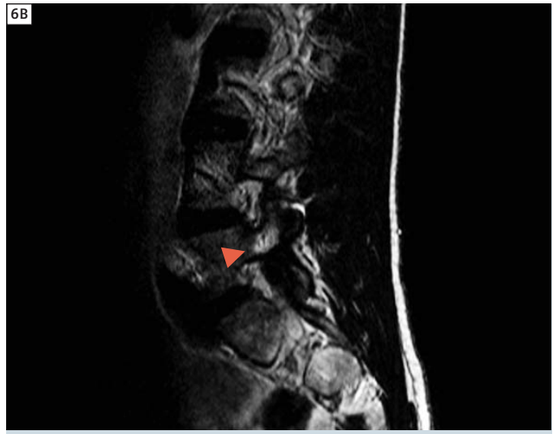

6B Sagittal T2w TSE.

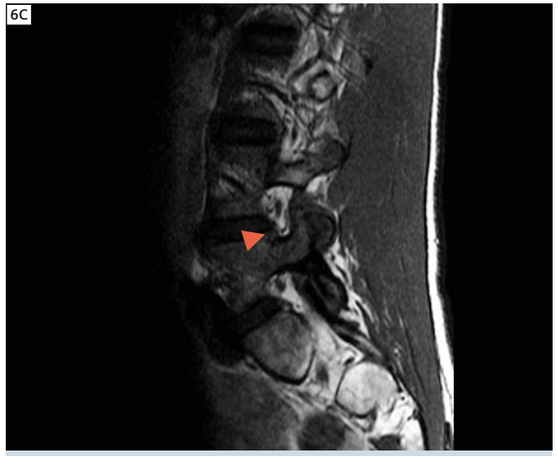

6C Sagittal T1w TSE.

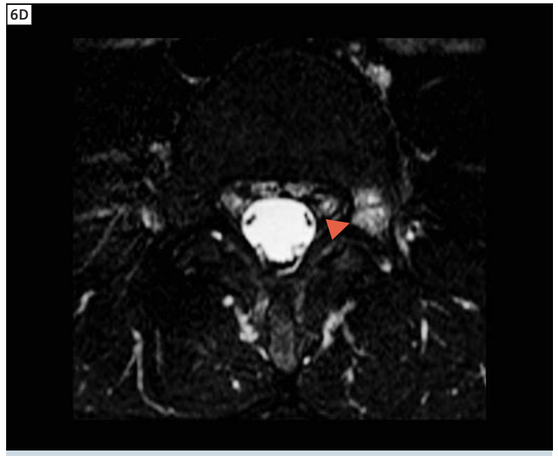

6D Oblique transversal T2w STIR.

Case 6

16-year-old female high-jumper with consistent pain during training sessions and while making sudden jerky movements.
High signal intensity within the bone marrow of the left pedicel of the 5th vertebra could be seen. Within this oedema, a continuous hypointense line was crossing the pedicel. This finding was rated as a 1st degree spondylolysis without signs of listhesis or cleft.
Images were acquired using the spine coil. Sequence parameters for the shown images were:

- Oblique transversal T2w TSE with spectral fat saturation: TR / TE = 3800 / 105 ms, SL 3 mm, FOV 180 x 180 mm, Matrix 192 x 256 px
- Sagittal T2w STIR: TR / TE / TI = 7300 / 63 / 150 ms, SL 3 mm, FOV 300 x 300 mm, Matrix 195 x 256 px
- Sagittal T1w TSE: TR / TE = 621 / 12 ms, SL 3 mm, FOV 280 x 280 mm, Matrix 269 x 384 px
- Sagittal T2w TSE: TR / TE = 8660 / 120 ms, SL 3 mm, FOV 280 x 280 mm, Matrix 269 x 384 px

Case 7

13-year-old female soccer player with pain within the right forefoot but without adequate corresponding trauma. Caudal of the epiphyseal line of the second metatarsal bone, an oedema of the bone marrow and very apical loss of shape of the bone and compression of bone trabeculae. The epihyseal line is of regular shape. The caudal head of the metacarbal bone is also surrounded by oedema and an effusion of the joint was present, too. These findings were concordant with an osteonecrosis in the stadium of vitrification (Morbus Köhler-Freiberg / Morbus Köhler II).
Images were acquired with the 4-channel flex coil. Sequence parameters for the shown images were:

- Coronal T2w STIR: TR / TE / TI = 4180 / 70 / 140 ms, SL 2 mm, FOV 140 x 140 mm, Matrix 460 x 512 px
- Coronal T1w TSE: TR / TE = 684 / 13 ms, SL 2 mm, FOV 140 x 140 mm, Matrix 256 x 512 px
- Sagittal T2w STIR: TR / TE / TI = 3700 / 70 / 140 ms, SL 2 mm, FOV 140 x 140 mm, Matrix 460 x 512 px
- Transversal T2w TSE: TR / TE = 3880 / 103 ms, SL 3 mm, FOV 89 x 130 mm, Matrix 352 x 512 px

Contact
Prof. Heinz-Peter Schlemmer, M.D; Ph.D.
Radiologie SpOrt Stuttgart
Fritz-Walter-Weg 19
D-70372 Stuttgart
Germany
h.schlemmer@Dkfz-Heidelberg.de
www.radiologie-neckarpark.de
www.sport-medizin.eu

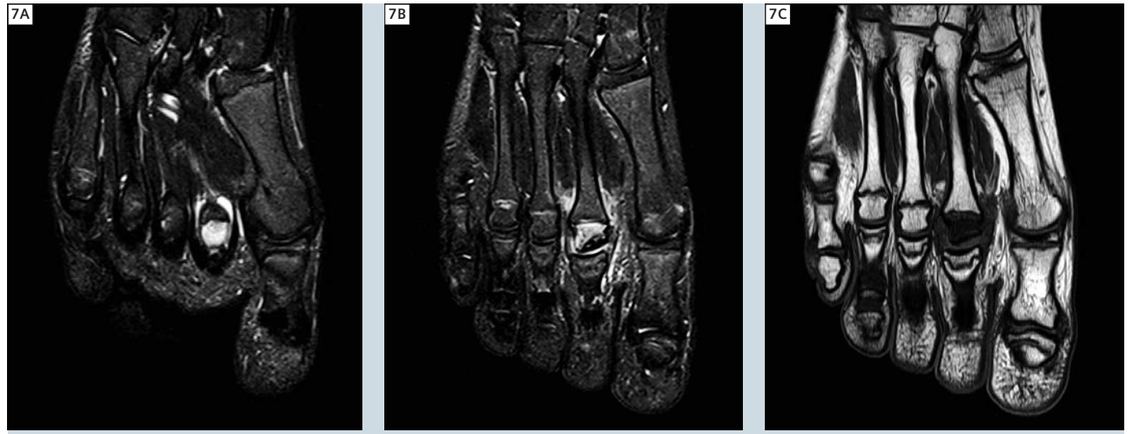

7A–C **A** and **B:** Coronal T2w STIR. **C:** Coronal T1w TSE.

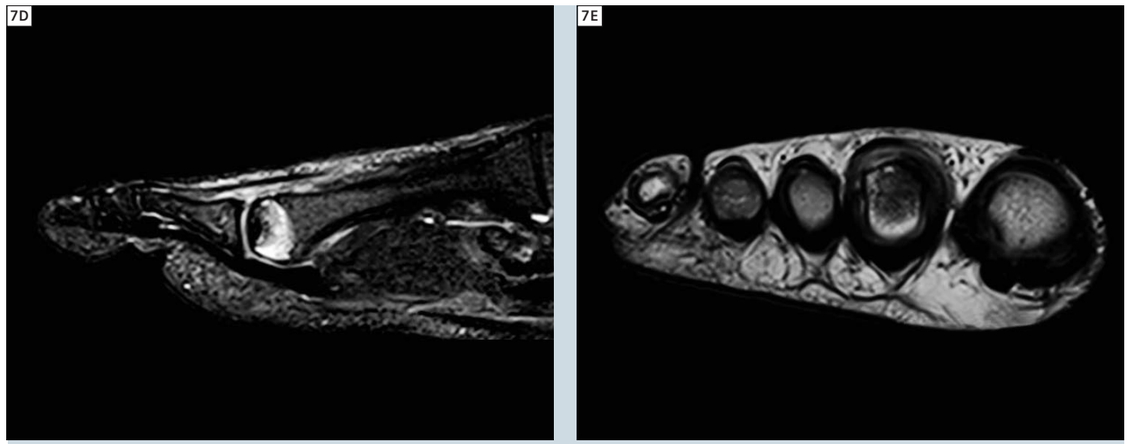

7D–E **D:** Sagittal T2w STIR. **E:** Transversal T2w TSE.

Case Report:
Traumatic Lesion of the Left Brachial Plexus

Markus Lentschig, M.D.

MR and PET/CT Imaging Center Bremen Mitte, Bremen, Germany

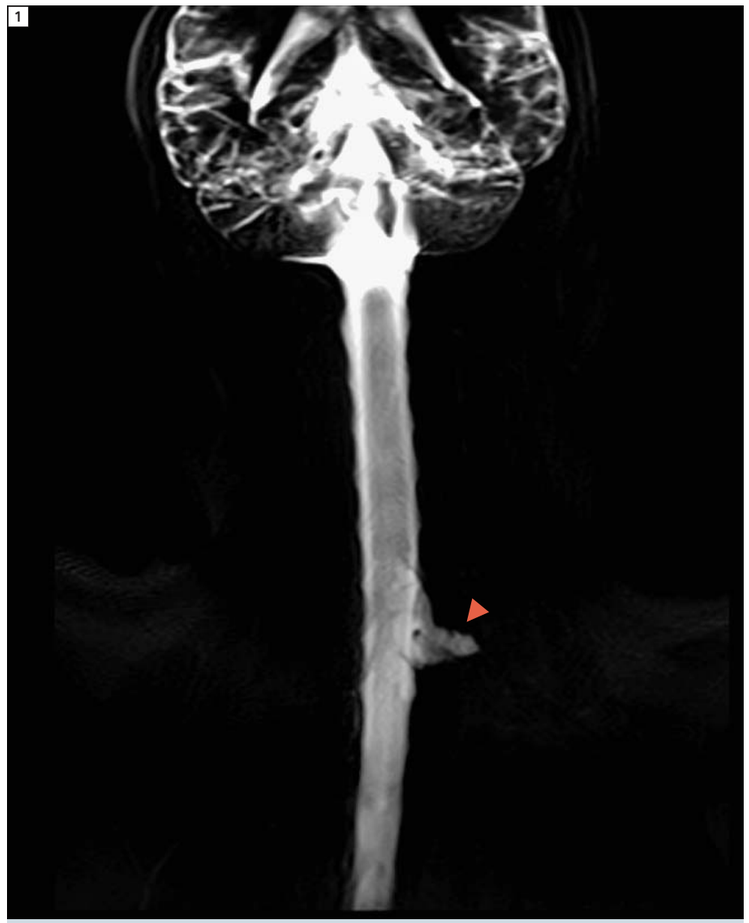

1 MR myelogram.

Patient history

An 18-year-old patient was referred to our institution for evaluation of the integrity of the left brachial plexus 4 weeks after a severe traumatic event. The presented symptoms at the time-point of MR imaging suggested an involvement of the medial and inferior left brachial plexus.

Sequence details

All images were acquired on our 1.5 Tesla MAGNETOM Espree with a combination of the dorsal elements of the head/neck and the spine matrix coils. The imaging protocol comprised a coronal single shot HASTE myelogram, sagittal T1w and T2w TSE, coronal T1w TSE and T2w TIRM, transversal fat saturated T2w TSE and MEDIC and finally 3D T2w TSE (*syngo* SPACE) in coronal orientation. No contrast media was applied in this patient.

Coronal HASTE Myelogram: TR / TE 4500 / 755 ms; FOV 350 x 350 mm; matrix 307 x 384; SL 60 mm; PAT 2; no averages; TA 1.8 s.

Sagittal T2w TSE: TR / TE 4274 / 113 ms; FOV 300 x 300 mm; matrix 314 x 448; SL 3 mm; no iPAT; averages 2; TA 4:13 min.

Sagittal T1w TSE (not shown): TR / TE 689 / 11 ms; FOV 241 x 300 mm; matrix 270 x 448; SL 3 mm; no iPAT; averages 3; TA 3:06 min.

Transversal T1w TSE wit spectral fat saturation (not shown): TR / TE 3740 / 93 ms; FOV 303 x 380 mm; matrix 204 x 512; SL 4 mm; no iPAT; averages 2; TA 3:56 min.

Coronal T1w TSE: TR / TE 639 / 20 ms; FOV 309 x 380 mm; matrix 250 x 512; SL 4 mm; no iPAT; no averages; TA 5:20 min.

Coronal T2w TIRM: TR / TE / TI 5940 / 36 / 160 ms; FOV 285 x 380 mm; matrix 192 x 512; SL 4 mm; no iPAT; no averages; TA 5:22 min.

Coronal 3D T2w TSE (*syngo* SPACE): TR / TE 1500 / 173 ms; FOV 280 x 280 mm; matrix 323 x 320; SL 1 mm; PAT 3; no averages; TA 3:56 min.

Imaging findings

A large cystic lesion at the level of the 1st thoracic and 8th cervical nerve root is obvious on the HASTE myelogram (arrowhead in Fig. 1). Accordingly a displacement of the dural border and widening of the subdural space is also obvious (compare transversal T2w MEDIC images in figures 2A, B). A displacement of the spinal dural mater (Fig. 2) can be found on transversal and sagittal T2w images. Edema of the left

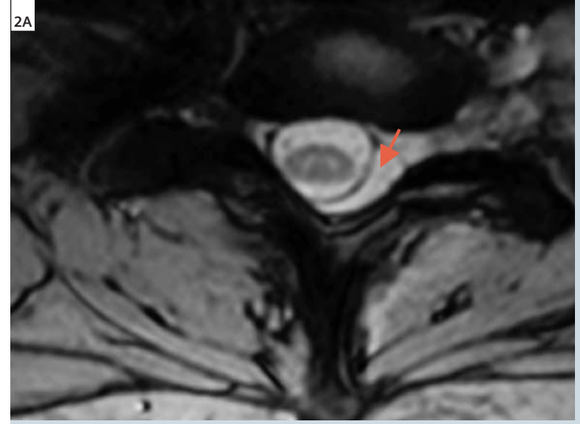

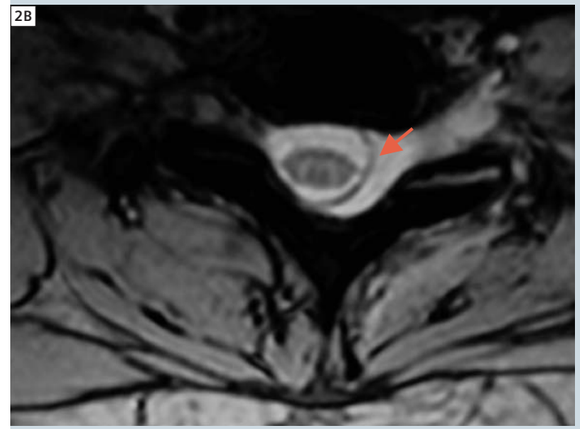

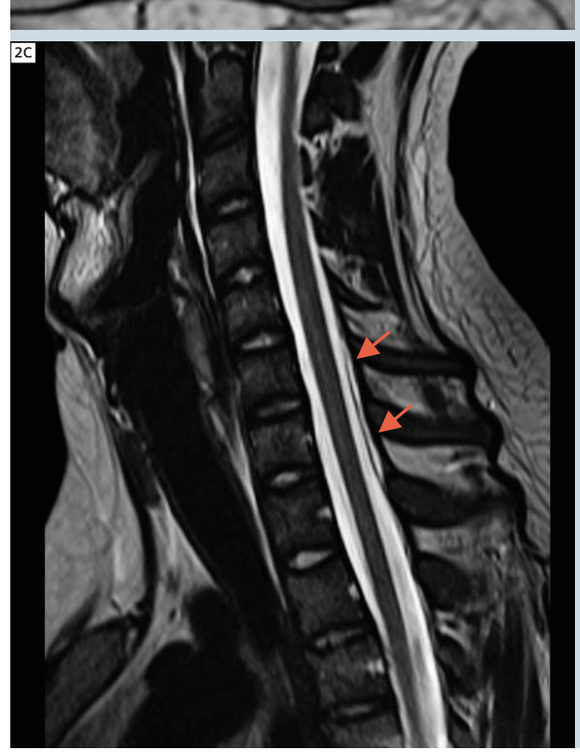

2 A and B transversal MEDIC, C sagittal T2w TSE.

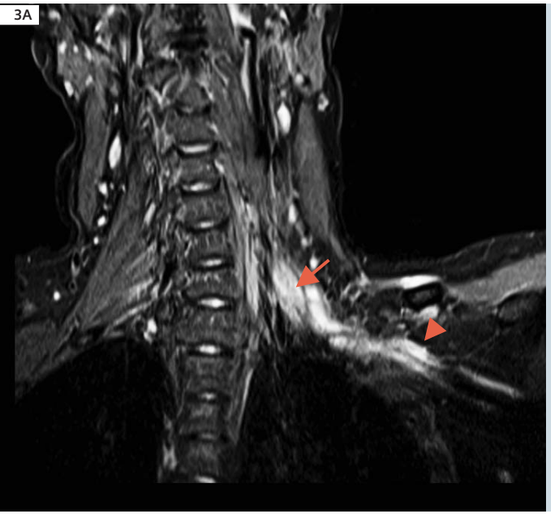

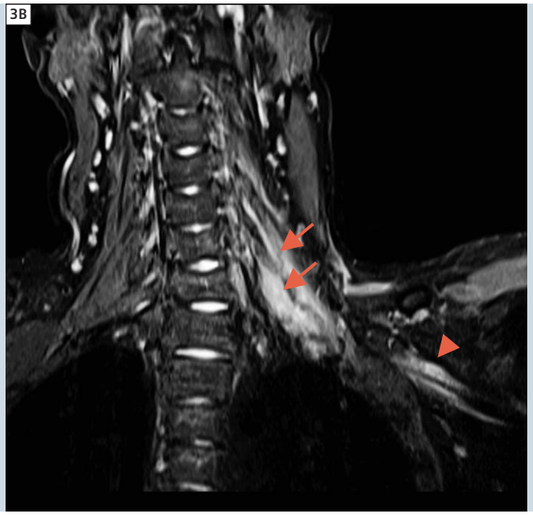

3 Coronal TIRM.

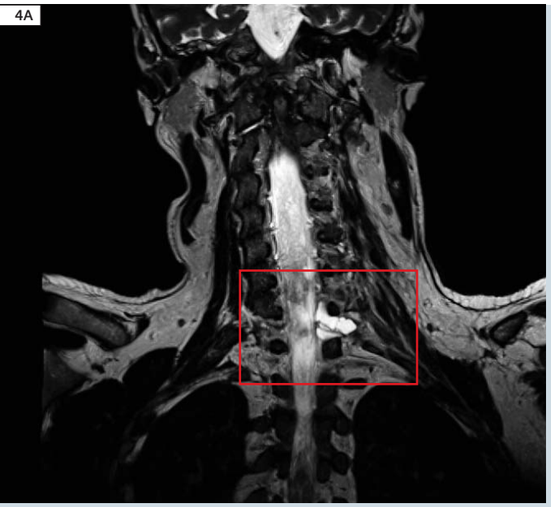

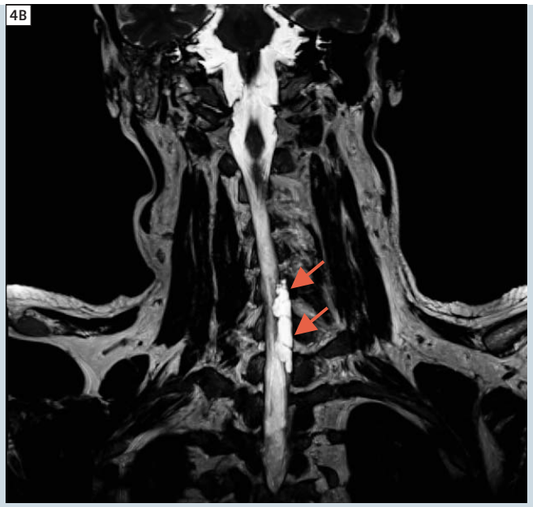

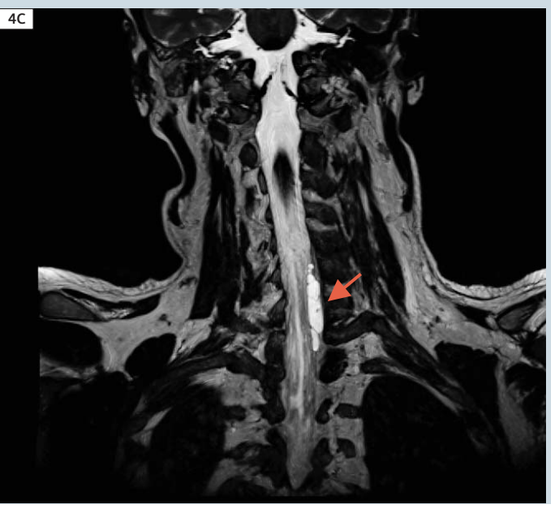

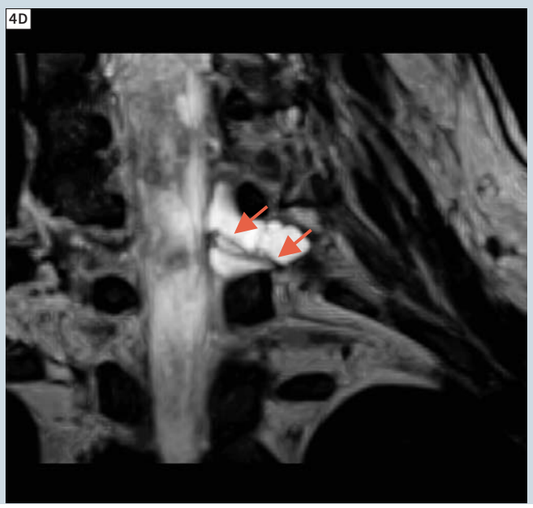

4 A, B, C coronal 3 mm thin-slice MPR based on a 3D T2w TSE scan (*syngo* SPACE).

D: magnified detail of Fig. 3A.

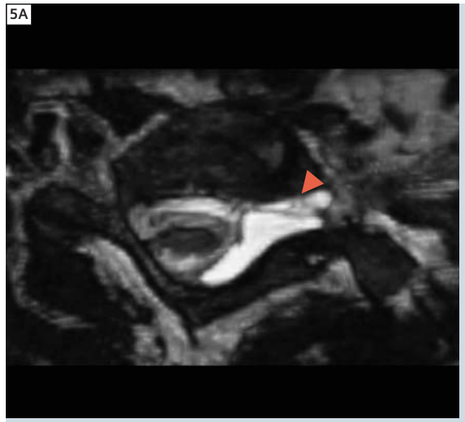

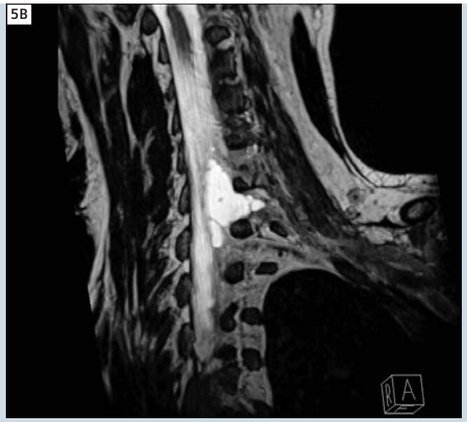

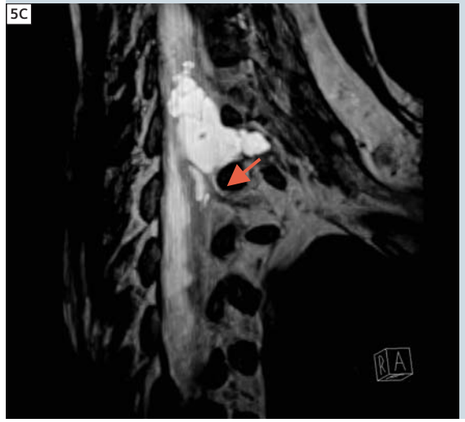

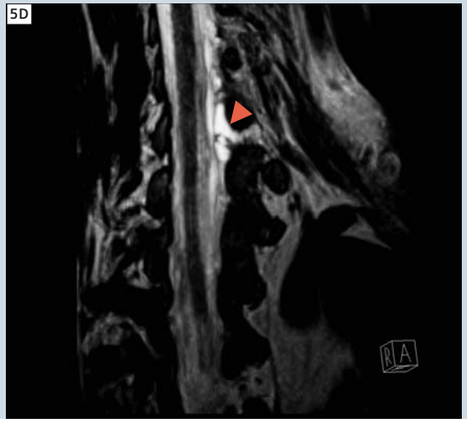

5 Oblique transversal **(A)** and coronal **(B–D)** 3 mm thin-slice MPR based on a 3D T2w TSE scan (*syngo* SPACE) for detailed visualisation of the nerve roots.

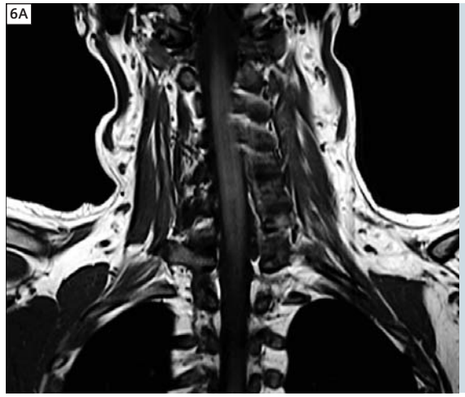

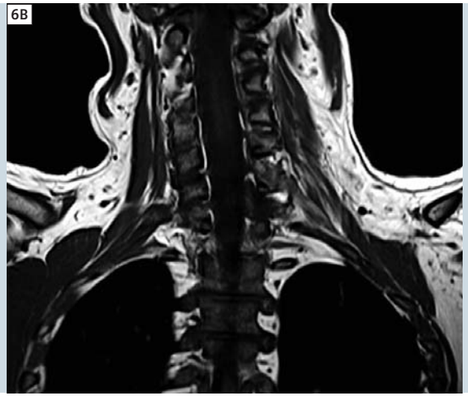

6 Coronal T1w TSE.

cervical muscles (arrows Figs. 3A, B) and of the inferior and medial trunc of the brachial nerve plexus (arrowhead Fig. 3) is clearly delineated on the coronal T2w TIRM images. Best visualized in the 3D T2w TSE (Figs. 4, 5), a nearly complete rupture of the 8th cervical nerve root is the obvious diagnosis, together with an affection and at least partial rupture of the 1st thoracic and 7th cervical nerve root. There is a regular alignment of the vertebra bodies and no evidence of a fracture. There are regular signal intensities of the myelon on the T1w and T2w images; there is no larger hemorrhage within either the myelon or the nerval plexus.

Contact
Markus G. Lentschig, M.D.
MR and PET/CT Imaging Center Bremen Mitte
Sankt-Juergen-Str. 1
28177 Bremen
Germany
www.mr-bremen.de

FABS View of the Elbow for Visualization of Distal Biceps Tendon

Peter Cazares, RT (R) (CT) (MR)

MR Clinical Education Specialist, Siemens Healthcare, Iselin, NJ, USA

Introduction

Imaging of distal bicep tendon in MR can be somewhat difficult at times given the position of the elbow in relation to the general scanning environment. Common axial / coronal sequences demonstrate the tendon in an oblique projection that make it difficult to appreciate it in its entirety. By using the FABS (**f**lexed elbow, **ab**ducted shoulder, forearm **s**upinated) technique, imaging of the distal biceps tendon can be acquired "in plane" with excellent visualization and comfortable patient positioning.

Conclusion

Distal biceps tendon pathology will be greatly appreciated using this technique and can be incorporated with standard elbow imaging when this clinical referral is presented. Also greater success can be achieved with greater patient comfort using this technique and position.

Contact
Peter Cazares
Siemens Healthcare USA, Inc.
HQ Application Specialist – MR
170 Wood Avenue South
Iselin, NJ 08830
USA
peter.cazares@siemens.com

Procedure

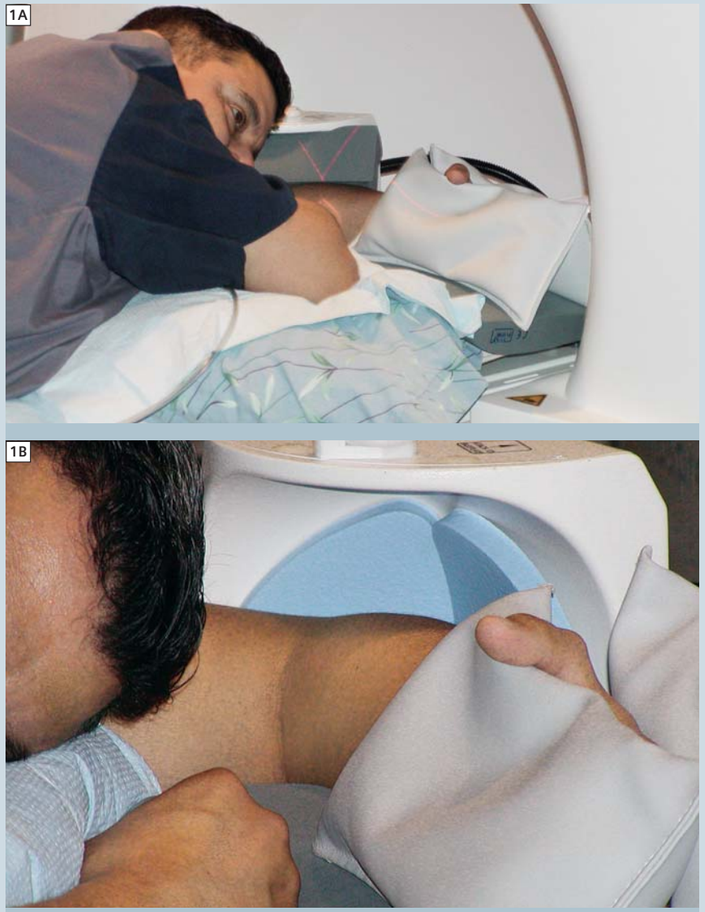

1 **Step 1:** We position the patient using our standard shoulder coil configuration. Have the patient lay on their stomach as comfortable as possible. Flex the elbow 90 degrees and place the elbow in the shoulder coil with the forearm and wrist supinated. Secure the forearm and wrist with either sandbags or a channeled positioning sponge to insure immobilization.

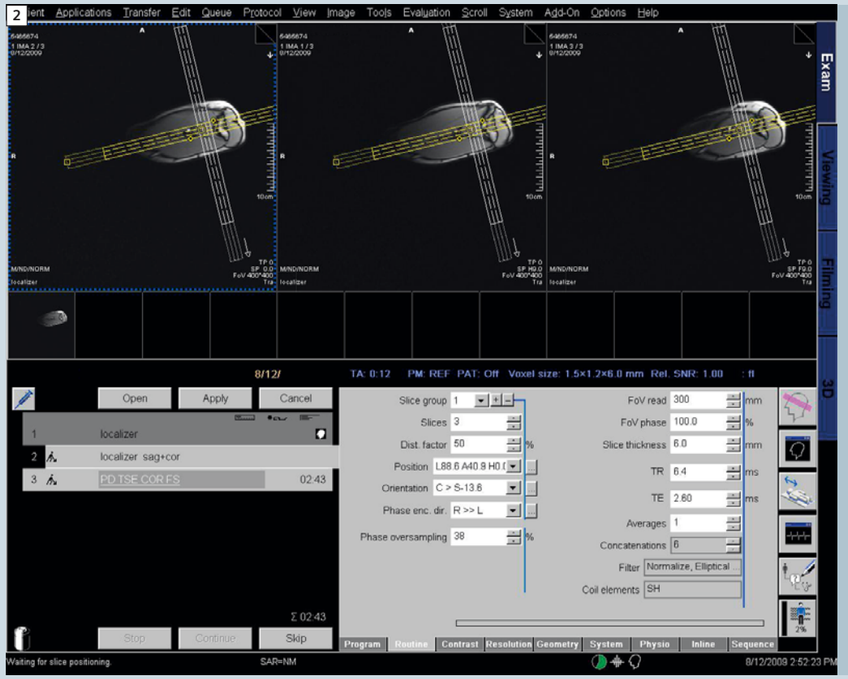

2 **Step 2:** Landmark at the center of the coil and localize. Perform two additional localizers in long and short axis in relation to the elbow.

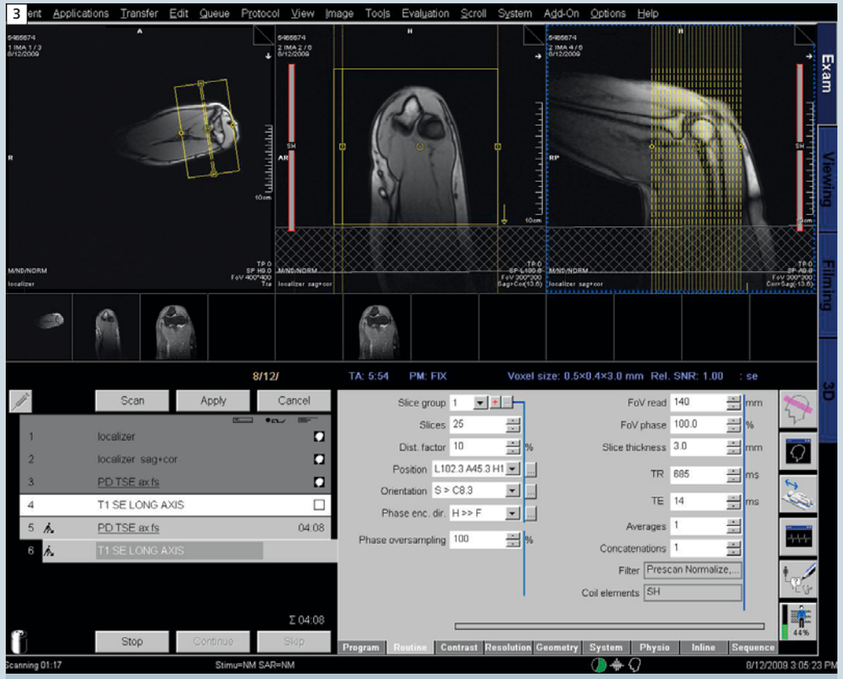

3 **Step 3:** Select sequences so as to image the biceps tendon "in plane". T1-weighted Spin Echo (SE) no fatsat, PD TSE fatsat are one recommendation.

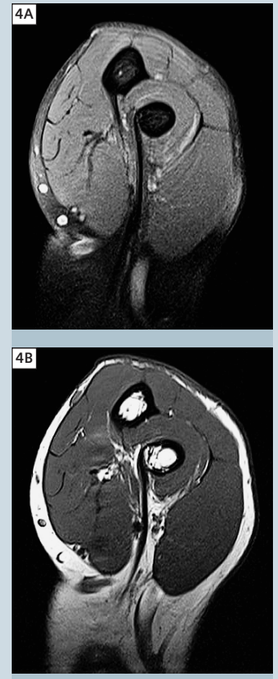

4 As seen, the distal biceps tendon is presented "in plane" along with the insertion at the radial tuberosity.

Tips for T2-weighted TSE Shoulder Imaging with Spectral Fat Saturation

Wei Jun Zhang[1]; Hans-Peter Hollenbach[2]

[1]*Siemens Mindit Magnetic Resonance Ltd., Shenzhen, China*
[2]*Siemens Healthcare, Erlangen, Germany*

Robust fat saturation can be achieved by different approaches including the application of inversion recovery sequences or advanced fat suppression pulses such as SPAIR. However, in some cases, such as the musculoskeletal imaging of the shoulders, the combination of a T2-weighted turbo spin echo (TSE) sequence with a conventional spectral fat saturation pulse is needed.
When imaging obese or very tall patients, the shoulder has to be positioned off-center in many MR exams and therefore several factors will affect image quality with spectral fat saturation:
B_0-inhomogeneity – if present – will cause a frequency shift, off-setting the frequency that has been implemented for spectral fat saturation relative to the fat peak. Consequently, fat will not be sufficiently suppressed. Secondly, the eddy current effect can be more serious at a very off-center position. And finally, distortions introduced by B0-inhomogeneity and non-linearity of the gradients at the edge of the maximum field-of-view can cause crosstalk effects.
The following hints on patient positioning and sequence set-up will help you to achieve high quality spectral fat saturation:

1. Try to position the shoulder as close to the magnet center as possible. (For further information on patient positioning, including a video and application hints, please visit the MSK Advisory Board on www.siemens.com/magnetom-world).
2. Try to reduce the eddy current effect by applying a lower bandwidth, changing the phase-encoding direction and using a lower sampling density. Keep in mind that the sampling density can also be influenced by the turbo factor for TSE sequences. With a fixed TR and number of slices, reducing the turbo factor will allow you to set a lower sampling rate.
3. Try to reduce the crosstalk effect by increasing the number of concatenation e.g. 2 instead of 1.

Imaging and sequence details

The shown images were acquired using a 1.5 Tesla MAGNETOM Symphony. Only one parameter was changed for best comparison. Sequence parameters for the shown T2-weighted TSE sequence were: TR / TE 3690 / 71 ms, slice thickness 3 mm, matrix 436 x 512 (interpolated), FOV 160 x 160; no averaging, no restore pulse used. In figure 1, the bandwidth was set to 120 Hz/px. Areas with insufficient spectral fat suppression are marked by an arrow in figures 1 and 2A).
In figure 1A the shoulder was placed at the very edge of the maximum field-of-view. Just by moving the region-of-interest a bit more to the isocenter of the magnet, a clear improvement in the quality of the spectral fat suppression can be achieved (Fig. 1B). In an open-bore magnet this is no problem, but even in a tighter bore, the shoulder can be moved away from the edge of the maximum field-of-view by slightly angulating the patient's position. In figure 2A the bandwidth was set to 90 Hz/px. By reducing the sampling rate to 50 Hz/px, eddy current effects are reduced and resulting in improved fat saturation.

Contact
Hans-Peter Hollenbach
Siemens AG
H IM MR PLM AW Orthopedics
Karl-Schall-Str. 6
91052 Erlangen
Germany
hans-peter.hollenbach@siemens.com

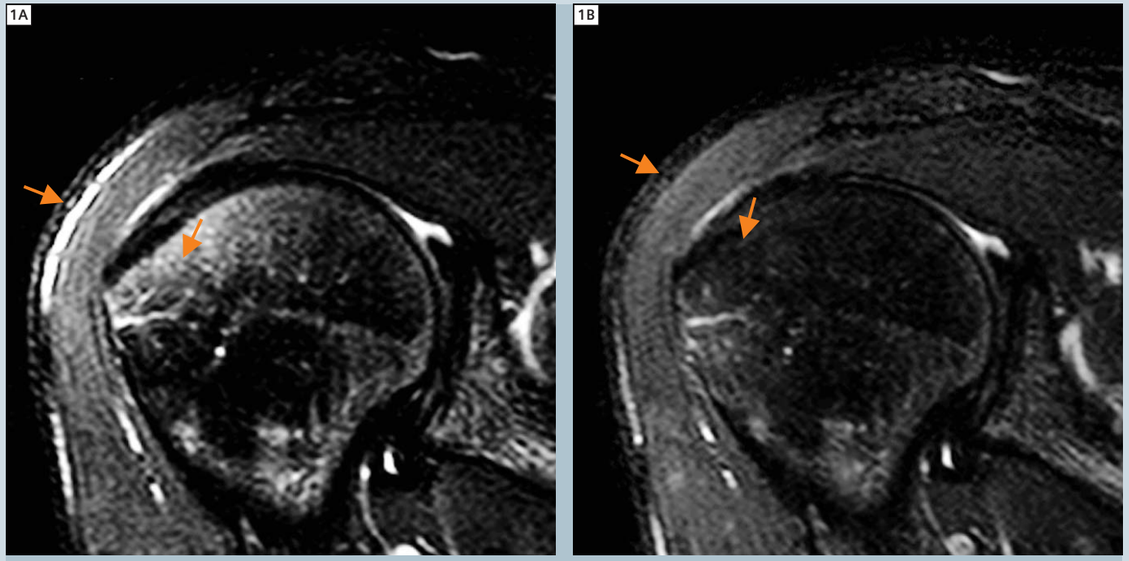

1 Improving the quality of fat saturation by moving the region of interest towards the isocenter.

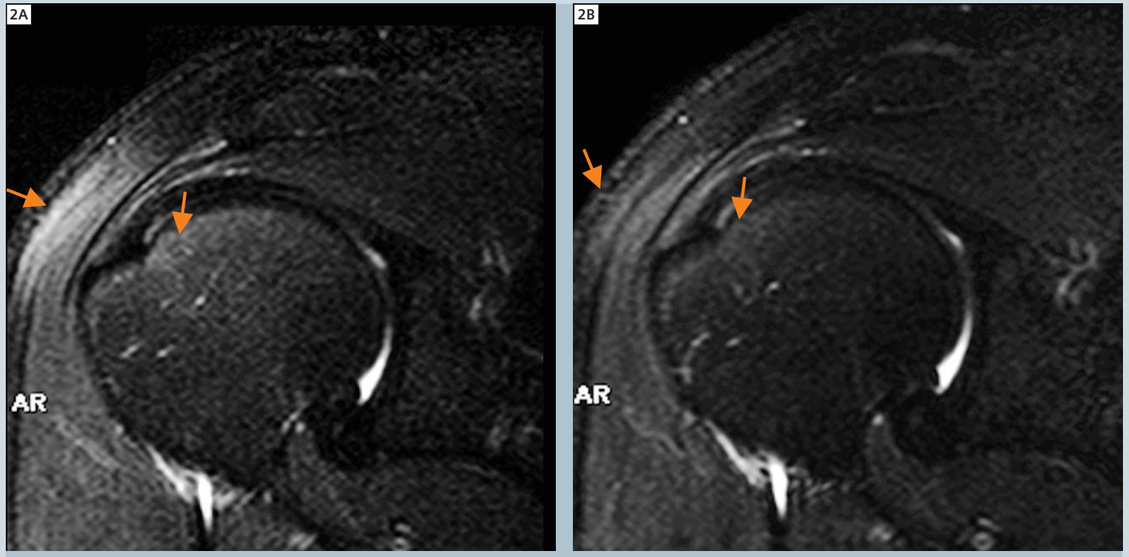

2 Reducing eddy current effects by decreasing the sampling rate.

Cerebral Blood Flow Imaging with 3D GRASE ASL Sequence Increases SNR and Shortens Acquisition Time

David A. Feinberg[1,2,3]; Matthias Günther[1,4,5]

[1]Advanced MRI Technologies, LLC, Sebastopol, CA, USA
[2]University of California, Berkeley and San Francisco, CA, USA
[3]Redwood Regional Medical Group, Santa Rosa, CA, USA
[4]mediri GmbH, Heidelberg, Germany
[5]University Hospital Mannheim, Neurology, Heidelberg, Germany

Abstract

Arterial Spin Labeling (ASL) is a technique capable of measuring cerebral blood flow (CBF) in humans. However, ASL is limited by low sensitivity given blood is ~3% by volume in brain parenchyma. Single-shot 3D GRASE ASL technique has made possible whole brain coverage with over twice the signal-to-noise ratio (SNR) of 2D EPI ASL. To achieve even higher spatial resolution in fast acquisitions, a segmented version of the 3D GRASE ASL sequence is combined with a 32-channel coil at 3 Tesla to achieve 128 and 256 matrix images in 1 to 2 minutes.

Introduction

In the early 1980s when the very first MRI blood flow images were shown at conferences, Nobel Prize laureate Prof. Paul Lauterbur commented, "As MR imaging techniques develop, blood flow imaging will advance with them." This is fortelling of the recent developments describing the uniquely powerful Arterial Spin Labeling (ASL) method of blood flow imaging [1–6], since it is very flexible and can be adapted to several different MR imaging sequences. Each imaging technique is differs in speed, image quality and ability to quantify blood flow. To be discussed below are the advantages of 3D sequences [1, 2, 26, 27] compared to 2D MRI in overcoming physiologic limitations in obtaining whole brain coverage. The 3D gradient and spin echo (GRASE) [1, 2, 18] readout scheme has advantages of refocusing many more signals than RARE / TSE / FSE or EPI sequences for higher SNR which translates into greatly reduced imaging time and much higher spatial resolution (Fig. 1). It has additional advantages of reduced susceptibility artifacts compared to Spiral and EPI techniques for improved image quality. Several examples of 3D GRASE ASL are presented here along with a fuller discussion of these differences.

1

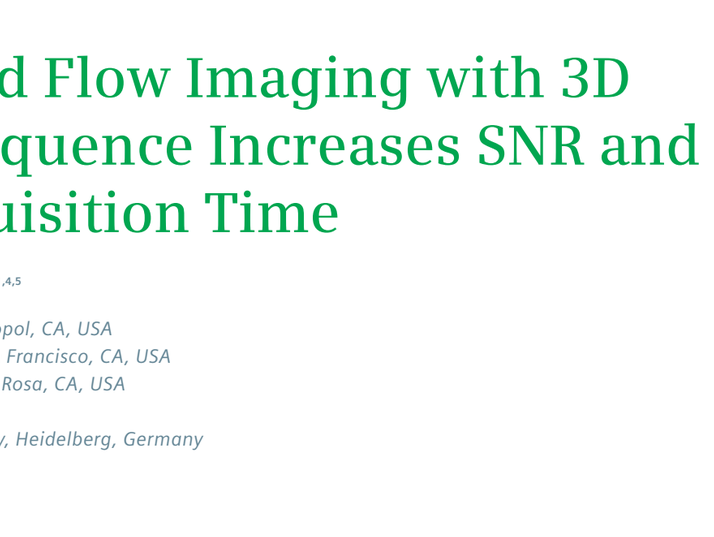

1 3D GRASE ASL with 32-channel coil **row 1)** 64 matrix, resolution 4 x 4 x 4 mm³ voxel, 26 images, 16 s, **row 2)** 128 matrix, resolution 2.5 x 2.5 x 2.0 mm³ in 1 min **row 3)** 256 matrix, resolution 1.5 x 1.5 x 3.0 mm³, 26 images, 2:04 min.

What is ASL imaging?

To measure blood perfusion in brain tissue, it is necessary to quantify signal changes independent of the signal from the partial volumed static brain tissue. ASL obtains two images, each with identical signals from brain tissue but different blood signal as affected by the presence / absence of blood labeling RF pulses (typically inversion RF pulses). Ideally, subtraction of the two images removes static brain tissue signal leaving only blood signal which intensity reflects hemodynamic parameters of cerebral blood flow (CBF) and the blood bolus arrival time (BAT) to the tissue. Critical to the success of ASL, the blood spin labeling is achieved by manipulating the longitudinal magnetization, which stores the "labeled" (tagged) spin magnetization with T1 decay (~1200–1500 ms) rather than with shorter T2 decay (~150 ms). The longer T1 decay enables enough time for the spins in blood to reach the brain tissue upstream from the arterial location of labeling. The tagging of the inflowing blood spins can either occur in a small localized region but over a long period of time of several seconds (continuous ASL [2, 3, 7, 9, 14, 24]) or at a larger region at a defined point in time (pulsed ASL [28–31]. After labeling preparation the tagged blood spins are given an inflow time TI to allow them to move into the microvasculature of the imaging region. A typical inflow time is 1500 ms. The beginning of the image readout sequence typically occurs with a 90° excitation pulse followed by either a gradient echo train sequence such as EPI or spiral, where the signal decays with T2* or by a spin echo based sequence like RARE or GRASE, where the signal decays with a combination of T2 and a component of stimulated echoes with longer T1 decay. As mentioned above, the measured signal will be dominated by brain tissue signal with blood signal being in the range of a few percent. Therefore, additional application of background suppression pulse schemes are incorporated to reduce the amplitude of static signal so errors in net subtracted signal is reduced for more reliable measurement of blood signal [32]. For quantification of cerebral blood flow several models exist [6, 12, 13] with the one-compartment model [12] being used most often. One of the most critical aspects of quantification is the variation of arrival times of the labeled blood bolus at different regions of the brain. Several techniques have been developed to reduce the sensitivity to this bolus arrival time (BAT) [4, 6]. Time-consuming sampling the inflow of the labeled blood into the tissue allows the measurement of BAT as an additional hemodynamical parameter. For whole brain application, this technique requires an efficient ASL technique, which provides sufficient SNR to reduce overall scan time and supports large region coverage.

2A

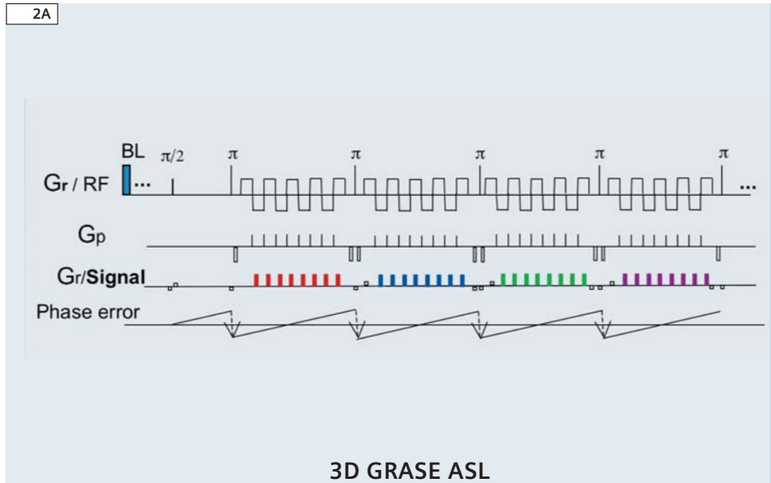

2B

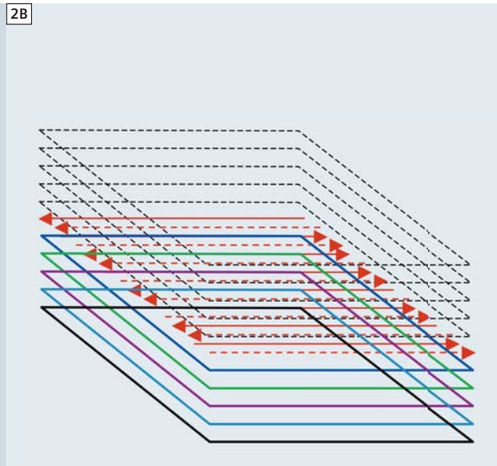

2 3D GRASE ASL. The 180° RF refocusing pulses (π) prevent large phase error. EPI type gradient refocusing (Gr) gives maximum number of signals, (BL) blood labeling and background suppression pulses.

2D and 3D ASL slice coverage limitations of hemodynamic timing

One of the major drawbacks of 2D EPI based ASL is a limitation on the number of images, preventing whole brain coverage. The EPI images are readout sequentially. With the acquisition of each EPI image ~50 msec, the blood inflow time of each slice increases with this time increment until the net range of inflow time is too large to ensure that the labeled blood is in the same vascular compartment in all slices. The 3D MRI sequences entirely overcome this problem because all images are readout

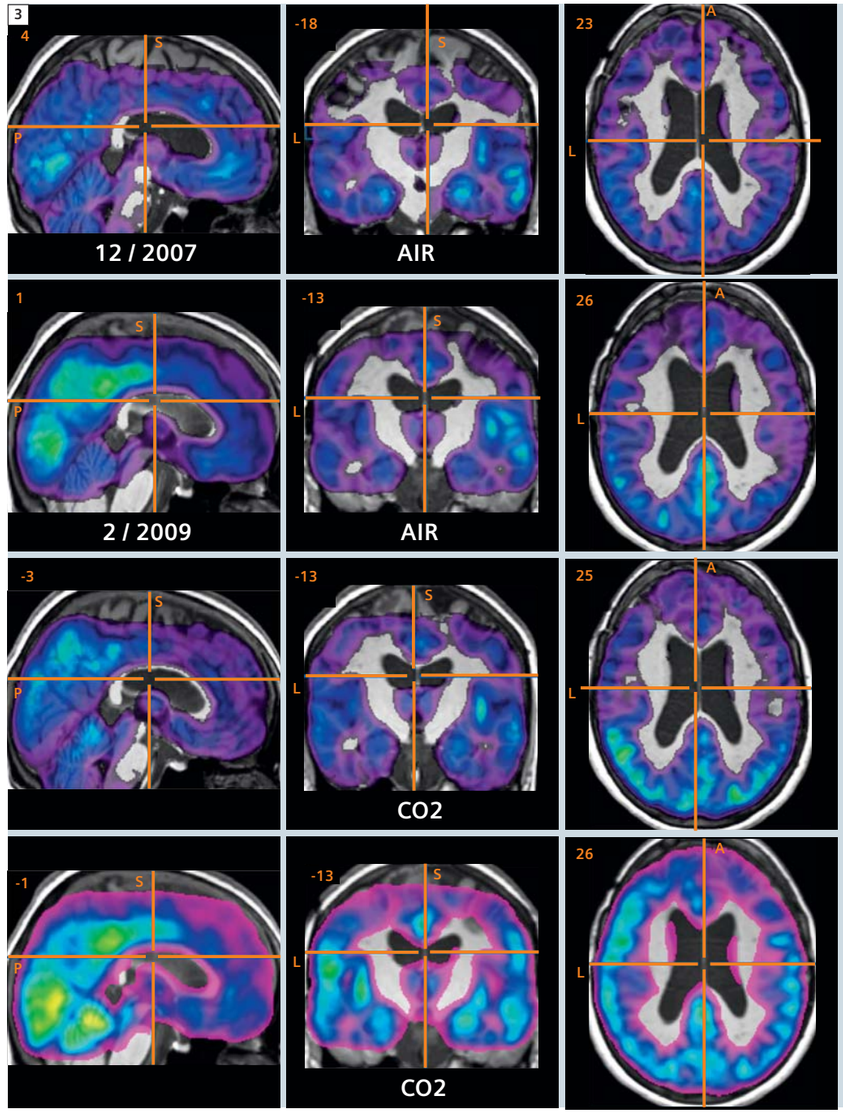

3 CBF maps of MoyaMoya patient.
Rows 1 and 2: control image while breathing air.
Rows 3 and 4: hypercapnia, CO_2 challenge.
Rows 1 and 3: 12/2007 pre-surgery.
Rows 2 and 4: 2/2009 post-surgery show greater vascular reactivity post-surgery. The CBF maps from 3D GRASE ASL overlaid on anatomic images. *(Courtesy of Rik Achten, GIfMI, UGent, Belgium.)*

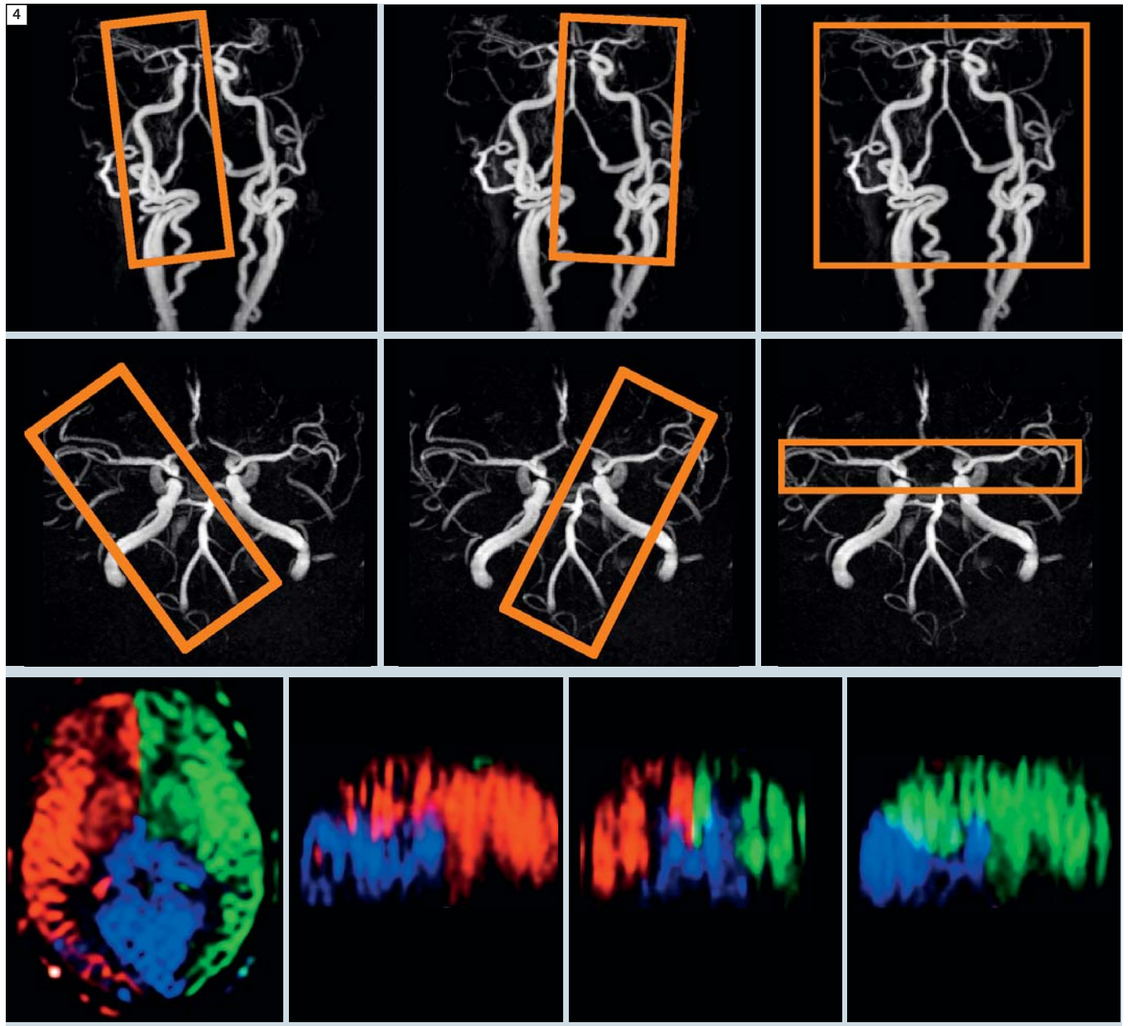

4 Color-coded visualization of vascular territories in transverse, sagittal and coronal orientation. Three excitation regions shown in MRA (yellow box) A–P (top) and C–C (middle).

simultaneously rather than in temporal sequential order. The spins move into the brain tissue and at a specified time, all slices are encoded simultaneously beginning with a single 90 degree pulse covering a thick slab 3D volume [1, 27], not a single slice [11]. The echo train reads out all slices together which are then separated by a 3D Fourier Transform, which has additional sqrt(N) advantage of higher SNR compared to 2D EPI. Similarly, in a 3D readout the inversion pulse timing for background suppression is optimal for all slices, while in sequential 2D imaging there is variation between slices in the effectiveness of background suppression [32].

Artifacts in 3D GRASE compared to RARE, Spiral, EPI

Basically any echo train sequence can be used for 3D ASL readout but each differs in their number of echoes, accumulative phase errors causing susceptibility artifacts, and SNR efficiency [25, 17]. Echo volume imaging (EVI) is the 3D variant of EPI which has an echo train time limited to under ~80 ms due to rapid T2* decay and it has large phase errors leading to susceptibility artifacts with regions of signal loss (similar to spiral and rectilinear EPI). 3D GRASE sequences has many RF refocusing pulses which maintains a low level of phase error and permits a sustainable echo train for up to 300 ms. RARE / TSE has similar net sequence time, however, there is a large fraction of time spent on RF refocusing pulses, 1 per signal. GRASE uses switched gradient rephrasing of signals to produce several times as many signals as TSE, which translates into faster imaging time and higher SNR per imaging time. A similar and useful variant, Spiral RARE (or Spiral GRASE) also has efficiency advantages, however, it places the beginning of the spiral, the center of k-space, on a gradient echo position at the beginning of each time interval between RF pulses, increasing susceptibility weighting. Furthermore, non-Cartesian image reconstruction methods are required. The key to success of 3D GRASE has been its high SNR, low arti-

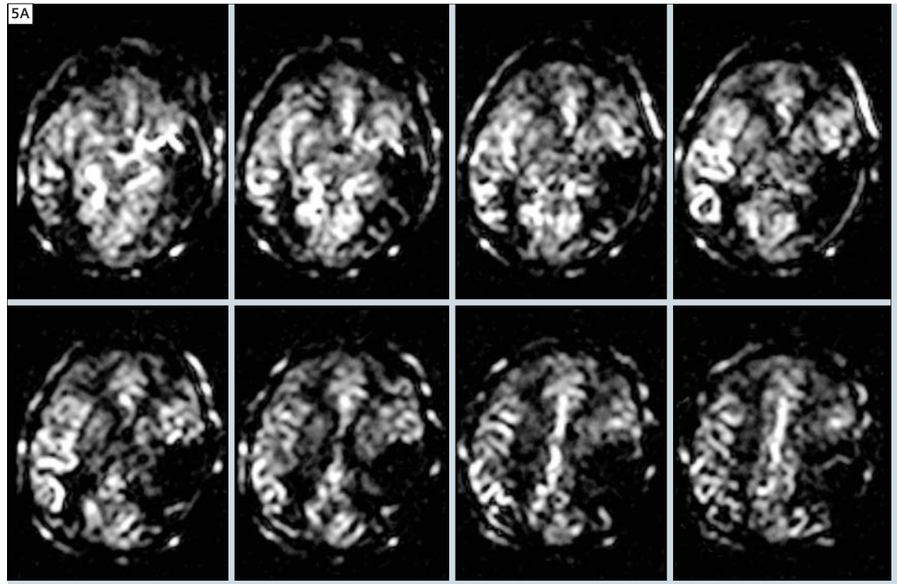

5 Single-shot 3D ASL of two patients with acute stroke. **A:** in left MCA territory, **5B** In second patient (48 hour) with hypoperfusion and delayed bolus arrival time (BAT) (red arrows) in ischaemic hemisphere, MRA reveals a near 100% occlusion in the left ICA (yellow arrow). *(Reproduced with permission of: BJ MacIntosh, P Jezzard et al., ISMRM 2009).*

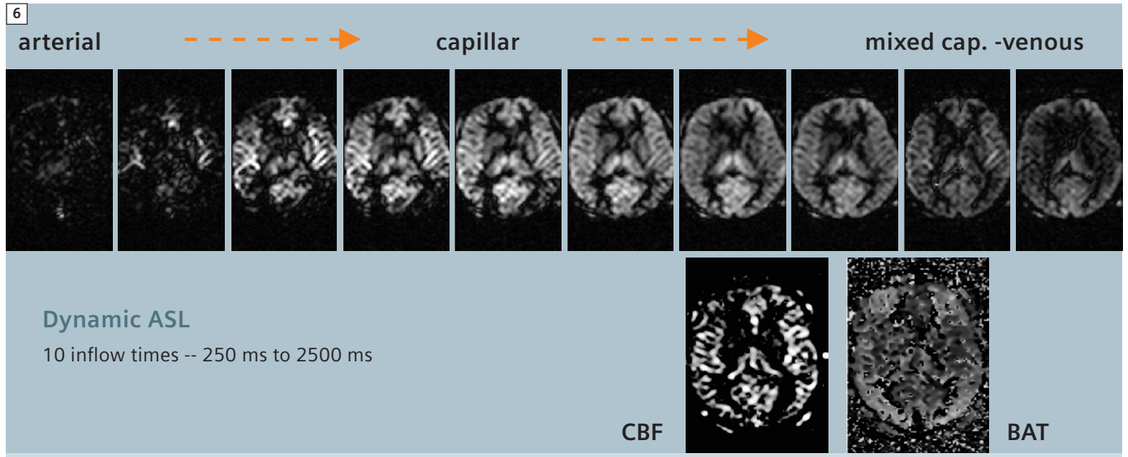

6 Dynamic ASL data acquisition with calculated CBF and BAT maps, 1 of 26 slices shown in a 3D whole brain coverage, inflow time (TI).

fact load due to the CPMG (Carr-Purrcell-Meiboom-Gill echos) timing, and whole brain coverage made possible with the simplified physiological timing in 3D acquisitions.

The source of high SNR and fast data acquisition of 3D GRASE

The number of echoes produced in a single echo train of EPI, TSE and GRASE is dependent on the rate of echo refocusing which is relatively slow in RF refocusing (~4 ms) versus fast with switched gradient refocusing (~0.2 ms). It is no less dependent upon the signal decay times of T2 and T1 stimulated echo compared to shorter T2* of EPI. In relative terms the number of refocused echoes is in EPI (2 signal / ms x 30 ms) 60 echoes, TSE (1 signal / 3 ms x 300 ms) 100 echoes, and 3D GRASE (1.5 signal / ms x 300 ms) 450 echoes. Therefore, EPI has the fastest rate of echo generation by means of gradient switching but the shortest 'echo train time', ETT, due to T2* decay. TSE has the slowest rate using RF refocusing but a long ETT, whereas 3D GRASE has the benefit of both a fast refocusing rate and a long ETT which are multiplicative for much higher net signal (Fig. 2). In addition to increasing spatial resolution and image speed, the image SNR is dependent on square root of N signals in the Fourier transform. Therefore, the relative SNR of EPI, TSE and 3D GRASE is sqrt(60), sqrt(100) and sqrt(450), 7.7, 10.0 and 21.2 respectively. The possible earlier TE of EPI to a lesser extent mitigates some of this large SNR disadvantage to 3D GRASE, which nets to nearly a factor of 2.5 higher SNR and, thus, 3D GRASE has a factor of 6–8 in scan time reduction (fewer signal averages) at constant SNR.

32-channel RF head coil effects speed and resolution

Utilizing a 32-channel coil yields another ~2 higher SNR in cortical brain regions for all imaging techniques, and these SNR gains are multiplied in 3D GRASE. This allows either extremely fast ASL acquisitions or higher resolution than previously achieved in ASL images at 3 Tesla [25] (Fig. 1).
The 32-channel coil has therefore been used to acquire larger matrix images with higher resolutions, with up to 256 matrix in reasonable scan times of 2 minutes. Instead of going to higher resolution, the reduced acquisition time can be used to sample variable inflow times to separately quantify CBF from bolus arrival time BAT using parametric curve fitting (Fig. 6). It should be noted that 3D GRASE can be combined with several different ASL encoding schemes [22, 24].

Resolving vascular territories in the brain

The images can be performed with separation of vascular territories by labeling different downstream vessels separately, (Fig. 4). Hadamard encoding has permitted to incorporate vascular territory sensitivity into an ASL protocol without loss of SNR compared to non-selective (standard) ASL to keep scan times in an acceptable range for clinical applications [21]. Stroke patients may be studied with 3D vascular territory ASL to evaluate changes occurring during recovery or to assess therapies (23). Patients with arterio-venous malformations (AVM) or aneurysms can have altered flow circuitry in the circle of Willis and downstream cerebral arteries identifiable as changes in vascular territory perfusion [20].

High spatial resolution ASL

The segmented sequence version of 3D GRASE ASL provides shorter RF pulse intervals in the CPMG spin echo sequence [27]. This reduces susceptibility artifact and concurrently shortens the time of

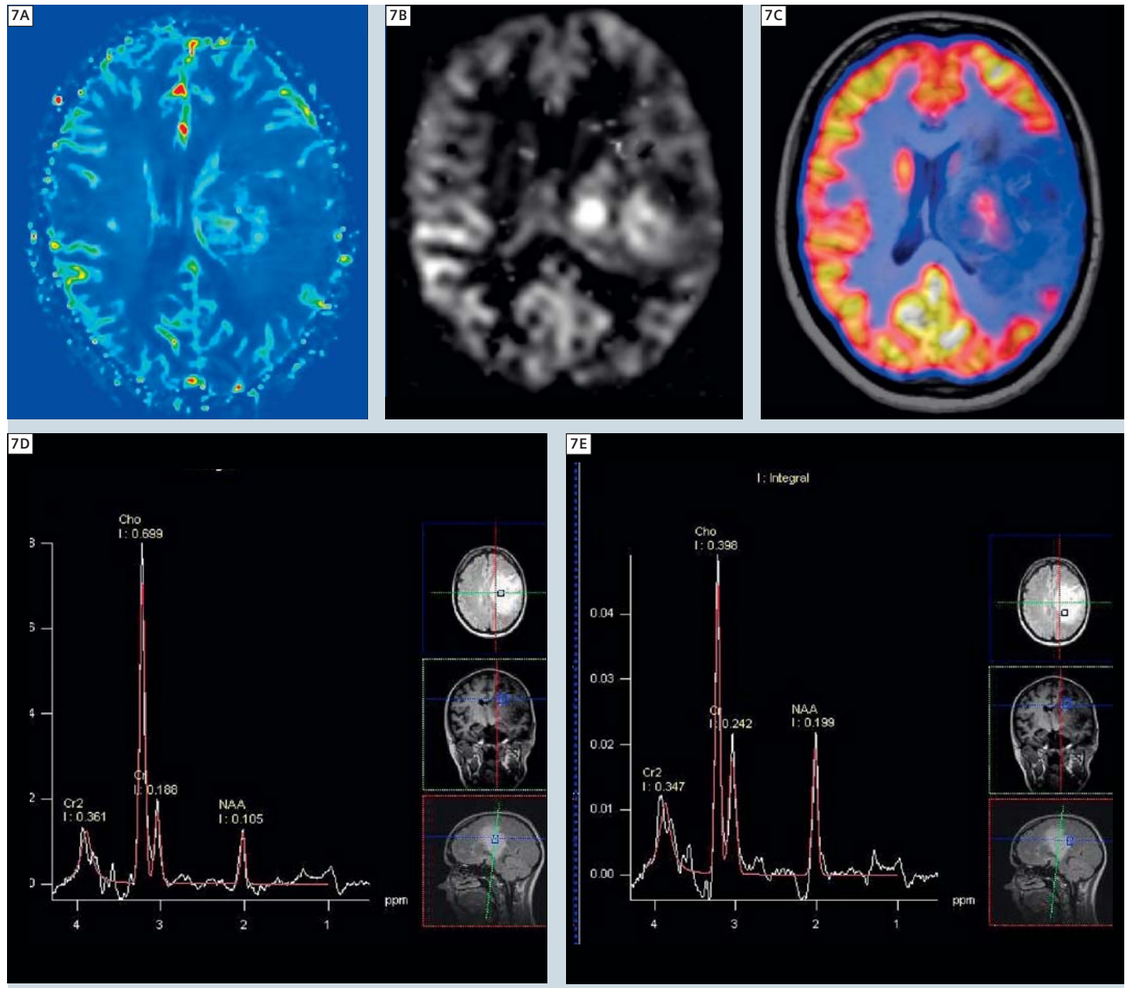

7 ASL perfusion of Glioma. **A:** Dynamic susceptibility contrast, increased perfusion in center of a recurrent Glioma, originally grade II, **B:** ASL CBF map from dynamic ASL, showing increased perfusion **C:** PET image fused to MRI. A biopsy was performed in the location of highest perfusion in ASL CBF and a grade III was diagnosed. **D, E:** At time of biopsy, MRS showed the Cho/Cr was highest in biopsy location. *(Courtesy of Rik Achten, GIfMI, UGent, Belgium.)*

each of several echo trains for reduced through-plane blurring compared to the single-shot sequences. Image distortions were also reduced using the 128 matrix instead of 64 matrix as the larger FOV allowed swapping the phase and read axes, placing the highly switched read axis onto the head's lateral axis with less physiologic stimulation to allow higher bandwidth and closer echo spacing for less distortions. One unexpected fortuitous finding is that the segmented 3D GRASE sequence does not have artifacts from CSF or brain motion and the labeling pulses normalizes blood inflow and the larger 3D volume further removes slice inflow artifacts.

The SNR gains from the 32-channel coil/receiver system enabled higher resolution ASL images. The ASL encoding used pulsed ASL (PASL) sequence with QUIPSS II (QUantitiativ Imaging of Perfusion using a Single Subtraction) variants and background suppression pulses, previously described [1].

One can incorporate the 3D ASL sequence into a clinical protocol, requiring only 8–16 second scan time for whole brain coverage at 4 mm isotropic resolution or 2–4 minutes to obtain highly quantitative BAT and CBF maps (Fig. 6), useful for evaluation of therapeutic responses to drugs and surgical interventions (Fig. 3), following brain recovery after stroke (Fig. 5), or evaluation of tumors (Fig. 7).

In conclusion, with ASL scan times now reduced from ~15 minutes 6 years ago, to ~16 seconds for a whole brain slice coverage, perfusion images should become just another image contrast mechanism, utilized in all routine clinical screening brain studies. With such fast scans and no need for contrast agents, ASL based perfusion imaging is an important new contrast mechanism that may be used by the radiologist in all routine clinical brain screening studies. Already with these refinements, ASL is faster than CT perfusion contrast imaging, and avoids x-ray dosage and risks of iodinated contrast agent to the patient. The rapid automated image processing of ASL perfusion maps enables their practical use in emergency medical studies. The ability of MRI to rapidly show several different contrast mechanisms in images (T1-weighted, FLAIR, diffusion-weighted imaging (*syngo* DWI)) and now CBF from 3D ASL without contrast injections, further establishes MRI as an invaluable diagnostic examination of brain disease.

Acknowledgment: N.I.H. National Inst. Neurological Disease and Stroke: grant no. 5R44NS059223

References

1 Gunther, M., K. Oshio, and D.A. Feinberg, Single-shot 3D imaging techniques improve arterial spin labeling perfusion measurements. Magn Reson Med, 2005. 54(2): p. 491–8.
2 M. A. Fernandez-Seara, Z.W., J. Wang, M. Korczykowski, M. Guenther, D. Feinberg, J. A. Detre. 3T Pseudo-continuous ASL Perfusion fMRI with Background-Suppressed Single Shot 3D GRASE During Memory Encoding. in International Society for Magnetic Resonance in Medicine. 2006. Seattle.
3 Detre, J.A., et al., Perfusion imaging. Magn. Reson. Med., 1992. 23: p. 37–45.
4 Alsop, D.C. and J.A. Detre, Reduced transit-time sensitivity in noninvasive magnetic resonance imaging of human cerebral blood flow. J. Cereb. Blood Flow Metab., 1996. 16: p. 1236–1249.
5 Gonzalez-At, J.B., D.C. Alsop, and J.A. Detre, Perfusion and transit time changes during task activation determined with steady-state arterial spin labeling. Magn. Reson. Med., 2000. 43: p. 739–46.
6 Wong, E.C., R.B. Buxton, and L.R. Frank, Quantitative imaging of perfusion using a single subtraction (QUIPSS and QUIPSS II). Magn Reson Med, 1998. 39: p. 702–8.
7 Yang, Y., et al., Transit time, trailing time, and cerebral blood flow during brain activation: measurement using multislice, pulsed spin-labeling perfusion imaging. Magn Reson Med, 2000. 44(5): p. 680–5.
8 Ye, F.Q., et al., Correction for vascular artifacts in cerebral blood flow values measured using arterial spin tagging techniques. Magn. Reson. Med, 1997. 37: p. 226–35.
9 Alsop, D.C. and J.A. Detre, Multisection cerebral blood flow MR imaging with continuous arterial spin labeling. Radiology, 1998. 208: p. 410–16.
10 McLaughlin, A.C., et al., Effect of magnetization transfer on the measurement of cerebral blood flow using steady-state arterial spin tagging approaches: a theoretical investigation. Magn Reson Med, 1997. 37(4): p. 501–10.
11 Wang, J., et al., Comparison of quantitative perfusion imaging using arterial spin labeling at 1.5 and 4.0 Tesla. Magn Reson Med, 2002. 48(2): p. 242–54.
12 Wong, E.C., R.B. Buxton, and L.R. Frank, A theoretical and experimental comparison of continuous and pulsed arterial spin labeling techniques for quantitative perfusion imaging. Magn. Rason. Med., 1998. 40: p. 348–55.
13 Buxton, R.B., et al., A general kinetic model for quantitative perfusion imaging with arterial spin labeling. Magn Reson Med, 1998. 40(3): p. 383–96.
14 Williams, D.S., et al., Magnetic resonance imaging of perfusion in the isolated rat heart using spin inversion of arterial water. Magn Reson Med, 1993. 30(3): p. 361–5.
15 Wang, J., et al., Empirical analyses of null-hypothesis perfusion FMRI data at 1.5 and 4 T. Neuroimage, 2003. 19(4): p. 1449–62.
16 Feinberg, D.A. and K. Oshio, GRASE (gradient- and spin-echo) MR imaging: a new fast clinical imaging technique. Radiology, 1991. 181(2): p. 597–602.
17 Feinberg, D.A., B. Kiefer, and G. Johnson, GRASE improves spatial resolution in single shot imaging. Magn Reson Med, 1995. 33(4): p. 529–33.
18 Feinberg DA, Kiefer B, Litt AW. High resolution GRASE MRI of the brain and spine: 512 and 1024 matrix imaging. J Comput Assist Tomogr. 1995 Jan-Feb;19(1):1–7.
19 Luh, W.M., et al., QUIPSS II with thin-slice TI1 periodic saturation: a method for improving accuracy of quantitative perfusion imaging using pulsed arterial spin labeling. Magn Reson Med, 1999. 41(6): p. 1246–54.
20 Sallustio F, Kern R, Günther M, Szabo K, Griebe M, Meairs S, Hennerici M, Gass A. Assessment of intracranial collateral flow by using dynamic arterial spin labeling MRA and transcranial color-coded duplex ultrasound.Stroke. 2008 Jun;39(6):1894–7. Epub 2008 Apr 10.
21 Günther M. Efficient visualization of vascular territories in the human brain by cycled arterial spin labeling MRI. Magn Reson Med. 2006 Sep;56(3):671–5.
22 Fernández-Seara MA, Edlow BL, Hoang A, Wang J, Feinberg DA, Detre JA. Minimizing acquisition time of arterial spin labeling at 3T. Magn Reson Med. 2008 Jun;59(6):1467–71.
23 MacIntosh BJ, Pattinson KT, Gallichan D, Ahmad I, Miller KL, Feinberg DA, Wise RG, Jezzard P. Measuring the effects of remifentanil on cerebral blood flow and arterial arrival time using 3D GRASE MRI with pulsed arterial spin labelling.J Cereb Blood Flow Metab. 2008 Aug;28(8):1514–22. Epub 2008 May 28.
24 Fernández-Seara MA, Wang Z, Wang J, Rao HY, Guenther M, Feinberg DA, Detre JA. Continuous arterial spin labeling perfusion measurements using single shot 3D GRASE at 3 T.Magn Reson Med. 2005 Nov;54(5):1241–7.
25 McKinstry RC, Feinberg DA. Ultrafast magnetic resonance imaging. A new window on brain research. Science. 1998 Mar 20;279(5358):1965-6. No abstract available.
26 Feinberg DA, Ramanna S, Gunther M, Evaluation of new ASL 3D GRASE sequences using Parallel Imaging, Segmented and Interleaved k-space at 3T with 12- and 32-Channel coils. ISMRM, Honolulu, 2009
27 Talagala SL, Ye FQ, Ledden PJ, Chesnick S. Whole-Brain 3D Perfusion MRI at 3.0 T using CASL with a separate labeling Coil, Mag Res Med, 52: 131–140 (2004)
28 Edelman, R. R., B. Siewert, et al. (1994). "Signal targeting with alternating radiofrequency (STAR) sequences: application to MR angiography." Magn Reson Med 31(2): 233–8
29 Kwong, K. K., D. A. Chesler, et al. (1995). "MR perfusion studies with T1-weighted echo planar imaging." Magn Reson Med 34(6): 878–87.
30 Luh, W. M., E. C. Wong, et al. (1999). "QUIPSS II with thin-slice TI1 periodic saturation: a method for improving accuracy of quantitative perfusion imaging using pulsed arterial spin labeling." Magn Reson Med 41(6): 1246–54.
31 Wong, E. C., R. B. Buxton, et al. (1998). "Quantitative imaging of perfusion using a single subtraction (QUIPSS and QUIPSS II)." Magn Reson Med 39(5): 702–8.
32 Ye, F. Q., J. A. Frank, et al. (2000). "Noise reduction in 3D perfusion imaging by attenuating the static signal in arterial spin tagging (ASSIST)." Magn Reson Med 44(1): 92–100.

Contact
David Feinberg, M.D., Ph.D.
Advanced MRI Technologies
652 Petaluma Ave.,
J Sebastopol, CA, 95472
USA
david.feinberg@advancedmri.com

Case Report:
Non-Contrast-Enhanced Evaluation of Perfusion Deficiencies of the Brain

David J. Panasci, M.D.; Steven L. Mendelsohn, M.D.

Zwanger-Pesiri Radiology, Smithtown, NY, USA

Background

Non-invasive and fast evaluation of the arteries and perfusion of the brain are common indications for MRI. Contrast-enhanced T2* perfusion MRI is used for this purpose and is playing an important role in stroke imaging in dedicated centres of care. However, contrast-enhanced perfusion measurements have practical limitations: First, renal function is often limited in elderly patients and may require dedicated preparation e.g. hydration. Second, T2* perfusion measurements require large gauge IVs for high-flow venous injection to achieve perfect bolus shape. Finally, the pressure to reduce costs and optimize the clinical cost-benefit ratio increases the demand for non-contrast enhanced MR methods which allow the evaluation of the vessel and perfusion status of the brain. With the clinical availability of arterial spin labelling techniques (*syngo* ASL), we established a fast, robust and contrast-media free imaging protocol at our imaging centres to meet the demands of a fast, clinical precise, error-robust and cost effective MR examination.

Patient history

The patient had a history of left internal carotid artery occlusion with stenoses of the cavernous segment of the right internal carotid artery and A1 segment of the right anterior cerebral artery. These were treated with angioplasty and stenting and angioplasty alone respectively.

Sequence details

The images have been acquired at 3 Tesla (MAGNETOM Verio) with the standard 12-channel head coil. The imaging protocol comprises 3D T1w FLASH, T2w fat-saturated FLAIR TSE, 3D TOF MRA and *syngo* ASL. For the evaluation of brain tissue perfusion, four different arterial labelling timepoints have been selected: 1.1, 1.5, 1.9 and 2.3 seconds.

Imaging findings

There is white matter microvascular disease involving both cerebral hemispheres with old infarcts in the medial aspect of the left parietal lobe in the watershed area between the middle cerebral and posterior cerebral territories on that side. A second area of infarction is seen in the deep white matter of the left frontal lobe (Fig. 1). The intracranial MRA demonstrates complete occlusion of the left internal carotid artery. Evaluation of the right cavernous carotid artery is limited because of artefact from the patient's stent. The A1 segment of the right anterior cerebral artery is normal in appearance (Fig. 2). No focal stenotic segment can be seen on this examination. The arterial spin labeling perfusion study demonstrates significant reduction in blood flow to the area of infarction in the left parietal lobe and to a lesser extent the left frontal lobe. There is progressively more perfusion seen on the studies performed

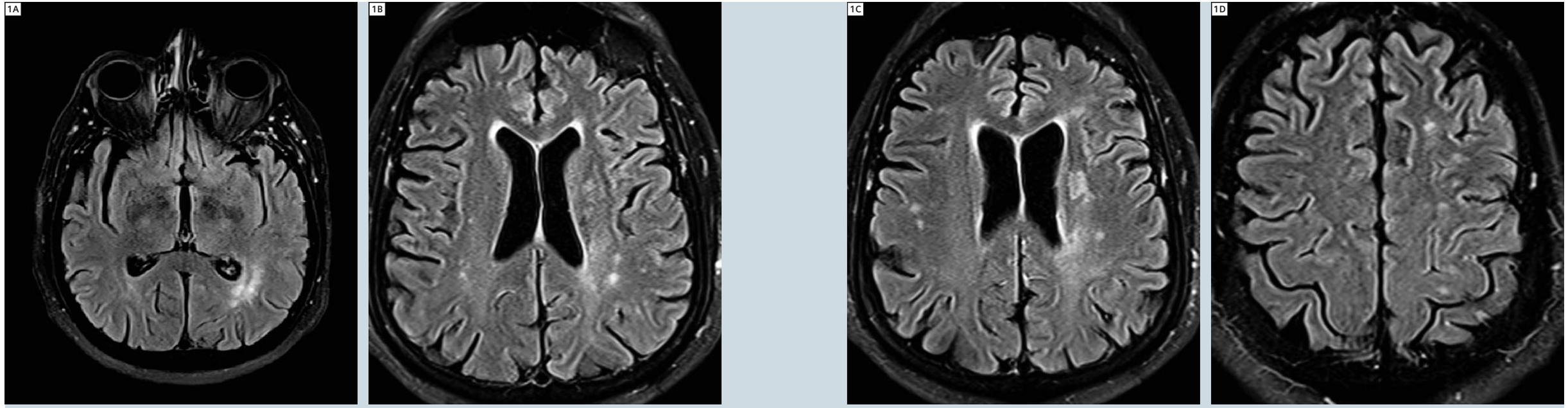

1 Transversal FLAIR images demonstrating multiple microvascular transformations of both cerebral hemispheres and old infarcts.

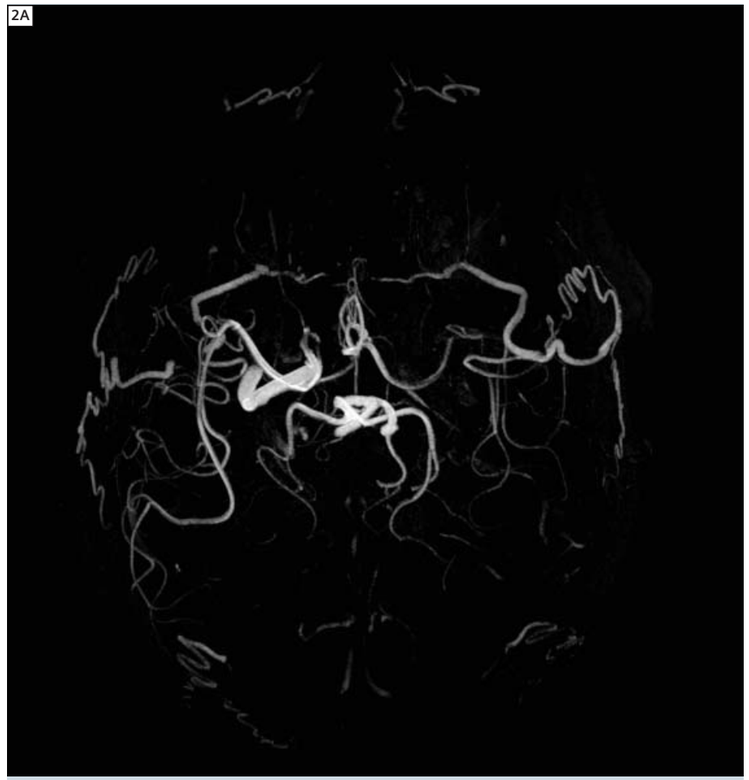

2 Transversal **(A)** and coronal **(B)** maximum intensity projection (MIP) of Time-of-Flight MR Angiography.

at 1.5 and 2 seconds after arterial labelling compared to the perfusion obtained 1 second after arterial labelling (Fig. 3). This would suggest there is delayed transit time into the left hemisphere secondary to the patient's carotid occlusion on that side.

Conclusion

The selected case of a post procedure study following angioplasty and stenting of a high grade right internal carotid artery cavernous segment stenosis and angioplasty of a right A1 segment anterior cerebral artery stenosis demonstrates the potential of this imaging protocol. The TOF MRA demonstrates a normal A1 segment of the right anterior cerebral artery and a patent cavernous segment. With *syngo* ASL, decreased perfusion in the patient's area of infarction in the left hemisphere in the left paretal and frontal lobes could be clearly visualized. In this case there also appears to be a delay in perfusion of the left hemisphere compared to the contralateral right side, another finding expected in this patient with occlusion of the left internal carotid artery.

Contact
David Panasci, M.D.
Zwanger-Pesiri Radiology
80 Maple Avenue
Smithtown, NY 11787
USA
Phone: +1 631-265-5777

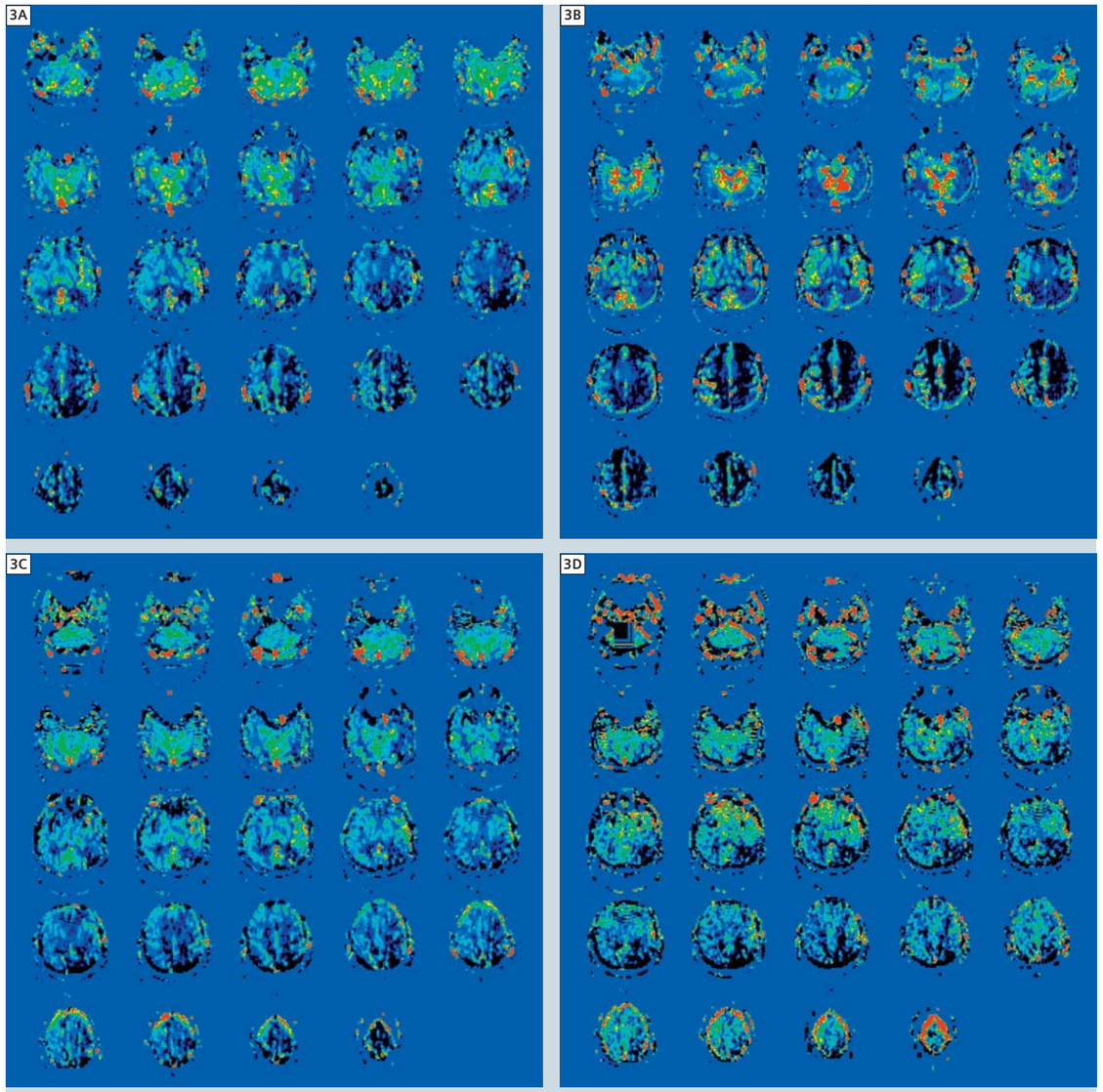

3 *syngo* ASL exam with different delays of blood labelling: 1.1 **(3A)**, 1.5 **(3B)**, 1.9 **(3C)** and 2.3 **(3D)** seconds. There is progressively more perfusion seen on the studies performed at 1.5 and 2 seconds after arterial labeling compared to the perfusion obtained 1.1 second after arterial labelling, suggesting that there is a delayed transit time into the left hemisphere secondary to the patient's carotid occlusion on that side.

Multimodal MRI of the Brain for Improved Diagnosis and Therapy Planning in a Case of Glioblastoma Multiforme

Elna-Marie Larsson, M.D., MSc

Uppsala University Hospital, Uppsala, Sweden

Patient history

A 60-year-old man with approximately one month history of depression, impaired working capacity and personality changes was consulting a psychiatrist due to increasing confusion. Computed Tomography (CT) of the brain was performed and showed a right-sided frontal tumor. The patient was referred to the department of Neurosurgery at the University Hospital. MRI of the brain including Perfusion MRI and MR spectroscopic imaging (MRSI) was performed for preoperative evaluation and guidance.

Sequence details

MRI of the brain with diffusion-weighted imaging (DWI), perfusion MRI and MRS was performed at 1.5 Tesla (MAGNETOM Avanto), using the standard Head Matrix coil.

The imaging protocol included:

- transversal T1w SE: TR/TE 593/9 ms, SL 5 mm
- transversal T2w TSE: TR/TE 4000/98 ms, turbo factor 13, SL 5 mm
- transversal DWI: ADC mapping with high b-value = 1000 s/mm^2, TE 89 ms, SL 5 mm.
- coronal T2w FLAIR: TR/TE 8000/90 ms, turbo factor 17, SL 5 mm
- Perfusion MRI: GRE EPI, TR/TE 1410/30 ms, SL 5 mm. Perfusion maps calculated using Nordic ICE software (NordicNeuroLab, Bergen, Norway, www.nordicneurolab.com)
- contrast-enhanced (Gadovist) transversal 3D T1w MPRAGE: TR/TE 1170/4 ms, SL 0,8 mm (MPR SL 5 mm)
- transversal 2D MRSI: PRESS, TR/TE = 1690/135 ms, 4 averages, matrix 16 x 16, nominal voxel size 10 x 10 x 15 mm^3

Imaging findings

In the right frontal lobe there is a 5 x 5 x 6 cm tumor with irregular contrast enhancement and necrotic portions. It is surrounded by extensive vasogenic oedema (with increased diffusion). Signal changes on T2-weighted images are also extending into the genu of the corpus callosum (Fig. 1). Perfusion with dynamic susceptibility contrast imaging (DSC) shows high relative cerebral blood volume (rCBV) corresponding to contrast enhancement, especially in the lateral portion of the tumor (Fig. 2). DWI with ADC map (Fig. 3) shows restricted diffusion in regions with high rCBV. 2D MRSI (Fig. 4A) shows a large lipid/lactate peak, low NAA and Cr, and elevated Cho in the tumor. Anteromedial to the enhancing tumor there is no lactate/lipid peak, moderately decreased NAA and elevated choline/creatine. The latter is also seen on the Cho/Cr image (Fig. 4B). The tumor with surrounding oedema has a considerable mass effect on the right lateral ventricle and there is a midline shift towards the left side. No other lesions are seen in the brain.

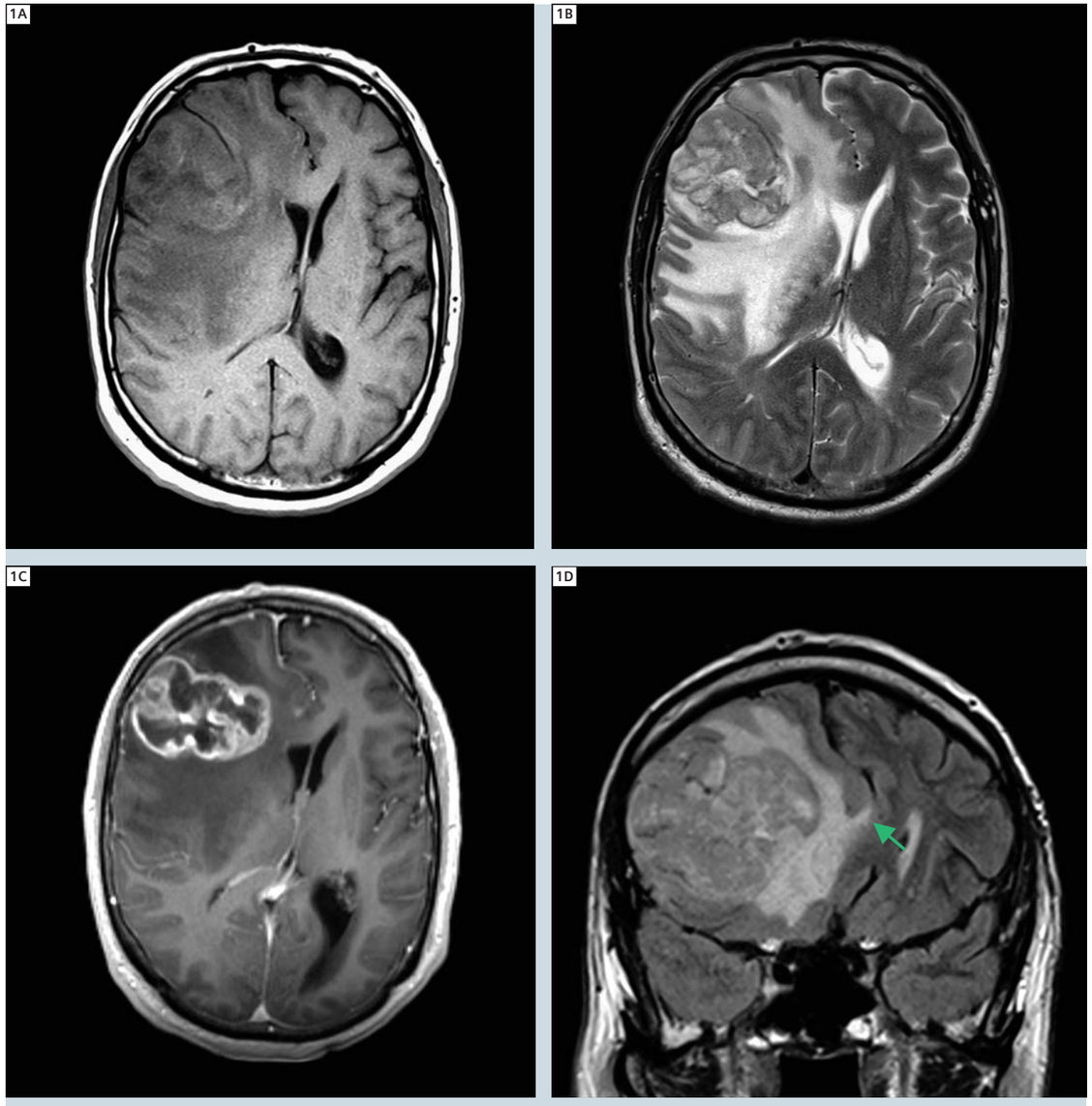

1 Transversal native T1w SE **(A)**, T2w TSE **(B)** and post-contrast T1w MPRAGE images of a tumor with central necroses and mass effect. Coronal T2w FLAIR image **(D)** demonstrating extension of the mass into the genu of the corpus callosum (arrow).

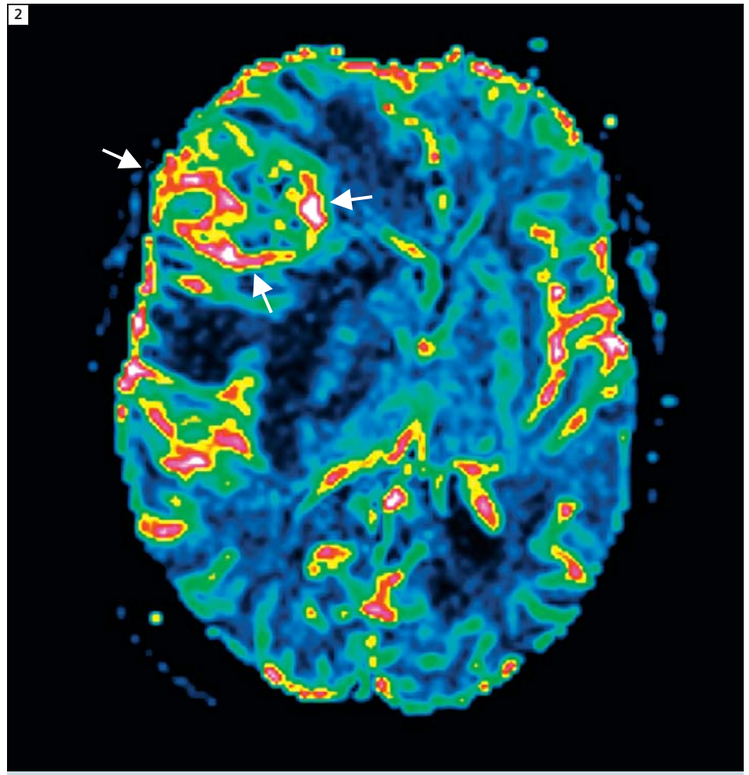

2 Corresponding results of the perfusion measurement is shown and rCBV map of the tumor does visualize high blood volume in areas of contrast-enhancment (arrows).

Discussion

In post-contrast T1w images (Fig. 1C), the contrast-enhancing lesion has the appearance of a malignant tumor with necrotic portions, which could be consistent with glioblastoma multiforme or a solitary metastasis. The signal changes in the genu of the corpus callosum (Figs. 1A, B and D) are most likely due to tumor growth, since oedema is usually not extending into the dense white matter fibres in the corpus callosum. The restricted diffusion (hypointense on ADC map (Fig. 3B) in portions of the tumor is a consequence of high cellularity seen in malignant tissue. The increased perfusion is consistent with malignant tumor and this is supported by the MRSI pattern with increased Cho and low NAA. Elevated superimposed lactate / lipid peaks reveal necrosis. The 2D MRSI imaging shows pathological spectra also outside the enhancing tumor (Fig. 4) speaking in favour of tumor infiltration as seen in malignant glioma but not in metastases. Abscess is not a likely diagnosis although the necrotic portion of an abscess usually has restricted diffusion. In our patient the restricted diffusion is seen in solid enhancing tumor portions and in addition the increased perfusion speaks in favour of malignant tumor (high perfusion is usually not seen in abscesses). The thick irregular contrast enhancement in this patient is not commonly seen in abscesses and the MRSI findings exclude abscess.
Thus the contrast-enhancement appearance, the restricted diffusion in solid tumor portions, the high rCBV and the MRSI pattern including pathological spectra in the tissue adjacent to the tumor strongly supports the diagnosis glioblastoma multiforme. The findings are also helpful for the neurosurgeon in selection of biopsy site in a malignant portion without too extensive necrosis. The MRSI is very helpful for the differentiation between glioma and solitary metastasis.
The patient underwent neurosurgery and the histopathological examination confirmed the suspected diagnosis glioblastoma multiforme.

Conclusion

Multimodality MRI with morphological images, DWI, perfusion and MRSI is thus helpful in the differential diagnosis of brain tumours and for the neurosurgical planning of biopsy locations.

Contact
Elna-Marie Larsson, M.D., D.MSc, Professor
Section of Neuroradiology
Department of Radiology
University Hospital
SE-75185 Uppsala
Sweden
elna-marie.larsson@radiol.uu.se

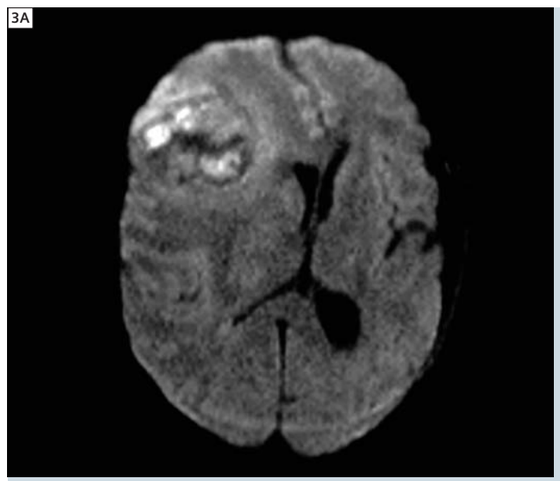

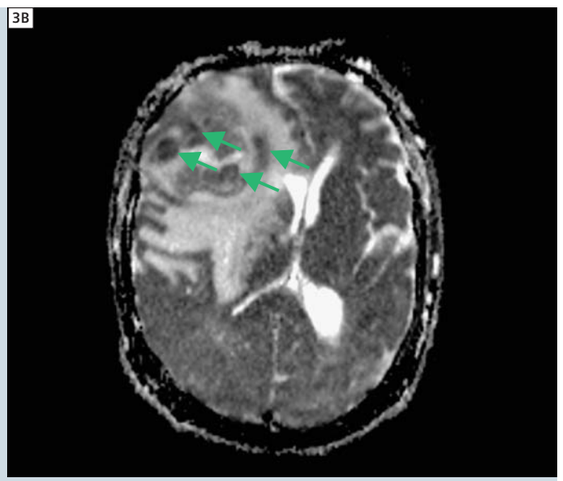

3 High b-value image at b = 1000 s/mm² and ADC map are shown. DWI shows clear restriction of water diffusion in non-necrotic areas of the mass (arrows).

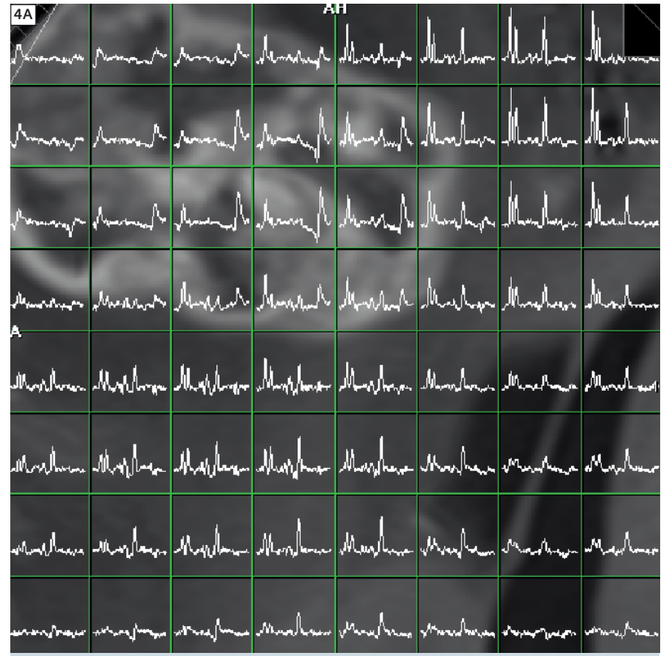

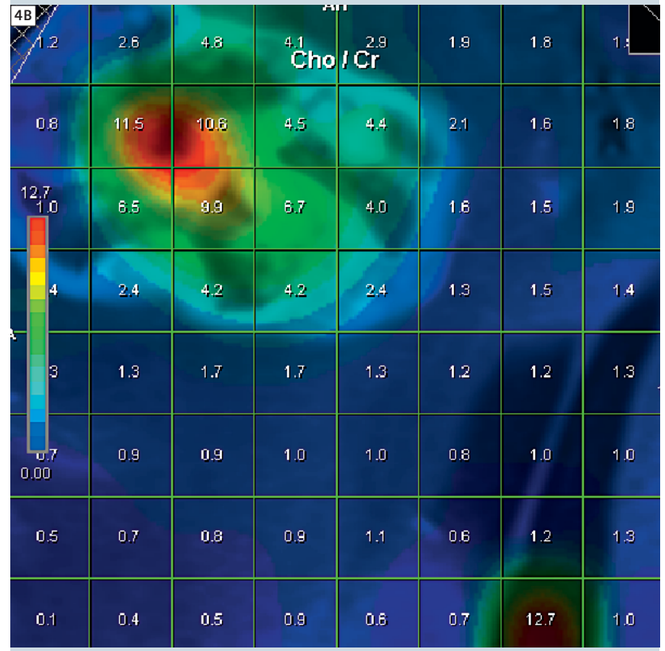

4 Spectra derived from 2D MR spectroscopic imaging are shown in **4A** (range 0.9–3.5 ppm). Choline/Creatine map **(B)** reveals high Cho/Cr ratio in the tumor and also increased ratio outside the contrast enhancing tumor region anteromedially (upper right corner of image, ratio around 1.8).

Try them on your system

Trial licenses for most of the applications featured in this issue of MAGNETOM Flash are available free of charge for a period of 90 days: Please contact your local Siemens representative for system requirements and ordering details or visit us online at **www.siemens.com/webshop** for further details, product overviews, image galleries, step-by-step demos, case studies and general requirement information.

1

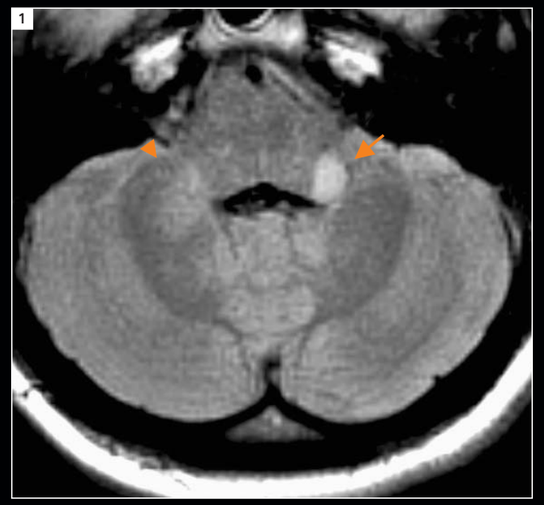

1 Reduced motion artifacts with *syngo* BLADE (page 10).

2

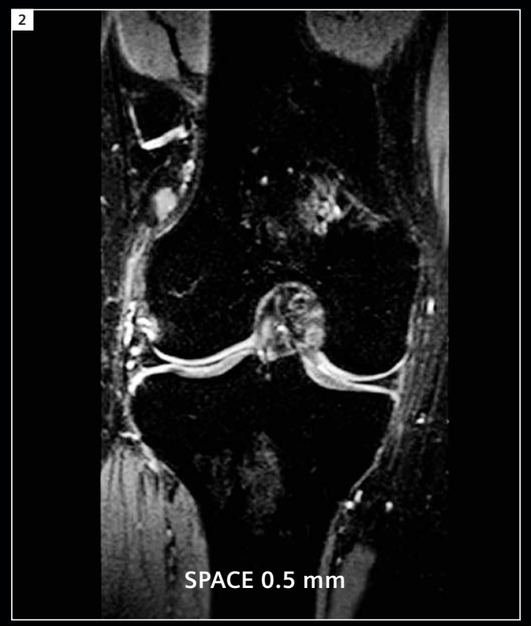

2 Coronal *syngo* SPACE reconstructions in 0.5 mm (page 13).

3

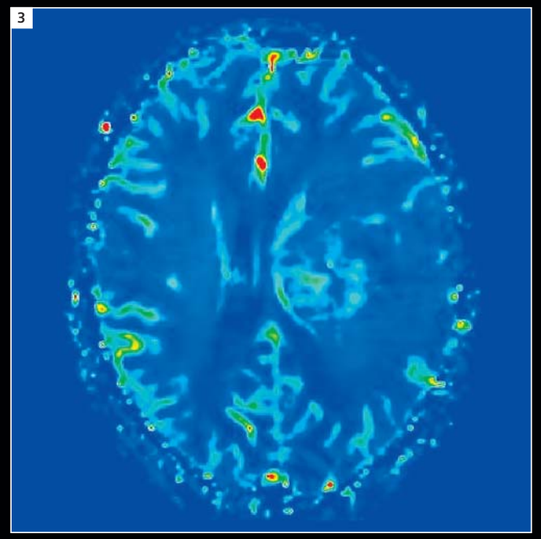

3 Non-contrast perfusion evaluation with *syngo* ASL (page 46).

4

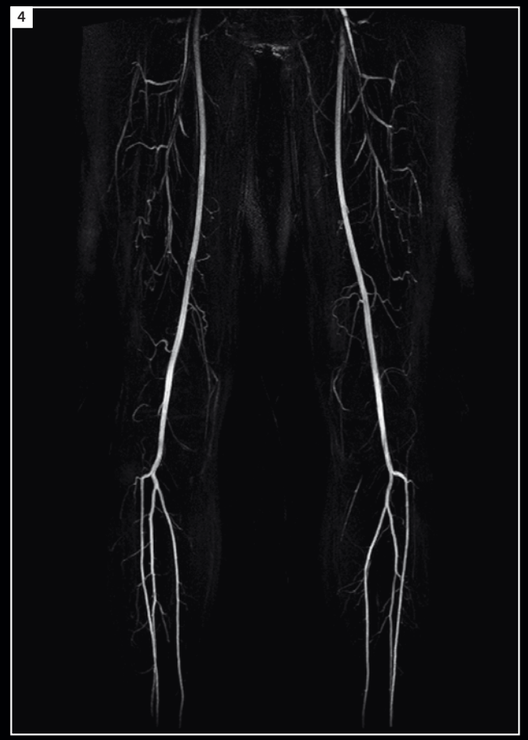

4 Non-contrast MRA and automatic composing from different table positions with *syngo* NATIVE SPACE and *syngo* Inline Composing (page 81).

Case Reports:
Tumor Detection by Diffusion-Weighted MRI and ADC-Mapping with Correlation to PET/CT Results

Matthias Philipp Lichy, M.D.; Philip Aschoff, M.D.; Christina Pfannenberg, M.D.; Schlemmer Heinz-Peter, M.D., Ph.D.

Department of Diagnostic and Interventional Radiology, University of Tuebingen, Germany

The early and correct estimation of metastatic spread is essential for a patient-specific and efficient therapy regime. Therefore knowledge of total tumor load, extent of lymph nodes and distant metastases as well as potential threats e.g. infiltration of vertebral body with high risk of fracture, is required. During recent years significant efforts have been undertaken to improve the detection of metastases – either by spiral multi-slice computed tomography (CT) or magnetic resonance imaging (MRI). By providing best soft tissue contrast compared to CT, high-resolution whole-body (wb) MRI proved itself as a powerful tool in oncology [1, 2, 3]. However, detection of metastases and therapy monitoring with wbMRI is mainly based on morphological changes. Integration of metabolic data (acquired e.g. by MR spectroscopic imaging) and functional information (e.g. dynamic contrast enhanced scans) is potentially possible with MRI, but due to time constraints these methods could prove its clinical impact only in dedicated applications e.g. detection of prostate cancer within the prostatic gland and cannot easily be implemented in wbMRI so far.
The amount and complexity of wbMRI data also hampers the widespread use of this technique in clinical routine. Positron emission tomography (PET) with an integrated CT scanner (PET-CT) provides combined morphological and metabolic information. Compared to wbMRI, however, PET-CT is associated to x-ray exposure and the tracer production, transport and its application are more labor- and cost intensive. Sensitivity and specificity of PET-CT and examinations depends also on tumor type, applied tracer and tissue of interest. Therefore, the selection of the appropriate staging modality is highly dependent on histology and the pattern of metastatic spread [4].
However, cancer is not only characterized by pathologic metabolism e.g. high glucose uptake; also higher cellularity and therefore restriction of water diffusion have also been found to be common features of tumors. Diffusion-weighted imaging (DWI) with high b-values has therefore been applied for imaging metastasis. However, comparisons of DWI with other imaging modalities and with special focus on wbPET/CT are not widely available. In the following two case reports, results of MRI and wbDWI are compared to 18F-FDG PET/CT findings.

Imaging techniques

CT was conducted with application of intravenous contrast agent (Ultravist 370, Schering AG, Germany) and oral administration of negative contrast dispersion as multi-phase protocols [7].
All PET-CT scans were performed on a single dual modality scanner (Biograph 16, Siemens Medical, Knoxville, USA) consisting of a 16-row multi-slice CT system (minimal rotation time of 0.5 sec) and a full ring lutetium oxortho-silicate (LSO) PET. WbMRI and DWI were performed on a 1.5 Tesla MR tomography with 32 receiver channels (MAGNETOM Avanto, Siemens Medical, Germany). For (wb) DWI application, a single-shot echo-planar-imaging (EPI) sequence with diffusion-module and fat-suppression-pulse was used (*syngo* REVEAL). This sequence has the ability for navigator-based respiratory triggering (PACE). For respiratory-triggered DWI sequence, data was acquired in expiration. In case of non-triggering, the patient was breathing freely. Water diffusion was measured with a 3-scan-trace technique and b-values of 0, 400 and 1000 s/mm^2; apparent diffusion coefficient maps were generated automatically (*syngo* Inline Diffusion). Sequence parameters of the single-shot echo-planar-imaging (EPI) sequence with diffusion-module and fat-suppression-pulse used in these two cases were: TR / TE 3900 (1500 for non-triggered DWI) / 76 ms, slice thickness 4 mm, FOV 380 x 380, 192 Matrix, EPI factor of 192, 4 averages, PAT factor of 2 (*syngo* GRAPPA), resulting voxel size 2 x 2 x 4 mm^3, TA 1:52 (non-triggered, 30 slices; for triggered DWI depending on respiration cycle TA approximate 5 min).

Case 1: Malignant Melanoma

This case shows the results of wbPET/CT and wbMRI including DWI of a female patient with an advanced malignant melanoma (stage IV). The DWI sequences were able to visualize even the extensive tumor spread within the bowel wall as well as lymph node metastasis in detail. All suspicious lymph nodes as well as the diffuse tumor infiltration of the bowel wall are characterized by a high restriction of water diffusion (compare with ADC map). However, the extension of this advanced melanoma and therefore the irresectability is already proven with the standard contrast-enhanced single-phase CT scan. However, comparing the thick-slice MIP of the inverted original b=1000 s/mm² DWI images, providing a "PET-like" image, with the corresponding PET image it is clearly shown that the resolution of the DWI here is clearly superior to the PET image and lymph node metastases and bowel infiltration are well delineated. However, fat-suppressed, contrast enhanced T1w and fat-suppressed T2w MRI are also able to display all metastases. While the ADC-map is essential to differentiate real restriction of diffusibility from T2-shine-through artifacts, this image cannot be used for a fast assessment of tumor spread. However, original b-value images especially at b=1000 s/mm² are characterized by suppression of all healthy tissue with exception of the spleen and clearly elevated signal intensity of the metastases.

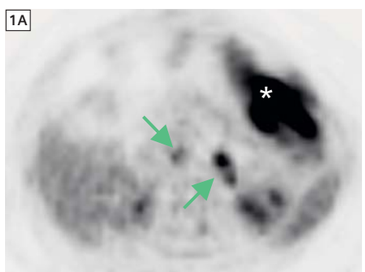

1 **A:** Corresponding original attenuation-corrected PET image (*bowel infiltration, arrows lymph node metastases).

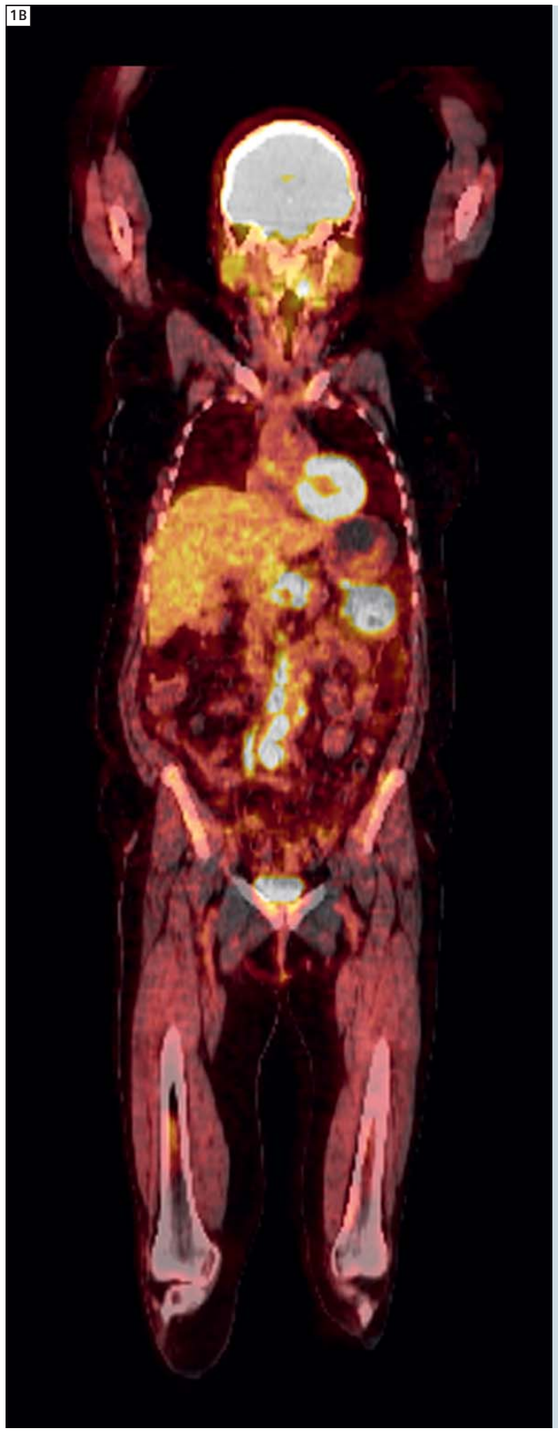

1 **B:** Fused 18F-FDG PET/CT demonstrating multiple paraortic metastases and diffuse bowel infiltration of a malignant melanoma (stage IV).

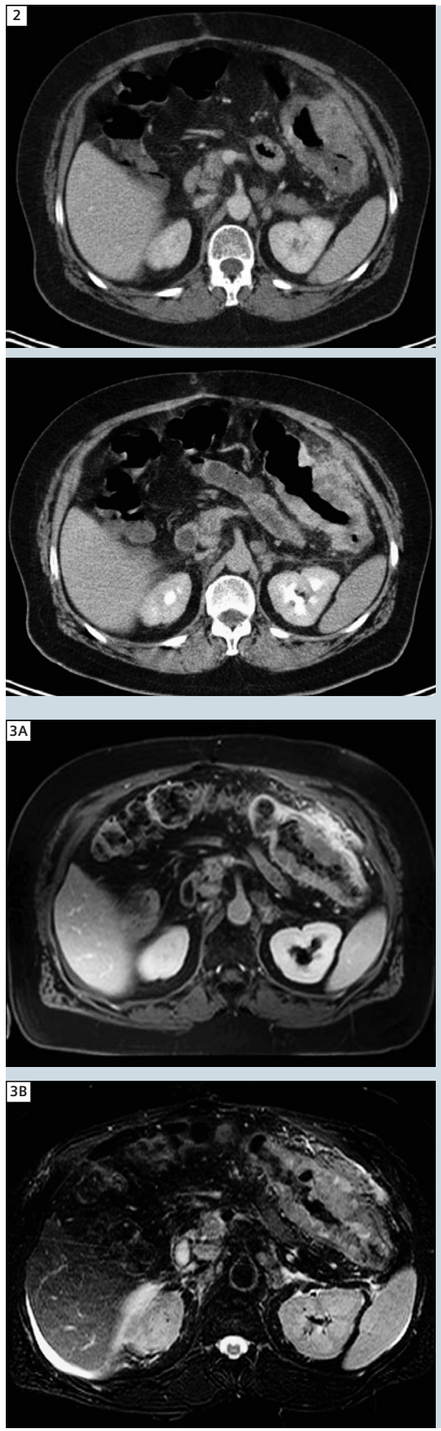

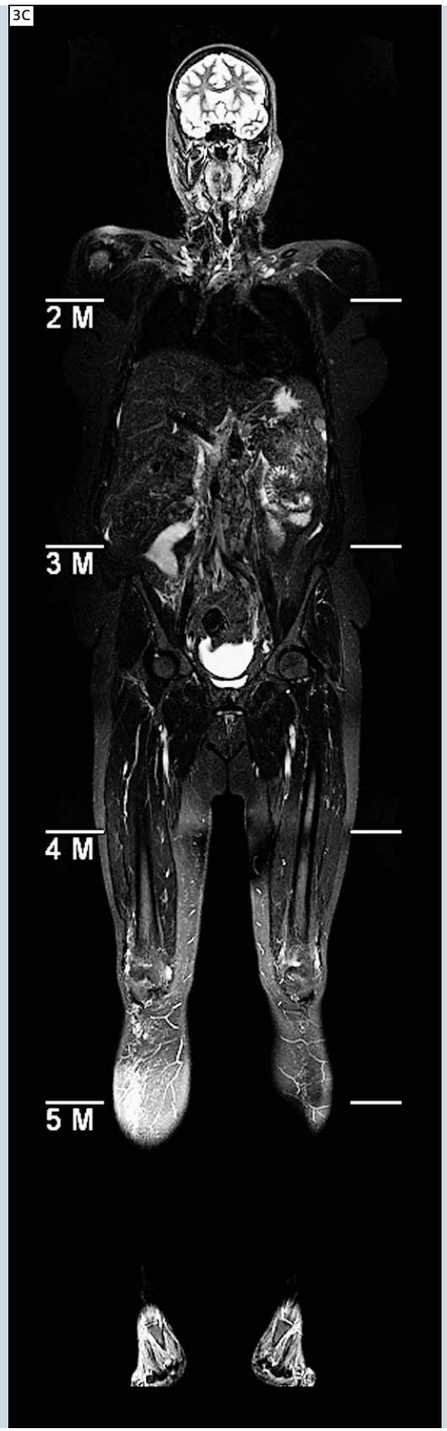

2 Corresponding single-phase CT scan (acquired during PET/CT scan).

3 **A:** Contrast-enhanced T1w 2D Flash MRI (breathhold).
B: T2w TSE with spectral fat-suppression (free breathing, triggered with PACE).
C: Composed whole-body T2 TIRM.

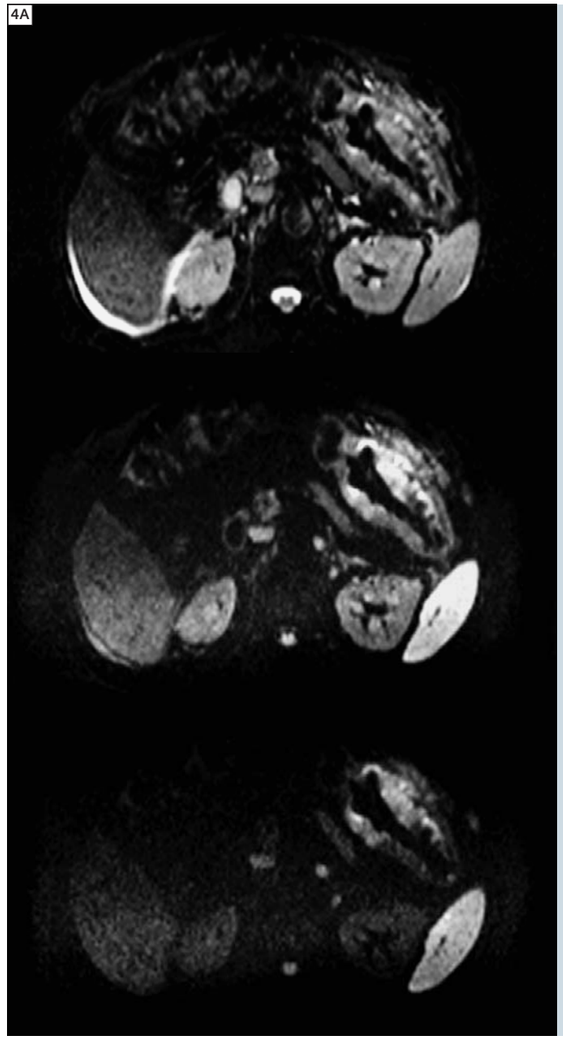

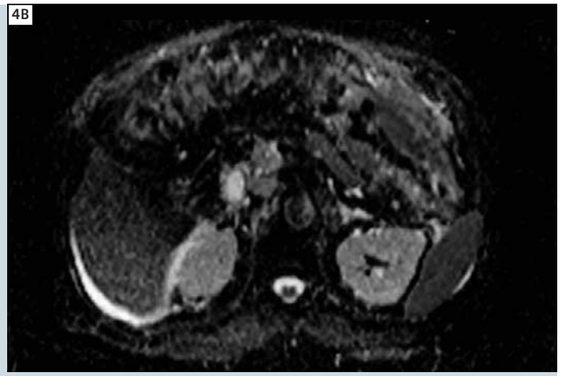

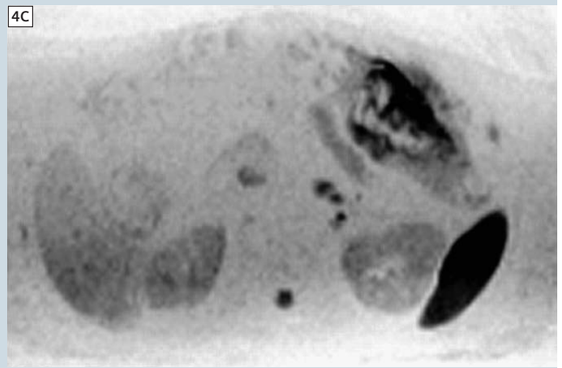

4 **A:** Original b-value images acquired at b = 0, 400 and 1000 s/mm² (from right to left). **B:** ADC map, generated from all three b-values (3-scan trace). **C:** Inverted thick-slice MIP, generated from images acquired with b=1000 s/mm².

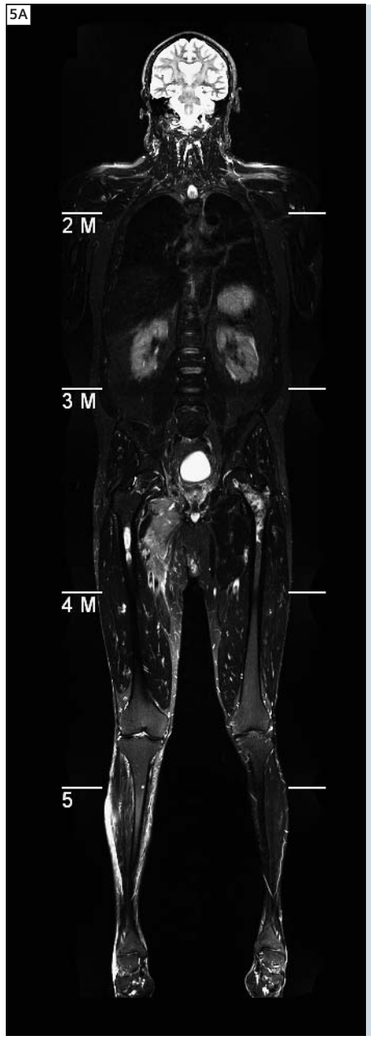

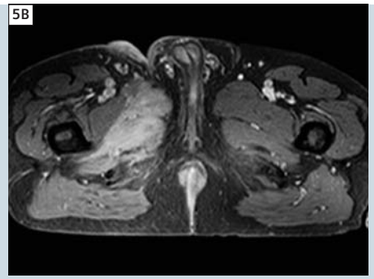

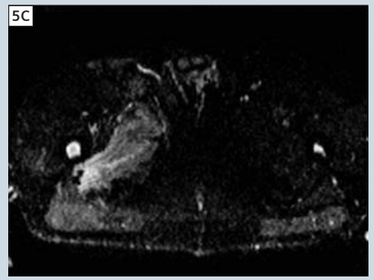

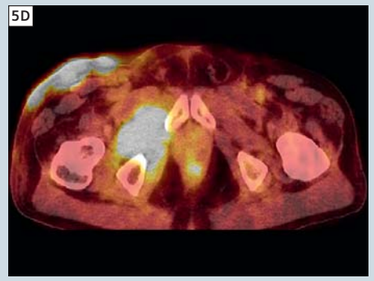

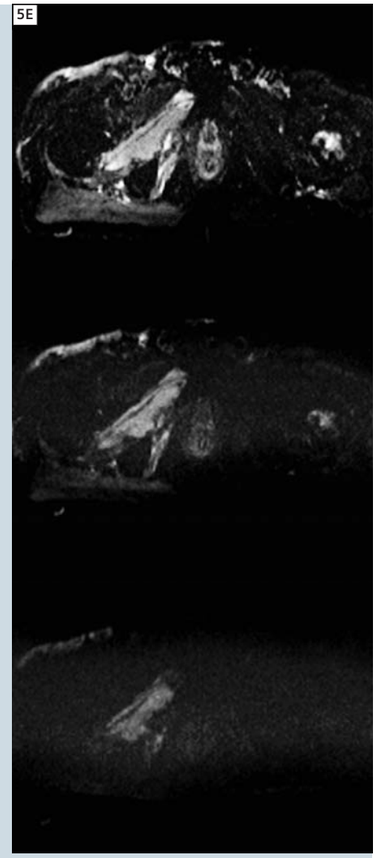

5 **A:** Composed whole-body T2 TIRM. **B:** Contrast-enhanced T1w 2D Flash MRI. **C:** Original b-value images acquired at b = 0, 400 and 1000 s/mm². **D:** ADC map, generated from all three b-values (3-scan trace). **E:** Fused 18F-FDG PET/CT demonstrating high metabolism in the ventral cutis as well as muscles, corresponding to diffuse non-Hodgkin lymphoma infiltration.

Case 2: Non-Hodgkin Lymphoma

In this case, the results of PET-CT and DWI examination of a male patient with a non-Hodgkin lymphoma are shown. PET-CT with ^{18}FDG revealed a diffuse tumor infiltration of the muscles and also of the right ventral skin of the right thigh. High b-value imaging was able to visualize diffuse tumor infiltration in detail even of the cutis. However, if one had to rely only on a single b-value image, in this case a clear differentiation of restriction of diffusibility from potential insufficient spectral fat suppression would be problematic and therefore hamper the correct diagnoses. Muscle atrophy of the right gluteal muscle results in restriction of water mobility, too, and also a pathologic signal of the femoral bone marrow is obvious at b = 0 and 400 s/mm² values. ^{18}FDG uptake was not suspicious, either in the bone marrow or in the atrophic muscles, but based on MRI tumor could not be ruled out. The ADC-map also shows unexpectedly high ADC-values in the muscles with high tracer uptake compared to the atrophic gluteal one. Atrophy of the right gluteal muscles is also obvious on fat-suppressed T2w and contrast-enhanced, fat-suppressed T1w MRI.

References

1 Walker R, Kessar P, Blanchard R, Dimasi M, Harper K, DeCarvalho V, Yucel EK, Patriquin L, Eustace S. Turbo STIR magnetic resonance imaging as a whole-body screening tool for metastases in patients with breast carcinoma: preliminary clinical experience. J Magn Reson Imaging 2000; 11(4):343-50.

2 Lauenstein TC, Goehde SC, Herborn CU, Goyen M, Oberhoff C, Debatin JF, Ruehm SG, Barkhausen J. Whole-body MR imaging: evaluation of patients for metastases. Radiology 2004; 233(1):139-48

3 Schlemmer HP, Schafer J, Pfannenberg C, Radny P, Korchidi S, Muller-Horvat C, Nagele T, Tomaschko K, Fenchel M, Claussen CD. Fast whole-body assessment of metastatic disease using a novel magnetic resonance imaging system: initial experiences. Invest Radiol 2005; 40(2):64-71.

4 Schmidt GP, Baur-Melnyk A, Herzog P, Schmid R, Tiling R, Schmidt M, Reiser MF, Schoenberg SO. High-resolution whole-body magnetic resonance image tumor staging with the use of parallel imaging versus dual-modality positron emission tomography-computed tomography: experience on a 32-channel system. Invest Radiol. 2005; 40(12):743-53.

Contact
Matthias Lichy, M.D.
Siemens AG, Healthcare Sector,
Marketing Magnetic Resonance
P.O. Box 32 60
91050 Erlangen
Germany
matthias.lichy@siemens.com

Whole-Body MRI for Accurate Assessment of Tumor Load of Bone Metastases Originate from Mamma Carcinoma

Philip Aschoff; Christina Pfannenberg; Claus Claussen; Heinz-Peter Schlemmer

Department of Diagnostic and Therapeutic Radiology, University Hospital of Tuebingen, Tuebingen, Germany

Background

While large efforts in the early and precise detection of mamma carcinoma and therefore detection in a potentially curative stage have been undertaken, mamma carcinoma remains the main leading cause of cancer-related deaths in women. It is also known from a variety of tumor entities that the accurate and precise detection of metastases and estimation of tumor load is of high relevance for patient-adopted individualized therapy regimes. While mammography and ultrasound do play an important role for local assessment of tumor extend / recurrence, ultrasound of, for example, the liver and to some extent also the conventional x-ray of, for example, the chest do play a role in detection of extended diseases; the indications and clinical benefit of these imaging modalities for staging of metastatic breast cancer is the subject of debate. Another routinely-used technique for detection of distant metastases is bone scintigraphy. However, it is not an uncommon finding of mamma carcinoma bone filiae that they are characterized as lytic lesions without surrounding reaction of the bone matrix. In combination with the limited spatial resolution, this fact reduces the sensitivity of bone scintigraphy and can result therefore in an inaccurate or even false negative estimation of metastatic spread [1]. Additionally the pressure to optimize the diagnostic pathways in regards to staging accuracy, time consumption (including multiple referrals), costs and finally patient comfort have lead to an increased usage of computed tomography for fast and precise coverage of soft tissue and bones in patients with extended tumor disease. But relying mainly on morphologic changes, small bone metastases, as well as diffuse bone marrow infiltration and small lymph node filiae, are missed easily [2]. Within recent years, the application of PET/CT has increased especially the specificity in the detection of malignant lymph nodes. In combination with contrast-enhanced CT scans, a clear advantage of an 18F FDG PET/CT exam compared to the M-staging with x-rays, ultrasound and CT alone can be claimed. In contrast to other tumor entities, like lung cancer or malignant melanoma, however, the larger variation of degree of increased glucose metabolism of mamma carcinoma cells can result in more false negative PET findings [3, 4]. It has already been shown by several working groups, and for different tumor entities including breast cancer, that MRI with T2w fat saturated imaging sequences is superior to bone scinitgraphy and CT [5]. In the following two cases we show the advantages of MRI for imaging bone metastases originating from breast cancer. In both cases, there was the high clinical suspicion of a tumor recurrence with metastastic spread. The patient underwent therefore a combined whole-body 18F FDG PET/CT and a whole-body MRI (32-channel MAGNETOM Avanto) to complete tumor staging with special focus on the brain, liver and bone marrow. The whole-body MRI protocols were performed according to [6, 7]. For detection of bone metastases mainly three sequences were used:

a) coronal TIRM
b) transversal T2w TIRM covering the body trunk from pelvis to skull base and
c) contrast-enhanced transversal 2D (pelvis and abdomen; FLASH) or 3D (chest, VIBE) GRE sequences with fat saturation.

In the presented cases, our imaging protocol did not include a whole-body DWI with ADC mapping for improved tumor detection and for providing additional functional parameter for follow-up of therapy responses. Nevertheless, in all three cases, MRI had to be considered the most sensitive methodology for detection of bone metastases; however, the influence of the whole-body imaging modalities on the clinical outcome with the given therapy options for such advanced breast cancer patients has still to be answered. Nevertheless, whole-body (bone) MRI presents itself as the imaging modality of choice when an accurate assessment of bone metastases is required. To increase further the diagnostic confidence and to provide additional information about tumor biology and biological activity, future developments will combine PET with MRI within one examination and also different PET tracers such as 18Fluoride will be used.

Case 1

In this case a 66-year-old patient underwent a breast-preserving mastectomy 12 years ago (R0 resection). Two years later a local tumor recurrence was observed and therefore a breast ablation and later augmentation was performed. Within a time-period of approximately 1 ½ years a slow but constant increase of the CA 15–3 tumor marker has been observed. In contrast to PET/CT, MRI showed multiple small lesions with T2w hyperintense signal and corresponding contrast-media uptake. Most of these lesions measured less than one centimeter in their maximum diameter (Figs. 1D, E). In retrospect, a discrete irregular bone configuration /sclerosis with implied focal FDG uptake can be found, corresponding to a larger metastases. Neither a further pathologic focal FDG uptake nor lytic / sclerotic CT lesions could be detected. Based on MRI and in concordance to the clinical follow-up, a diffuse metastatic spread had to be diagnosed in this case.

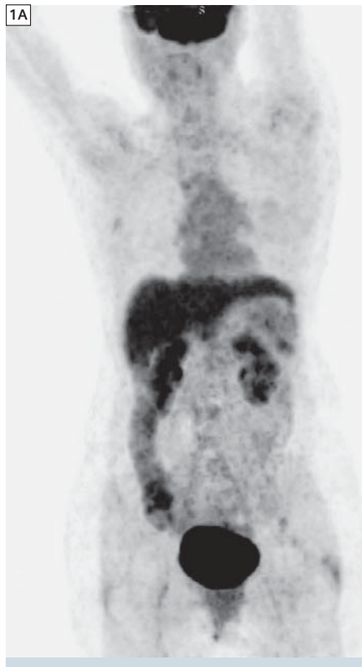

1A MIP of the FDG-PET examination.

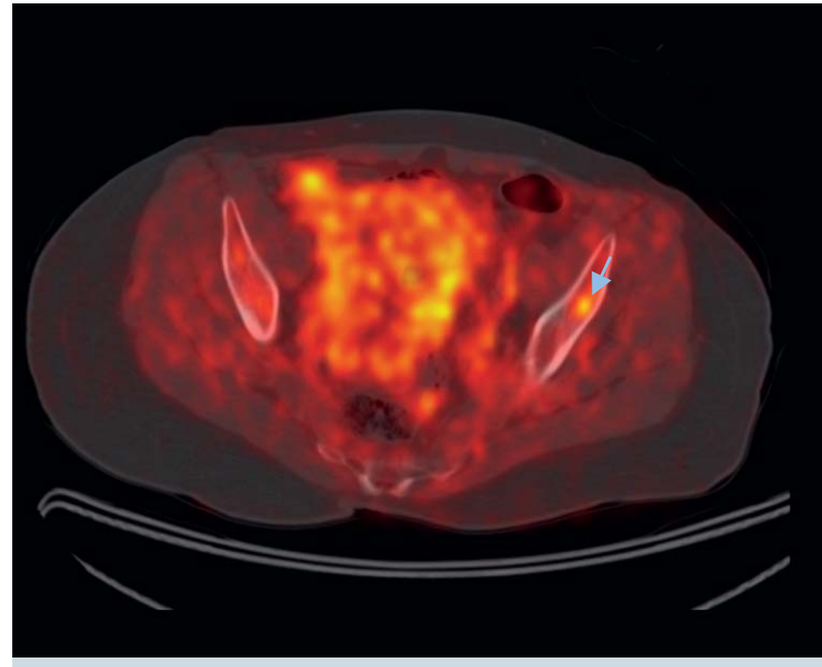

1B Focal uptake within the left iliac bone.

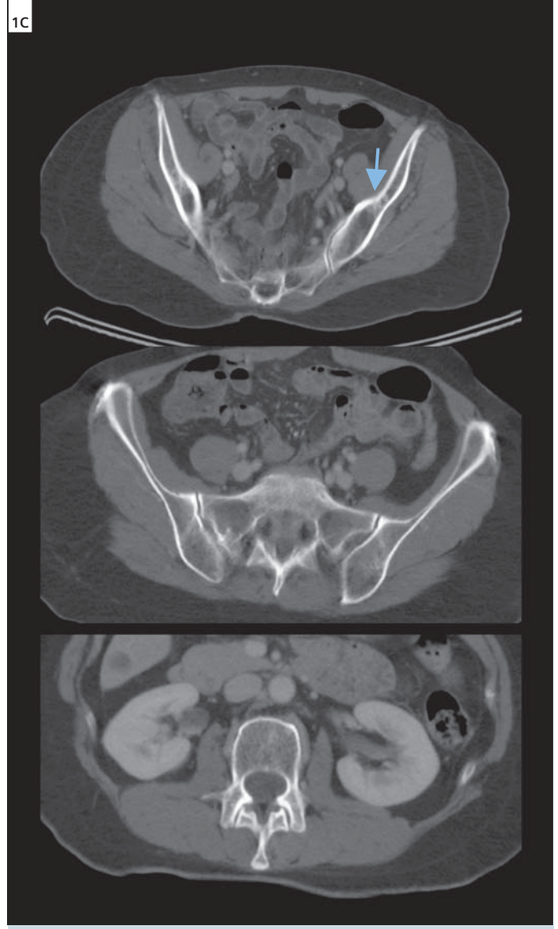

1C Corresponding to the PET scan, CT was able to visualize a small irregular sclerosis; further bone lesions could not be detected by FDG PET/CT.

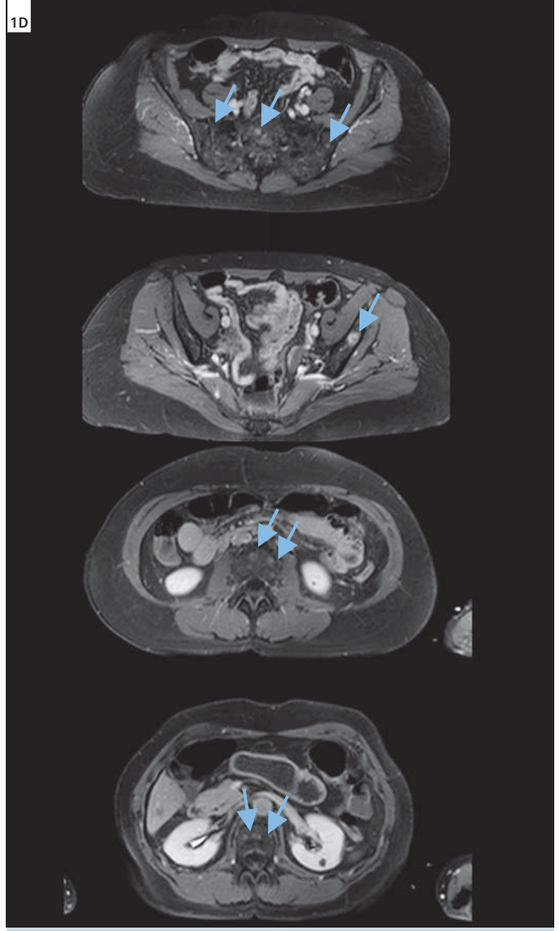

1D Contrast-enhanced T1w 2D FLASH, demonstrating multiple smallest bone metastases.

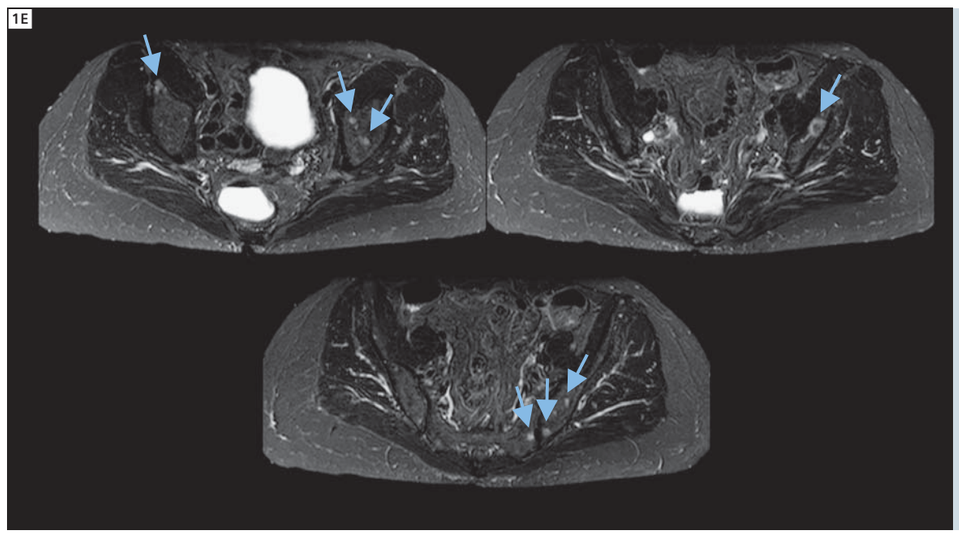

1E T2w TIRM; diffuse metastatic spread is obvious.

Case 2

A 46-year-old patient underwent whole-body imaging because the routinely-acquired bone scintigraphy was inconclusive for bone metastases (Fig. 2A). A CT scan was performed directly after the bone scan but did not lead to a clear rule out or confirmation of a tumor recurrence. It should be mentioned that there were no other signs of tumor recurrence reported than the unclear bone scan, and the tumor markers were within normal range. The patient was initially diagnosed

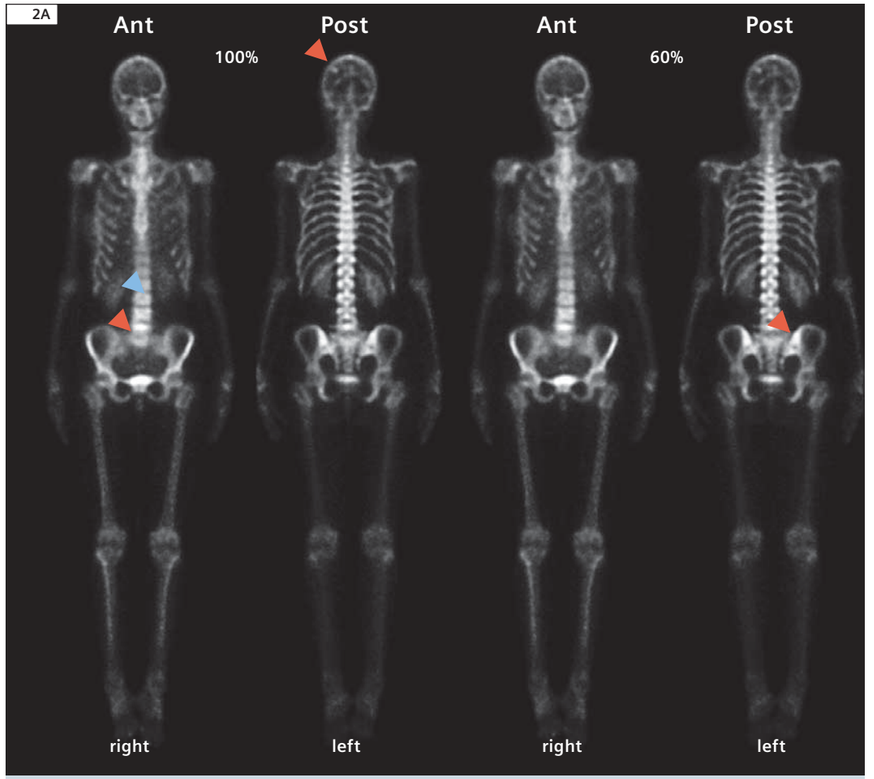

2A Bone scan suspicious for metastases (arrows).

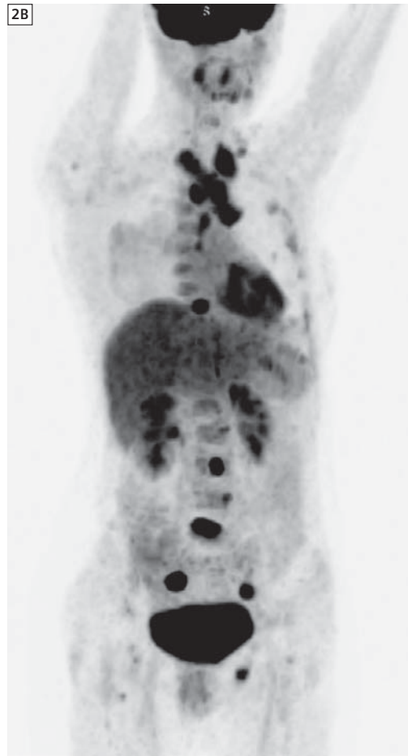

2B MIP of the FDG PET: multiple bone and lymph node metastases with clearly increased glucose metabolism are shown.

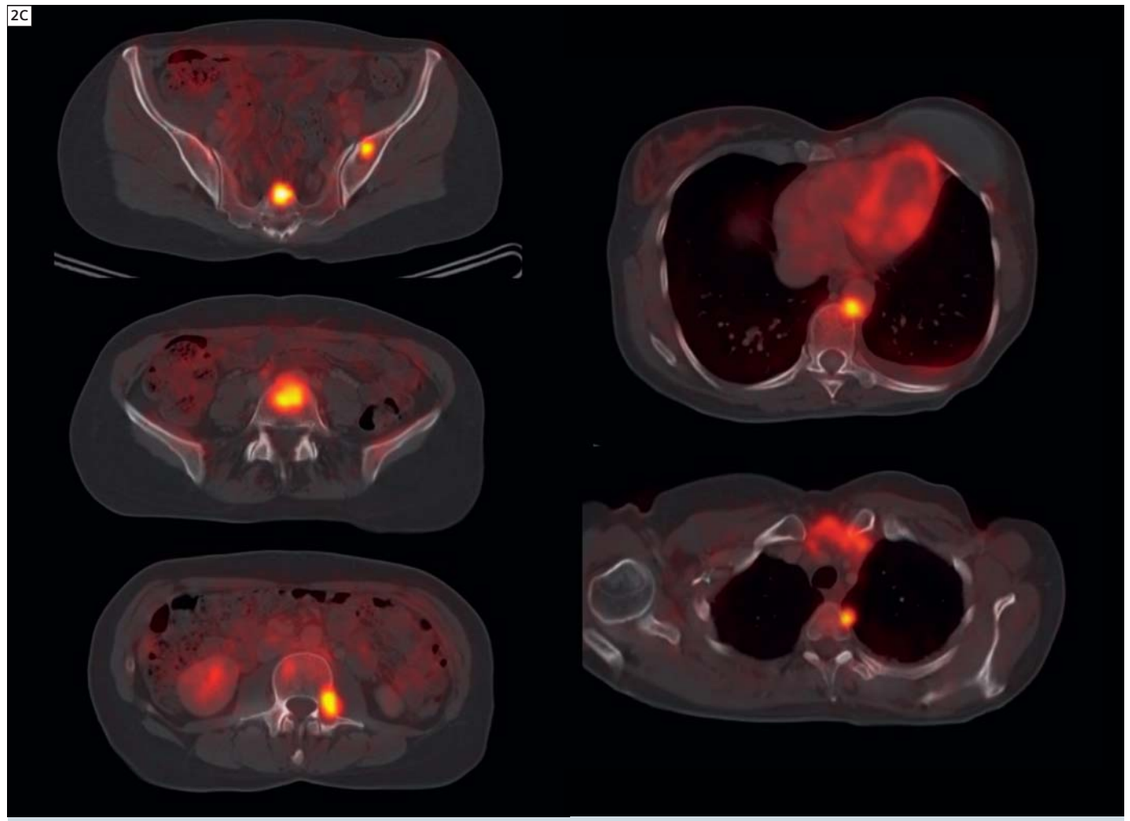

2C Corresponding PET/CT images demonstrating the extend of the multiple lytic bone metastases.

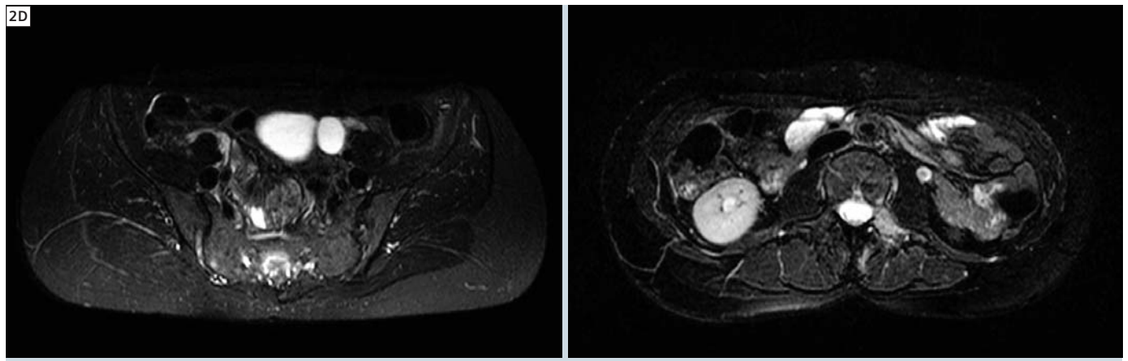

2D T2w TIRM MRI provides best delineation of bone metastases and the relationship to the spinal canal.

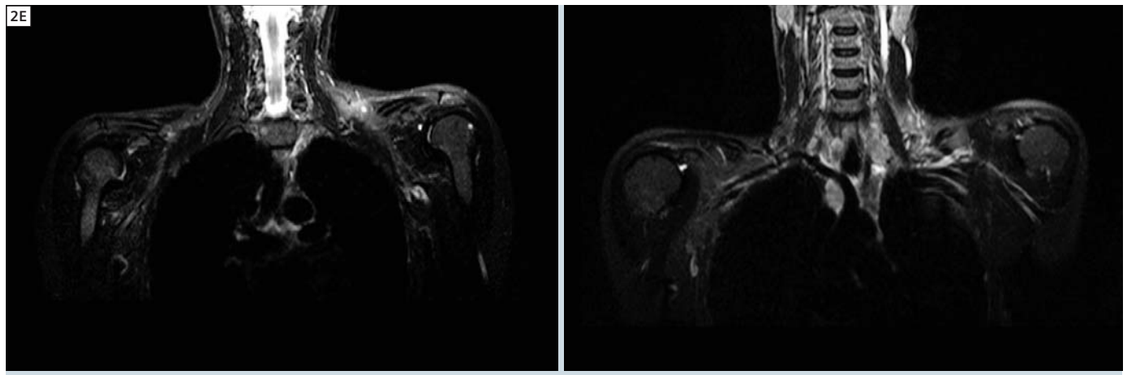

2E While PET/CT shows a higher diagnostic accuracy for small lymph nodes, in the presented case, MRI (coronal TIRM) could also stage the extension of the lymph node involvement correctly.

ten years ago with a breast cancer (pT1c pN1a (1/21) G2-3 M0) und underwent R0 breast ablation and LNE. Two years later a local tumor recurrence was diagnosed which resulted in a re-surgery, radiotherapy and chemotherapy. To definitively answer the question of a tumor recurrence, the patient was than sent to our department for a whole-body PET/CT and MRI. Based on PET/CT and MRI findings, an advanced tumor recurrence was diagnosed. Multiple osseous as well as mediastinal and cervical lymph node metastases are detected by high glucose metabolism on PET/CT (Figs. 2B, C) and MRI (Figs. 2D, E). MRI could visualize bone infiltration in more detail and its relationship to the spinal canal; however no differences in the total tumor load are obvious between the two imaging modalities. A hormone therapy was started and a partial remission could be achieved for this patient to date (18 months follow-up period; not shown).

References

1 Hamaoka T, Madewell JE, Podoloff DA, Hortobagyi GN, Ueno NT. Bone imaging in metastatic breast cancer. J Clin Oncol. 2004 Jul 15;22(14):2942-53.

2 Groves AM, Beadsmoore CJ, Cheow HK, Balan KK, Courtney HM, Kaptoge S, Win T, Harish S, Bearcroft PW, Dixon AK. Can 16-detector multislice CT exclude skeletal lesions during tumour staging? Implications for the cancer patient. Eur Radiol. 2006 May;16(5):1066-73.

3 Du Y, Cullum I, Illidge TM, Ell PJ. Fusion of metabolic function and morphology: sequential [18F] fluorodeoxyglucose positron-emission tomography/computed tomography studies yield new insights into the natural history of bone metastases in breast cancer. J Clin Oncol. 2007 Aug 10;25(23):3440-7.

4 Gil-Rendo A, Martínez-Regueira F, Zornoza G, García-Velloso MJ, Beorlegui C, Rodriguez-Spiteri N. Association between [18F]fluorodeoxyglucose uptake and prognostic parameters in breast cancer. Br J Surg. 2009 Feb;96(2):166-70.

5 Costelloe CM, Rohren EM, Madewell JE, Hamaoka T, Theriault RL, Yu TK, Lewis VO, Ma J, Stafford RJ, Tari AM, Hortobagyi GN, Ueno NT. Imaging bone metastases in breast cancer: techniques and recommendations for diagnosis. Lancet Oncol. 2009 Jun;10(6):606-14.

6 Walker R, Kessar P, Blanchard R, Dimasi M, Harper K, DeCarvalho V, Yucel EK, Patriquin L, Eustace S. Turbo STIR magnetic resonance imaging as a whole-body screening tool for metastases in patients with breast carcinoma: preliminary clinical experience. J Magn Reson Imaging. 2000 Apr;11(4):343-50.

7 Schlemmer HP, Schäfer J, Pfannenberg C, Radny P, Korchidi S, Müller-Horvat C, Nägele T, Tomaschko K, Fenchel M, Claussen CD. Fast whole-body assessment of metastatic disease using a novel magnetic resonance imaging system: initial experiences. Invest Radiol. 2005 Feb;40(2):64-71.

Contact
Philip Aschoff, M.D.
Department of Diagnostic and Therapeutic Radiology
University Hospital of Tuebingen
Hoppe-Seyler-Strasse 3
72076 Tuebingen
Germany
philip.aschoff@med.uni-tuebingen.de

Case Report: Klippel-Trénaunay-Weber Syndrome

Chawla Tanya, M.D.[1]; Scott Enns[1]; Melissa Charette[1]; Nancy Talbot[1]; Karen Bodolai[1]; Sunil Kumar S. L., M.D.[2]

[1]Princess Margaret Hospital, University Health Network, Toronto, Canada
[2]Siemens Healthcare, Toronto, Canada

Patient history

We report on a 31-year-old female patient with known Klippel-Trénaunay-Weber syndrome. The patient was gravid and at 27 weeks gestation*. Referral to our institution was to confirm the presence of a venous malformation and aid obstetrical planning to determine if a Caesarean section was technically feasible.
The Klippel-Trénaunay-Weber syndrome is a rare congenital disease characterised by a triad of capillary hemangioma (port-wine stain), large venous malformations as well as lymphangiomas. The haemangioma is of variable depth and can involve the deep sub-cutaneous tissues as well as involving adjacent visceral organs or bowel. It is also associated with focally limited gigantism (in very rare cases also dwarfism). The Klippel-Trénaunay-Weber syndrome is therefore also described as angiodysplasia with dominantly venous-cavernous type and hypertrophy of the affected extremity. Most cases are sporadic, although a few cases in the literature report an autosomal dominant pattern of inheritance. If arteriovenous malformations are present within the affected extremities, this special form is often described as Parkes Weber syndrome.

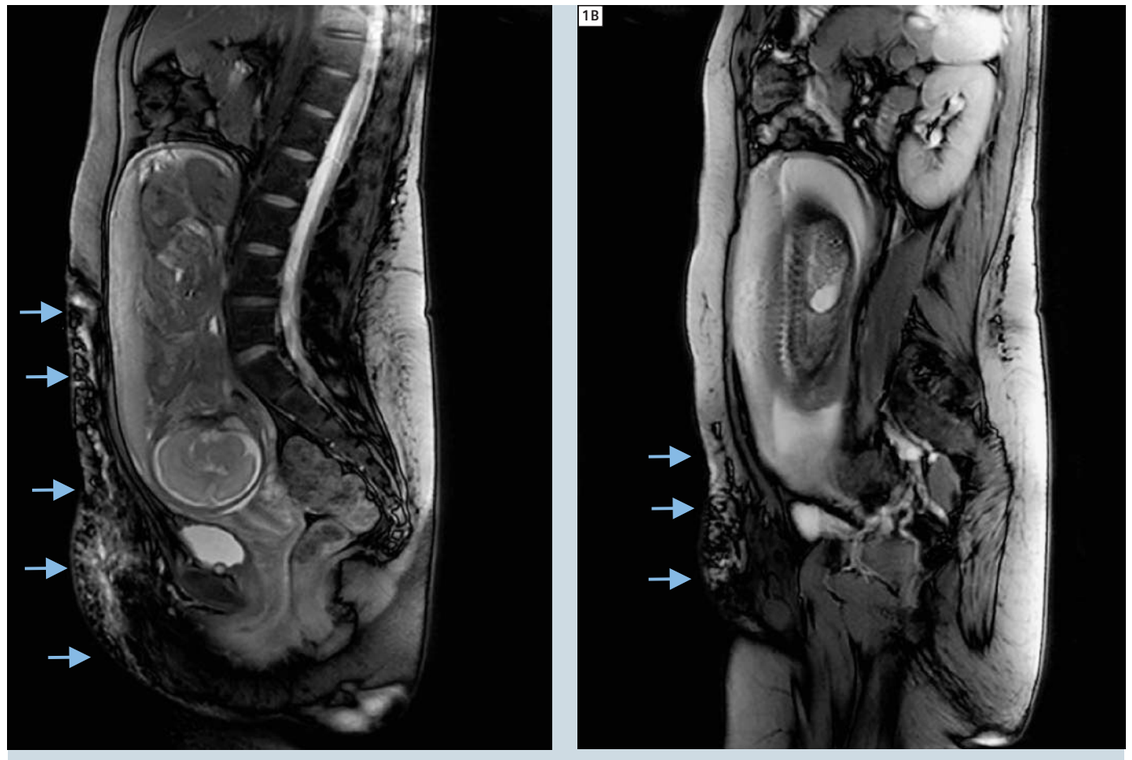

1 Composed sagittal TrueFISP images, consisting of two measurements. The extensive venous malformation is well delineated (arrows).

Sequence details

All images were acquired at 1.5T (MAGNETOM Avanto, 32-channel, SQ-Engine) with the usage of two Body Matrix coils and the integrated spine coil. The anatomical area covered with this MR exam reached from the upper lower extremities towards the upper abdomen. The examination was performed as a multistep MR exam. The scanner is equipped with the Tim Planning Suite. Because of the limited breath-hold capabilities of the patient, short and robust imaging sequence were mainly used (HASTE, TrueFISP). The protocol comprised: transversal (TR / TE 1380 / 76 ms, FOV 317 x 315 mm, matrix 220 x 256 Px, SL 7 mm), coronal (TR / TE 1375 / 76 ms, FOV 350 mm, matrix 243 x 256 Px, SL 7 mm) and sagittal (TR / TE 1380 / 76 ms, FOV 350 x 350 mm, matrix 243 x 256 Px, SL 7 mm) HASTE and TrueFISP (TR / TE 3.69 / 1.85 ms, FOV 350 x 350 mm, matrix 486 x 512 Px, SL 7 mm, respectively). For evaluation of potential large arterial feeder of the large vascular malformation, a dynamic MR sequence was used (3D FLASH in coronal orientation, 41 measurements, temporal resolution 6 seconds, TR / TE 2.13 / 0.76 ms, FOV 450 x

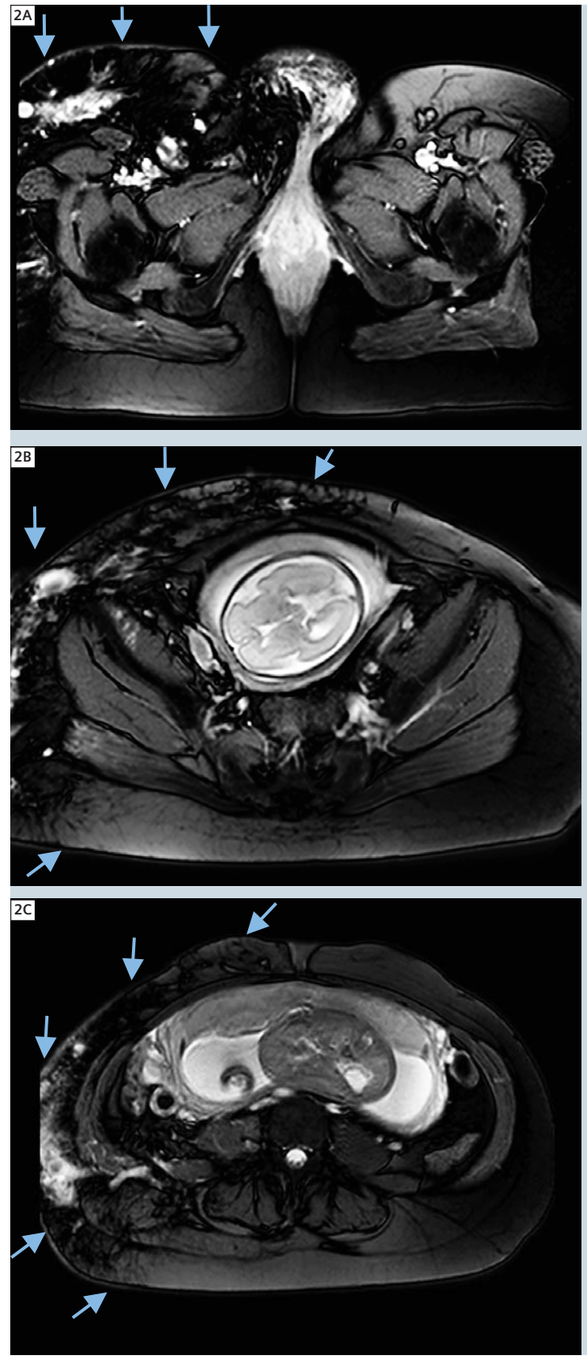

2 Transverse TrueFISP images. The involvement of the right thigh, pubis and abdominal wall by the vascular malformation is well visualised.

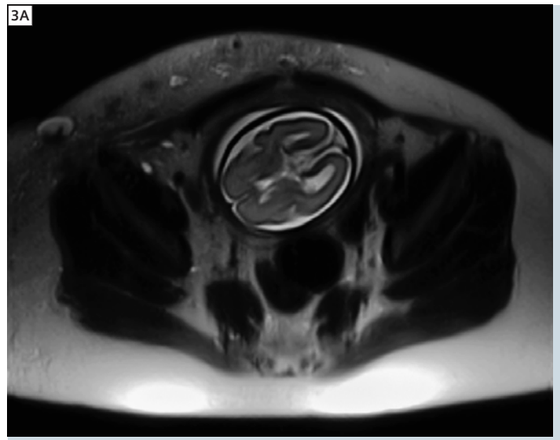

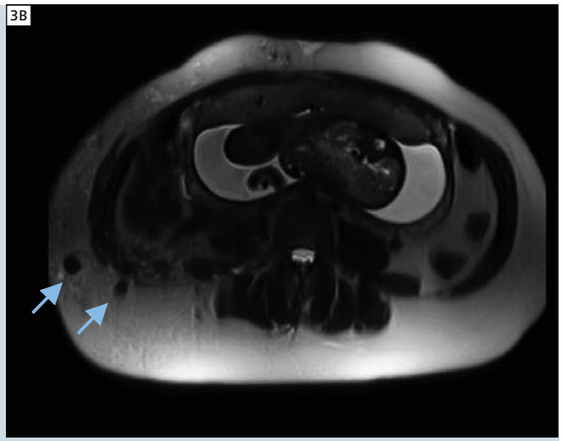

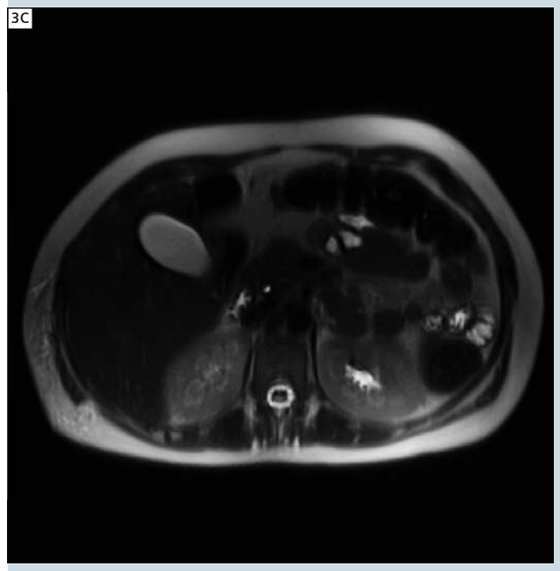

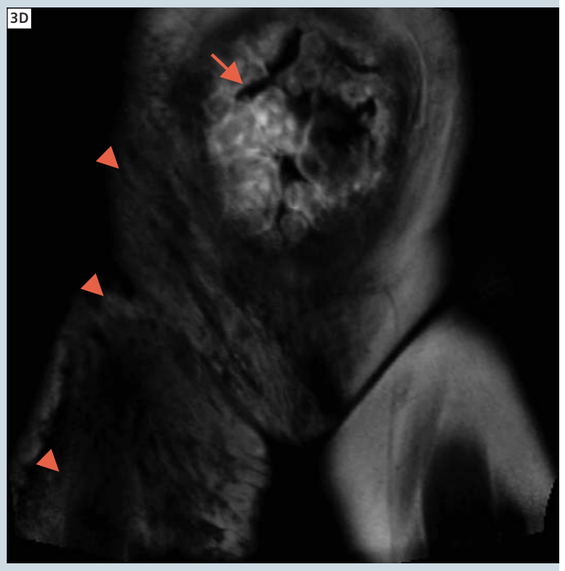

3 Corresponding transverse HASTE images **(3A–C)** show bright signal of the vascular malformation, indicating a low flow. However, two large vessels are shown with a clear flow-void (arrows, **3B**). Based on dynamic MRI, no arteriovenous malformation can be detected within the large vascular malformation (red arrowheads). Enhancement of the placenta is noted (red arrow).

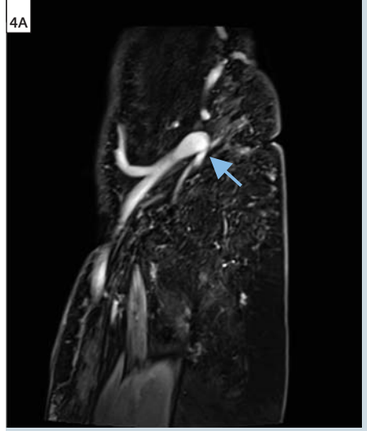

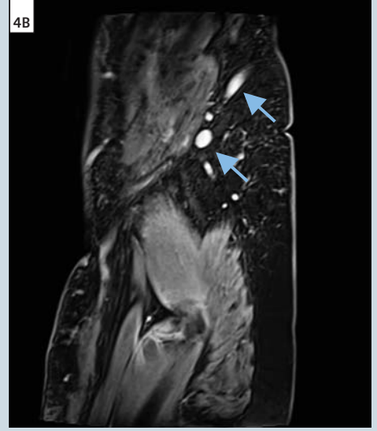

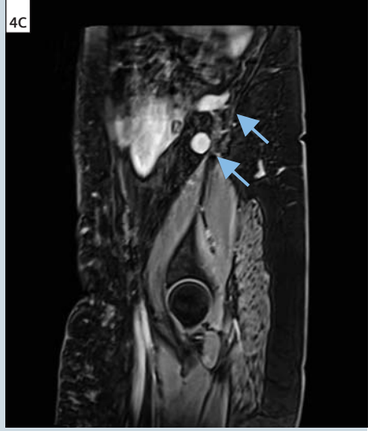

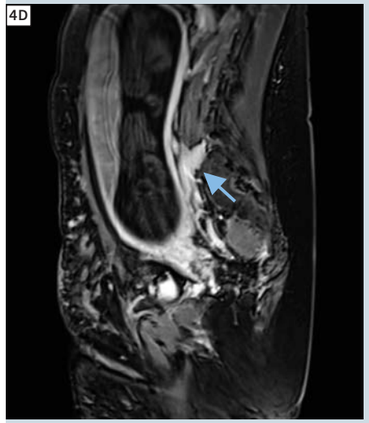

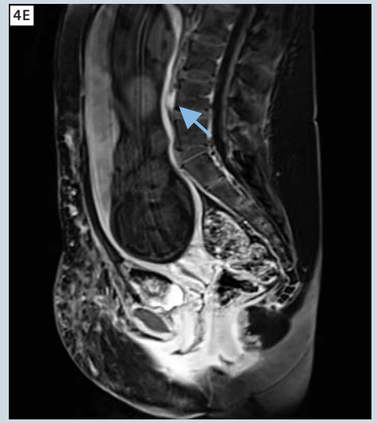

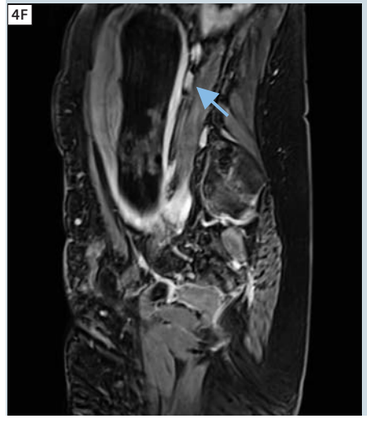

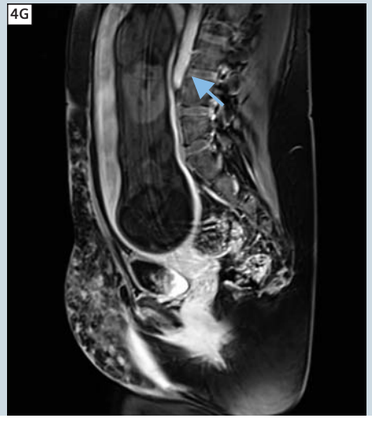

4 A large subcutaneous vein drains the malformation and enters the right retroperitoneum posteriorly at the level of L5/S1. The images are sequentially arranged from right lateral **(4A)** to medial **(4G)** slice position.

450 mm, matrix 240 x 320 Px, SL 7 mm). Venous drainage was visualized by applying a 3D VIBE in sagittal orientation (TR / TE 5.41 / 1.72 ms, FOV 400 x 400 mm, matrix 240 x 320 Px, SL 5 mm).

Imaging findings

An extensive subcutaneous slow flow vascular malformation extending from the right thigh involving the right vulva, pubis, right lower abdomen and right flank was found. A large subcutaneous vein drained the malformation and entered the right retroperitoneum posteriorly at the level of L5/S1. An additional large subcutaneous vessel was identified in the right lower abdominal wall, which was favoured to comprise part of the venous drainage of the large malformation. No pelvic vascular malformations were seen. Also based on the dynamic MR scan, no evidence of an arteriovenous shunt was found. The venous malformation crossed the midline to the contralateral abdominal wall; however, there were no venous malformations visible on the left side of the abdomen.

*The safety of imaging fetuses has not been established.

Contact
Dr. Chawla Tanya
Assistant Professor and Staff Radiologist
MRCP FRCR FRCPC
Princess Margaret Hospital, University Health Network
610 University Avenue
Toronto, ON M5G 2M9
Canada
nancy.talbot@uhn.on.ca

syngo NATIVE TrueFISP in the Assessment of the Transplanted Kidney

Peter Weale[1]; Jeremy Collins, M.D.[2]; James C. Carr, M.D.[3]

[1]Staff Scientist ,Siemens Healthcare, Cardiovascular MR Research and Development, Chicago, IL, USA
[2]Fellow, Department of Radiology, Northwestern University Medical School, Chicago, IL, USA
[3]Associate Professor, Director, Cardiovascular Imaging, Department of Radiology, Northwestern University Medical School, Chicago, IL, USA

Introduction

Assessment of the vascular integrity of a transplanted kidney is a request we receive occasionally, most commonly when transplant recipients present with compromised renal function.
The fact that the patient presents with impaired renal function and has recently undergone transplant surgery makes the nephrologist understandably nervous about referring them for contrast-enhanced MR Angiography of the transplanted kidney. While the risk may be small, it makes sense to use a completely non-invasive method without the potential risk of Nephrogenic Systemic Fibrosis, if the diagnostic yield can be sufficient to answer the clinical question.
In our institution we recently published a study [1] where the effectiveness of TrueFISP with selective inversion recovery preparation, now known as *syngo* NATIVE TrueFISP, was evaluated for its utility in the assessment of the transplanted renal artery. Our results showed that the technique was essentially the same in diagnostic performance as low dose contrast-enhanced angiography and the method provides a low-risk method for the initial evaluation of the transplanted kidney.

Principles

syngo NATIVE TrueFISP is a method which generates angiographic contrast by preparing the region which contains

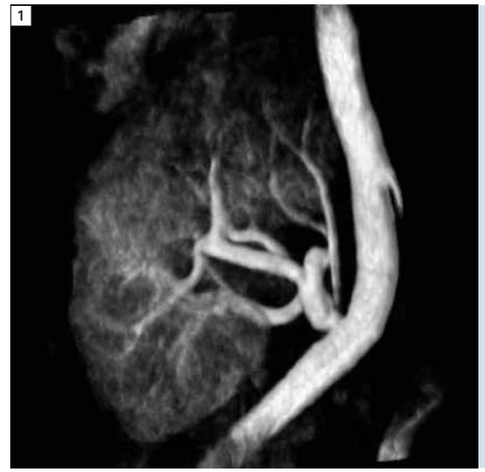

1 Volume rendered depiction of the anastomosis and proximal branches in this transplanted kidney. A slight "waisting" is seen at the site of the anastomosis.

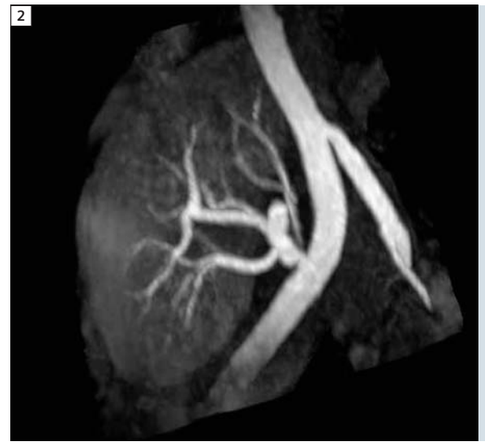

2 Thin MIP (50 mm) demonstrates the anastomosis and the upper pole accessory / early branching artery which originates very close to the site of the anastomosis. Depiction of 2nd and 3rd order branches of the renal artery provides qualitative evidence of good perfusion as the mechanism behind this technique relies upon in-flow during the prescribed inversion time. In this case blood depicted at the distal ends of the demonstrated arteries has travelled from the top if the inversion band (essentially top of this image) within 900 ms.

the vascular territory of interest by use of a selective inversion recovery pulse. The inversion pulse reduces the signal from the static tissue and blood which remains in the area but blood which flows into the slice during a defined inversion time is not inverted and, when the image data (3D TrueFISP) is collected there is a large difference in signal between blood which has moved into the area and other tissues which remain attenuated as a consequence of the inversion preparation.
This preparation region is not simply slice selective but has a graphically positioned inversion preparation which allows targeting of the desired vessel, independent of the orientation of the imaging volume.

Case study

A 64-year-old male patient with hypertension and type-2 diabetes who had been the recipient of a transplanted kidney was referred for evaluation of the transplanted renal artery to rule out an anastomotic stenosis as a cause for diminishing renal function. Recent Doppler ultrasound had demonstrated elevated velocities in the transplant renal artery, raising the suspicion of transplant arterial stenosis.
The patient and referring physician had concerns relating to the administration of Gadolinium containing contrast agents as his eGFR was reduced (35 ml/min/1.73 m^2). 30 ml/min/1.73 m^2 is the cut off point for administration of contrast in our institution.
After localization with 2D HASTE images the imaging volume of the *syngo* NATIVE TrueFISP protocol was positioned to depict the iliac arteries and the renal transplant anastomosis. The selective inversion band was positioned transversely with its upper border a few cm proximal to the assumed position of the anastomosis. The inversion preparation was larger than the imaging volume in the superior-inferior direction and covered around 4 cm distal to the imaging volume to invert any inflowing blood in the iliac veins (Fig. 3).
In this case, we used ECG triggering but in practice this is largely optional for renal transplants. We have found that the degree of respiratory motion in the pelvic region is small enough so as not to be a significant source of artifact in most patients, where the transplanted kidney is positioned against the pelvic sidewall and largely free of any significant respiratory motion.
The spatial resolution of this protocol was 1.25 x 1.25 x 1.25 mm (interpolated to 1 mm in the slice direction). 112 slices per 3D slab were acquired giving just over 11 cm of head-to-foot coverage. An inversion time of 900 ms was used which allowed the TI and acquisition to be completed within one heart beat resulting in completion of the scan in 3 minutes.
The TrueFISP readout scheme used a flip angle of 90 degrees.

Findings

The renal artery to external iliac artery anastomosis was well demonstrated and depicts a mild stenosis which is probably not a factor in this patient's diminishing renal function (Fig. 2).
The upper pole accessory artery (or what was probably an early branching upper pole artery in the native kidney) is also well seen distally, though the spatial resolution of this protocol inhibits the confident depiction of this very small vessel to the degree where an assessment of its diameter or severity of stenosis can be given.
The physiological nature of the contrast mechanism in NATIVE TrueFISP, however, gives some indication that this branch does not have a hemodynamically significant stenosis as the upper pole branch is filled with fresh blood within one cardiac cycle.

Conclusion

syngo NATIVE TrueFISP is a technique which allows depiction of the anastomotic site of a transplanted renal artery and the major branches of the implanted organ.
The mechanism whereby the angiographic contrast is generated in this sequence has a physiological component which can be seen as both a positive and a negative feature.
In the absence of sufficient flow, or in significantly impaired flow, the lumen of the vessel of interest may not be filled with sufficient "non-inverted" blood. This can be addressed to a degree by careful planning of the position of the inversion region so that large volumes of blood proximal to the vessel of interest are not inverted, which will reduce the available contrast.
In the example of renal transplants, if blood flow is compromised, the inversion preparation can be targeted so that the proximal external iliac artery is outside the preparation region, so that the non-inverted blood which gives the required signal has less far to travel – so less "fresh blood" is wasted filling a vessel of no clinical significance. Increasing the inversion time may also help in depiction of arteries where inflow into the kidney is reduced.
The physiological nature of the contrast mechanism is a benefit in that it gives a qualitative feel to the significance of any demonstrated stenosis.
In this example the mild stenosis seen at the anastomosis seems to have no significant effect on the filling of the distal branches of the intra-renal arteries suggesting that the kidney is well perfused.
syngo NATIVE TrueFISP is a useful addition to the available methods for performing MR angiography. As with all techniques a full understanding of the mechanisms behind the technique will give more consistent results and provide additional diagnostic information.

References

1 Liu X, Berg N, Sheehan J, Bi X, Weale P, Jerecic R, Carr J. Renal transplant: nonenhanced renal MR angiography with magnetization-prepared steady-state free precession. Radiology. 2009 May;251(2):535-42.

Contact
Peter Weale
Siemens Healthcare
Cardiovascular Research and Development
737 N Michigan Ave
STE 1600
Chicago, IL 60611
USA
peter.weale@siemens.com

3

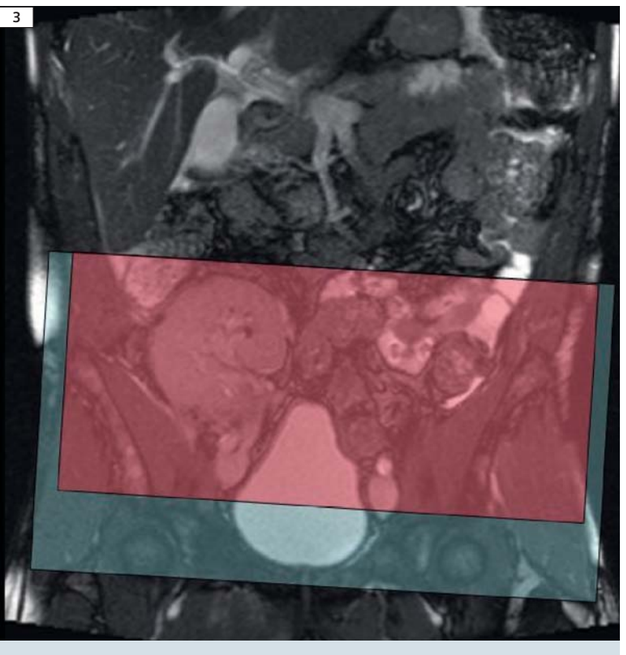

3 In this example the inversion preparation (gray) was positioned asymmetrically in the head-foot direction in relation to the imaging volume (red) to reduce the signal from any inflow via the iliac veins.

4

4 A cross sectional thin MIP of the iliac artery at the level of the anastamosis showing the main renal artery demonstrates a minor degree of narrowing which is probably of limited hemodynamic significance as the artery is well seen with 2nd and 3rd order branches well seen.

5

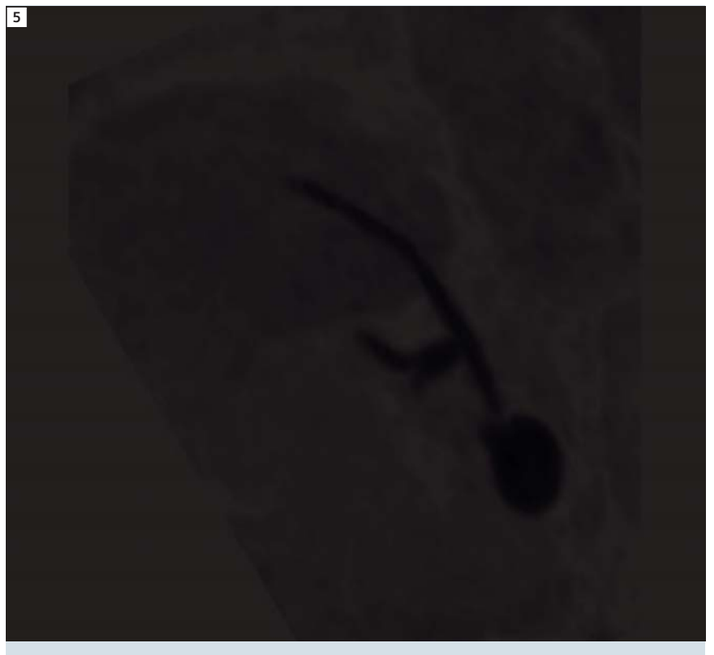

5 The upper pole accessory artery is well demonstrated, though the assessment of the lumen of this very small artery at the site of the anastomosis is somewhat compromised due to spatial resolution limitations.

How I do it: Non Contrast-Enhanced MR Angiography (*syngo* NATIVE)

Manuela Rick, Nina Kaarmann, Peter Weale, Peter Schmitt

Siemens Healthcare, Erlangen, Germany

Introduction

The realization that the administration of gadolinium-based contrast agents may be a factor in the development of Nephrogenic Systemic Fibrosis (NSF) in patients with renal failure has created a renewed interest in the in angiographic methods using intrinsic rather than extrinsic contrast mechanisms. The current economic climate in the Healtcare industry means that there is an increasing need to develop more cost-effective methods and reduction of contrast agent utilization is one element which might contribute to this. The existing non contrast-enhanced sequences, such as the Time-of-Flight (TOF) sequence, have their advantages in regions like the intracranial vasculature, but may have limitations for abdominal or peripheral imaging.

syngo NATIVE was introduced with software version *syngo* MR B17. It comprises two different non-contrast MRA techniques:

- *syngo* NATIVE TrueFISP (optimized for the renal arteries)
- *syngo* NATIVE SPACE (optimized for peripheral regions)

Both applications use mechanisms for contrast generation which depend on physiological processes. In NATIVE TrueFISP the inflow of non-inverted blood is exploited to depict the vessels. In NATIVE SPACE the image contrast is based on the pulsatility of the blood flow. Hence, the methods might be limited (reduced or no contrast-to-noise-ratio (CNR)) for patients with severe pathologies that have a direct influence on these physiological processes. This article not only demonstrates how to plan and perform a *syngo* NATIVE examination, but also gives some hints and tricks in cases where it may be difficult to get good image quality.

A clear understanding of the technical background of these measurements gives the user the opportunity to adapt the scan parameters individually, with respect to the patient's physiology. The ability to tailor the measurement can maximize the success rate.

The theory behind *syngo* NATIVE TrueFISP

syngo NATIVE TrueFISP is based on the TrueFISP sequence which typically yields a bright blood signal.

To enhance the contrast between flowing and static magnetization, an inversion pulse is applied to the region of interest. When imaging takes place after an inversion time TI, when the magnetization of surrounding tissue is close to zero, the background will have low signal. During the TI, however, fresh blood, with no history of inversion, enters the inverted slab, and the filled vasculature appears bright. The higher the more blood volume entering the inverted region, the better the contrast and the assessment of the small branches of the vessels. Figure 1 shows the basic principle of *syngo* NATIVE TrueFISP. With *syngo* NATIVE TrueFISP, respiratory synchronization can be realized with the 1D PACE Navigator. In this case the images are usually acquired in end-expiration to prevent breathing artefacts.

To increase the effectiveness and to reduce further artefacts from pulsatile vessels, you can combine 1D PACE with ECG-triggering. When a new inversion is played out with each ECG trigger signal, the total blood volume available for imaging is proportional to the stroke volume within one heartbeat.

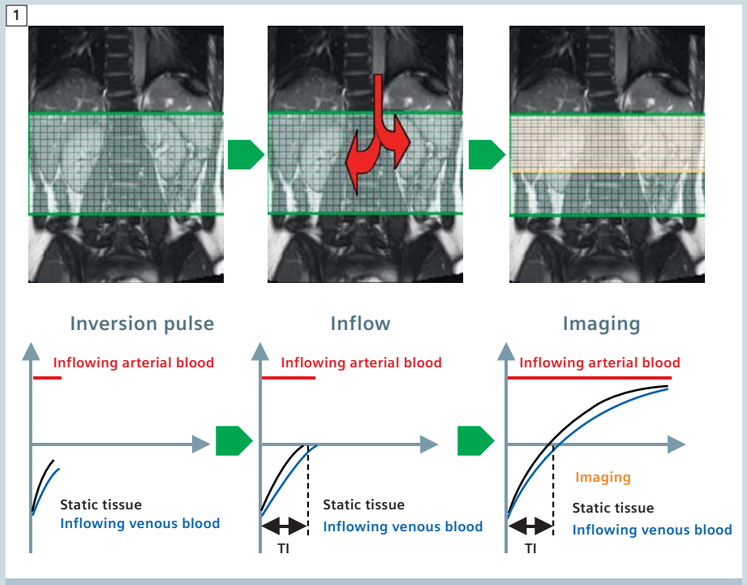

1 Basic principles of *syngo* NATIVE TrueFISP

Patient preparation

The patient is positioned supine, head or feet first.

It is highly recommended to use ECG-triggering. To reduce patient set-up time, *syngo* NATIVE TrueFISP data can be acquired without ECG triggering. If doing so it is necessary to ensure that the inversion time is long enough so that that there is sufficient inflow into the area of interest – with pulsatile flow if the TI chosen is too short (shorter than the RR interval of the patient) there is the likliehood that a significant proportion of the acquired data is acquired without capturing an inflow event. To reduce this likelihood set the TI to be long enough to always include an inflow episode (eg 1200 to 1400 ms). Remember that the volume of non-inverted blood has to be large enough to fill all the small vessel branches.

Position the Body Matrix coil on the patient, so that both regions the kidneys and the diaphragm are covered. The respiratory gating is usually performed with the 1D PACE Navigator, alternatively the respiratory cushion can be used. All the protocols are set up in the reference mode. This is essential on the Siemens open bore systems MAGNETOM Espree and MAGNETOM Verio, to achieve a good signal-to-noise-ratio for the renal arteries and the navigator. Position the laser marker in the middle of the renal hilum and the dome of the diaphragm. On the MAGNETOM Avanto, the examination can also be performed in the isocenter since the FOV in z-Axis is 50 cm. With software version *syngo* MR B17, a new functionality regarding the ECG display has been introduced. The learning cycle is demonstrated with a count-up mechanism, to show when the necessary 10 heartbeats are covered. The learning phase reduces the likelihood of inappropriate trigger detection, for example from artefacts due to the magneto-hydrodynamic effect.

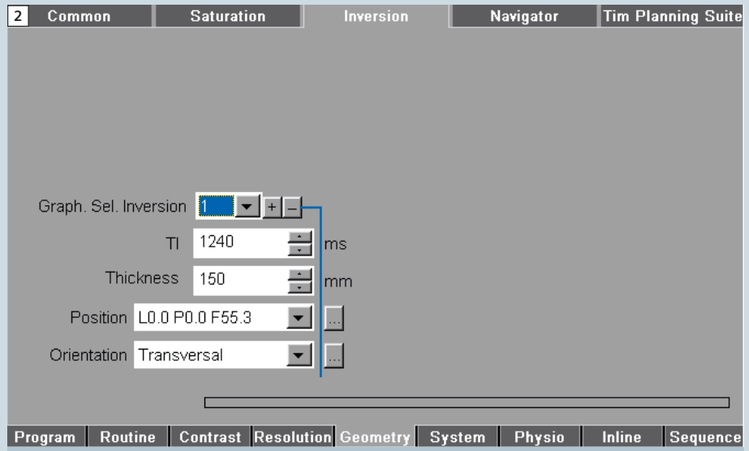

2 "Inversion" Subcard

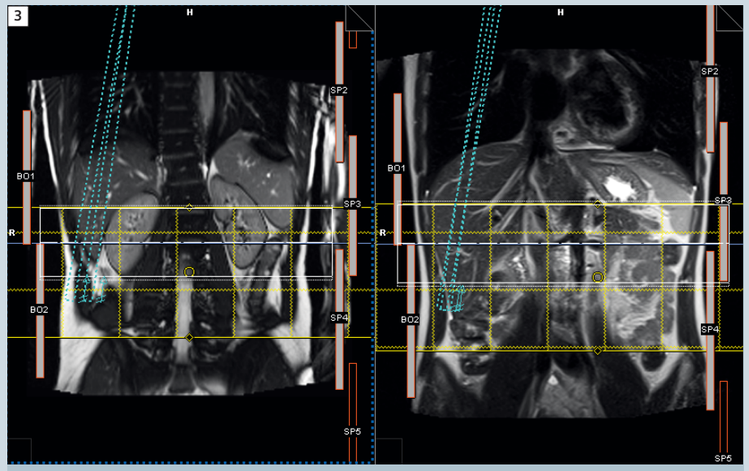

3 Coronal localizers. The TrueFISP localizer (left image) is standard in the protocol set-up, the HASTE sequence (right image) can be used alternatively.

Protocol set-up

The axial and coronal TrueFISP localizers are acquired as non-breath-hold examinations.

When opening the *syngo* NATIVE TrueFISP protocol, three graphical elements are shown, which have to be positioned correctly. We recommend to start with the navigator positioning, so that the center of the navigator is located at the dome of the diaphragm. Tilt the navigator beams, so that the signal intensity of the kidneys is not affected (compare Fig. 2).

The navigator has a new off-center readout support. If you shift the center of the navigator to the dome of the diaphragm, the respiratory trace, generated by the interface between the lung and liver, will be shown in the middle of the Inline Display. A scout mode is therefore no longer necessary. Due to the automatic tracing, the system will

detect the end expiration phase automatically. This new capability to off-center the navigator in the Z direction is essential for applications where the anatomy of interest is significantly offset from the diaphragm in the Z direction. Make sure that the coils for the kidneys, as well as for the navigator in z-axis direction, are selected.
The next step is to position the imaging FOV. Set the upper border of the FOV very close to the origin of the vessel of interest. Do not include too much proximal aorta in the FOV. To maximize the inflow effect, the upper limit of the inversion band should exactly match the upper limit of the FOV. This way, there will be no loss of signal of the inflowing, arterial blood. For the inversion pulse, a new graphical element has been designed and a new parameter subcard implemented into the UI (Fig. 3). The graphical element of the inversion pulse covers
a larger area inferiorly, to also saturate the inflowing blood from the veins and therefore, prevent the veins from causing unwanted signal in the images.
Finally, set the captured cycle. The maximization of the inversion time is automated within the sequence and there is usually no need to change this parameter. To verify this value, it can be checked on the Geometry-Inversion subcard.
The acquisition time is usually between 2–5 minutes, strongly depending on the heart rate and the breathing cycle of the patient. Monitor the navigator signal and the ECG- triggering during the measurement, to ensure a successful completion.

4

4 Example of a *syngo* NATIVE TrueFISP MIP reconstruction (healthy volunteer).

Postprocessing

Coronal and axial Maximum Intensity Projections (MIPs) are reconstructed Inline. For reconstruction of radial ranges, load the 3D dataset to the 3D-card and use the MIP and radial ranges button.
For further evaluation, the ThinMIP button can also be used and the volume adapted to the maximum possible. Figure 4 shows a radial ThinMIP reconstruction of a healthy volunteer.

Challenges and possibilities

- Imaging of renal transplants: In the pelvis region motion artifacts due to breathing are not usually of great significance. Thus, the respiratory gating is not needed in this region. There is a dedicated protocol for this specific application in the Siemens Exam Explorer.
- In elderly patients or patients with a known heart failure, the stroke volume may not be sufficient to fill the complete arterial tree of the kidneys with fresh blood within one heart cycle. In this case longer TI values such as 1400 ms may be useful. The UI allows 1400 ms when both acquisition window and TR are long enough. Keep in mind, that this leads to a situation where every second trigger signal is used, while the value of the trigger pulse parameter remains 1 (Fig. 5).
- Patient is dehydrated: Elderly patients in particular tend to drink less, which can have a negative influence on the blood volume and flow. Ensure that the patient is well-prepared for the examination. Perhaps communicate that topic with the responsible medical doctor.
- ECG-signal is disturbed during the measurement. Try to position the ECG amplifier in the direction of the head rather than the feet.
- In some cases, the detection of the renal arteries may be difficult on the TrueFISP Localizer. Alternatively, an axial and coronal multi-breath-hold HASTE sequence can be run.

5

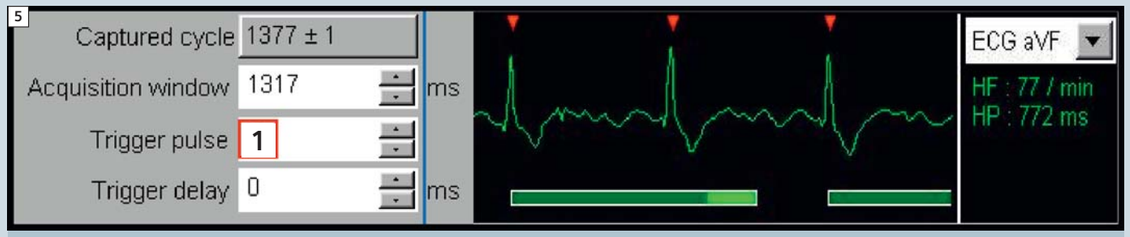

5 Trigger settings for long TI values (every second trigger used).

The theory behind *syngo* NATIVE SPACE

The *syngo* NATIVE SPACE sequence is a flow-sensitive 3D Turbo Spin Echo (TSE) sequence which allows fast scanning with high spatial resolution.
The sequence offers non-selective refocusing pulses and thus ultra-short echo-spacing.
The contrast of the *syngo* NATIVE SPACE sequence is based on the difference in the signal-intensity between static or slow-flowing blood (diastole) and fast-flowing blood (systole).
In diastole, the arteries appear bright (bright blood image). In systole, the arteries are dark (black blood image).
syngo NATIVE SPACE includes two measurements in one protocol, each with a different trigger delay. One measurement is acquired when the blood within the vessel is at its peak velocity, the other at its lowest velocity. The two images are subtracted voxel-wise, which removes background and venous signals, and the user is presented with immediate results (Inline subtraction and Inline coronal MIP). The Inline functionalities are chosen on the subcard Inline-Common. To manipulate the sensitivity to moving spins, different flow spoiling gradients can be selected.
The key to obtaining best image quality is to clearly identify the flow patterns in the R-R cycle. For this purpose, a cine FLASH sequence with a fairly high flip angle is used. The high flip angle enhances the in-flow effect.
Another important point is a stable ECG-signal, since the data must be collected consistently at the right time in the cardiac cycle. Therefore, ensure the correct positioning and preparation of the ECG device.

Patient preparation

The patient is positioned feet-first supine. The protocol in the Siemens Exam Explorer is set up with the peripheral angiography coil and the upper spine coil elements. Position the laser marker on the centre of the lower leg.

Protocol set-up

The standard exam consists of three protocols:

- a TrueFISP localizer including imaging of coronal and transversal slices
- a Cine_TDscout, and
- the NATIVE_SPACE_3D sequence.

The localizer starts automatically.
Position the FOV of the Cine_TDscout sequence transversely in the middle of the scan range. Use the captured cycle button to set the number of phases.
Load the images of the Cine_TDscout to the Mean Curve Application and draw a circle over an artery in each leg and begin the evaluation.
The scale on the curve image can be changed to Trigger Time, using the right mouse-button and selecting Scaling/Sorting.
Figure 6 shows a typical result of a healthy volunteer. In this case, you can easily identify the peak flow and the slow flow period.
The Cine_TDscout may also be used as a predictor for the chance of success. If the selected vessel does not show pulsatility in the flow pattern, it is very likely that the NATIVE SPACE technique will not provide enough contrast.
When running a multi-step protocol, it is beneficial to perform as many cine scouts as imaging steps. The trigger delay for each step may vary significantly (normally around 20–30 ms for each step). If a peripheral angiography with multiple steps is preferred, use the Tim Planning Suite and add as many steps as necessary. Figure 7 shows the

6

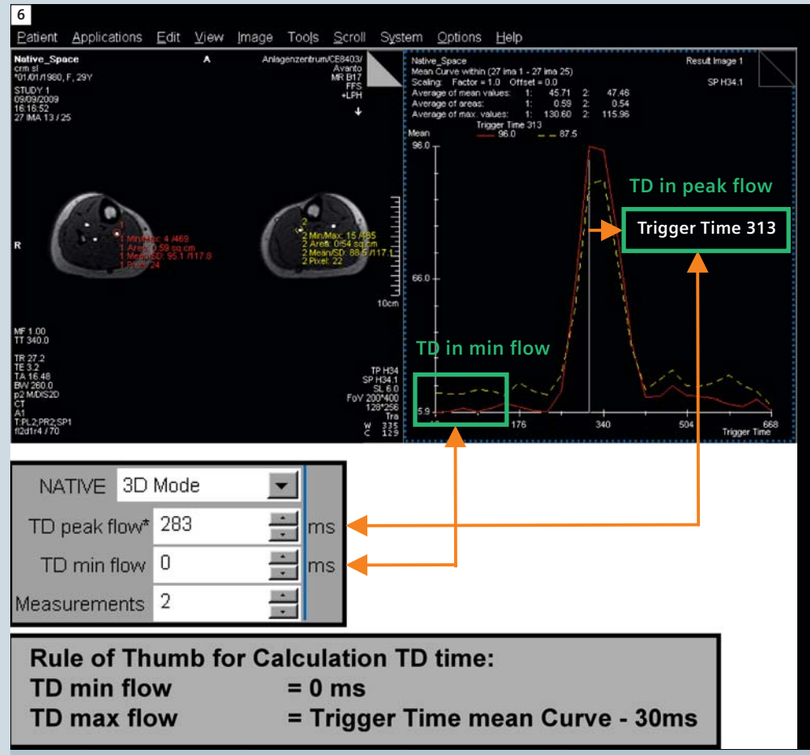

6 Mean Curve Application within the *syngo* NATIVE SPACE protocol and calculation of the delay times.

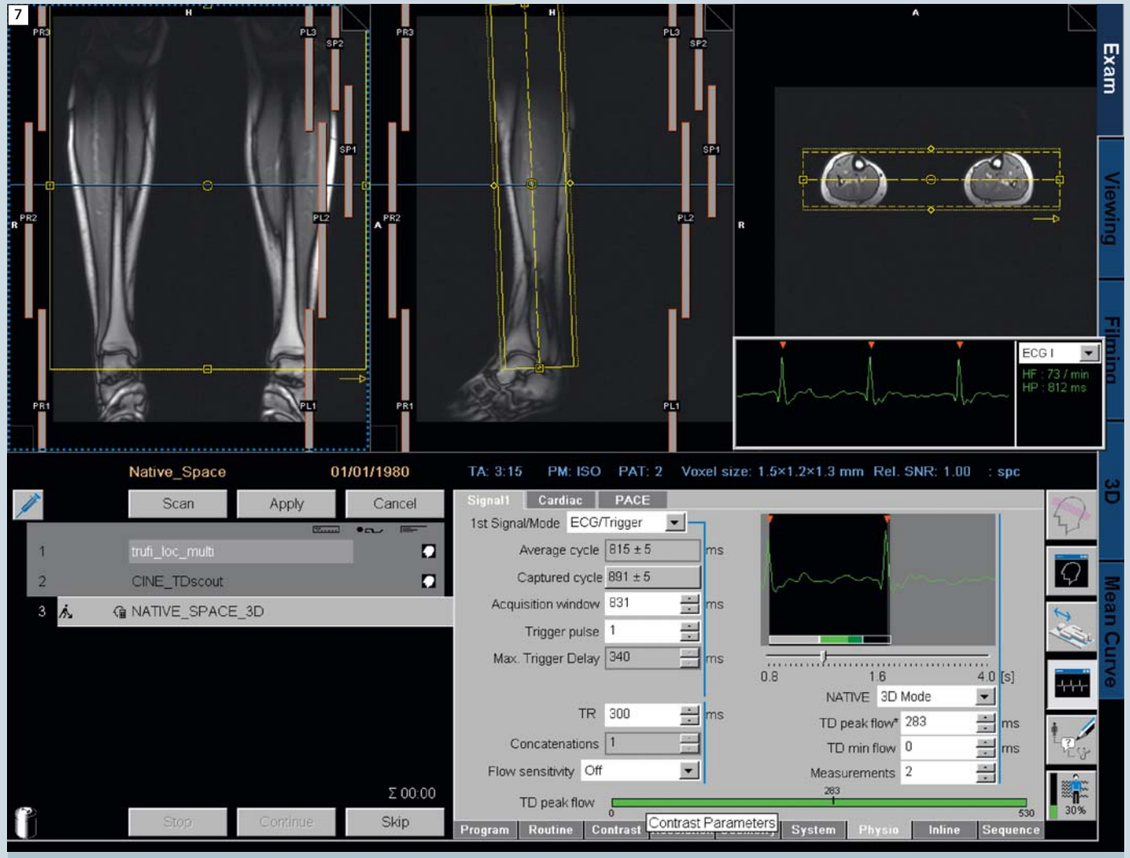

7 Planning of a single-step standard protocol in the lower leg region.

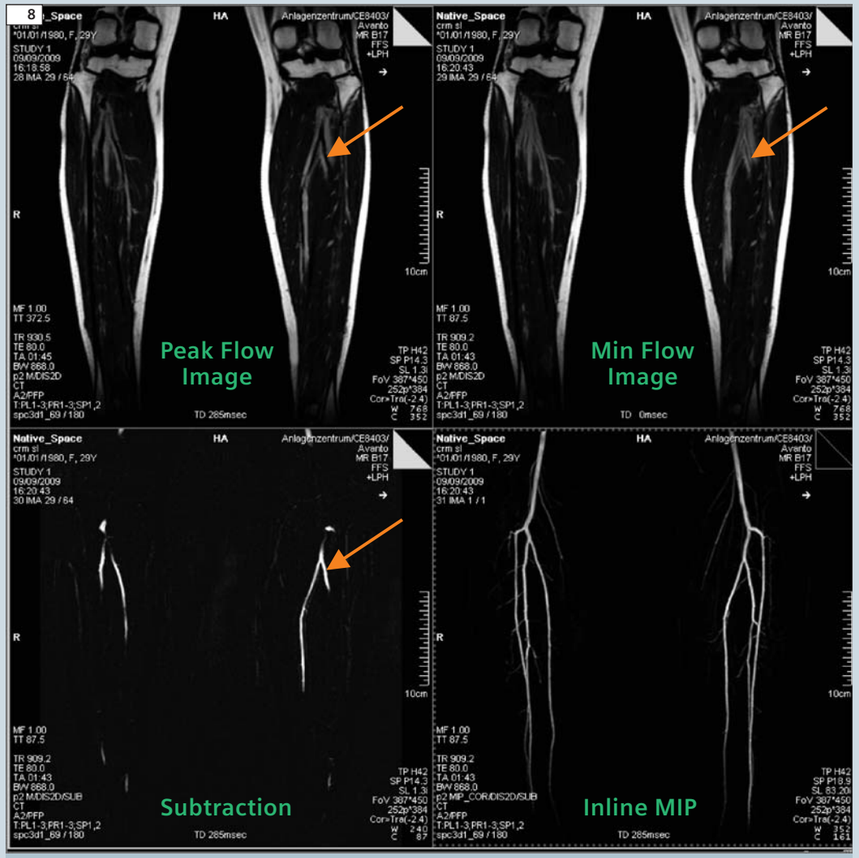

8 Results derived from a *syngo* NATIVE SPACE non-ce MR angiography exam.

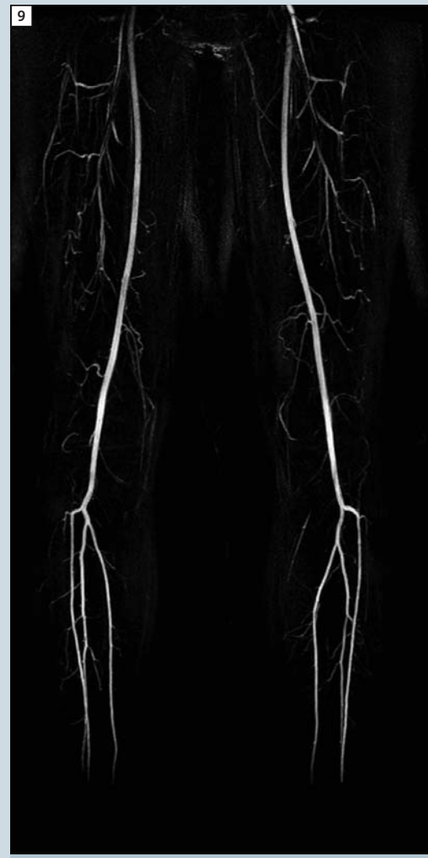

9 Coronal MIP of a multistep protocol.

planning of a single-step standard protocol in the lower leg region.
Do not forget to adapt the time delay for the peak flow to the corresponding area. To set the Trigger Delay times for the peak and the minimum flow, open the 3D SPACE sequence on the Physio – Signal 1 subcard. We have good results by subtracting 30 ms from the peak trigger time in the Mean Curve Application, as shown in Fig. 6. In most cases, a trigger delay of 0 ms should be well-suited for the minimum flow acquisition.
During the scan remember to monitor the stability of the ECG.
As a result of the *syngo* NATIVE SPACE sequence, four different image series are displayed in the Viewing Card:

- Peak Flow image with dark arteries
- Min Flow image with bright arteries
- Inline subtraction showing arteries only, and
- Inline coronal MIP (Fig. 8).

Postprocessing

Similar to the *syngo* NATIVE TrueFISP sequence, an Inline coronal MIP is reconstructed to give a first impression. For further manipulation, load the subtracted data to the 3D card. Comparable to the *syngo* NATIVE TrueFISP postprocessing, also try the ThinMip button for refinements. Figure 9 shows a multi-step MIP approach on a healthy volunteer.

Challenges and Possibilities

- The method can be considered as robust even if contrast agent has already been applied. Therefore, the technique may be used as a backup, if a contrast-enhanced examination did not work out perfectly.
- If there are different blood transit times on each leg due to a severe stenosis in one extremity (seen on the Cine_TDscout images in the Mean Curve application card), consider running two measurements, each of them optimized for one leg.
- Reduced contrast behind stenosis due to lack of pulsatility of flow and high-grade change of direction: To enhance the flow sensitivity, work with the extra flow sensitizing spoiler gradients. They support the collection of dark blood images since they additionally destroy the signal in moving blood. There are four different possibilities available (found on Physio-Signal1 subcard):
  - **off –** means the normal way of using the flow-spoiling gradients as implemented in the *syngo* SPACE sequence. (Value between weak and medium.)
  - **weak** – no flow-spoiling gradient used (Value = 0%)
  - **medium** – higher flow sensitivity than "off", due to sophisticated spoiler gradients (Value = 25%)
  - **strong** – highest flow sensitivity (Value = 50%)

Conclusion

syngo NATIVE SPACE and *syngo* NATIVE TrueFISP do not claim to replace contrast-enhanced angiography, but are complementary methods in cases where contrast agent is not applied for different reasons or where the contrast technique did not turn out well.
With these techniques, the user can overcome known weaknesses of the non-contrast enhanced MR angiographies used to date and may improve the overall diagnostic value of the MRI examination.

Contact
Manuela Rick
Siemens Healthcare
MR CRM-SL
Postbox 32 60
91052 Erlangen
Germany
Phone: +49 (9131) 84-4126
manuela.rick@siemens.com

Siemens Healthcare – Customer Magazines

Our customer magazine family offers the latest information and background for every healthcare field. From the hospital director to the radiological assistant – here, you can quickly find information relevant to your needs.

Medical Solutions
Innovation and trends in healthcare. The magazine, published three times a year, is designed especially for members of the hospital management, administration personnel, and heads of medical departments.

News
Our latest topics such as product news, reference stories, reports, and general interest topics are always available at www.siemens.com/healthcare-news

AXIOM Innovations
Everything from the worlds of interventional radiology, cardiology, fluoroscopy, and radiography. This semiannual magazine is primarily designed for physicians, physicists, researchers, and medical technical personnel.

MAGNETOM Flash
Everything from the world of magnetic resonance imaging. The magazine presents case reports, technology, product news, and how-to's. It is primarily designed for physicians, physicists, and medical technical personnel.

SOMATOM Sessions
Everything from the world of computed tomography. With its innovations, clinical applications, and visions, this semiannual magazine is primarily designed for physicians, physicists, researchers, and medical technical personnel.

Perspectives
Everything from the world of clinical diagnostics. This semi-annual publication provides clinical labs with diagnostic trends, technical innovations, and case studies. It is primarily designed for laboratorians, clinicians and medical technical personnel.

For current and older issues and to order the magazines, please visit **www.siemens.com/healthcare-magazine**

Market your MAGNETOM system

All the tools necessary to market your facility to patients and referring physicians are waiting for you in the **Your MAGNETOM** section on **www.siemens.com/magnetom-world**

Here you will find everything you need from patient pamphlets to advertisements, to trailers and press releases, postcards, posters, event checklists, high-resolution images and much more – ready for immediate use.

MAGNETOM Flash – Imprint

Publisher:
Siemens AG
Medical Solutions
Business Unit Magnetic Resonance,
Karl-Schall-Straße 6, D-91052 Erlangen, Germany

Editor-in-Chief: Dr. Matthias Lichy, M.D. (matthias.lichy@siemens.com)

Associate Editor: Antje Hellwich (antje.hellwich@siemens.com)

Editorial Board: Okan Ekinci, M.D.; Ignacio Vallines, Ph.D.; Wellesley Were; Milind Dhamankar, M.D.; Michelle Kessler; Gary McNeal; Sunil Kumar, M.D.

Production: Norbert Moser, Siemens AG, Medical Solutions

Layout: independent Medien-Design Widenmayerstrasse 16, D-80538 Munich

Printers: Farbendruck Hofmann, Gewerbestraße 5, D-90579 Langenzenn, Printed in Germany

MAGNETOM Flash is also available on the internet:
www.siemens.com/magnetom-world

Note in accordance with § 33 Para.1 of the German Federal Data Protection Law: Despatch is made using an address file which is maintained with the aid of an automated data processing system.
MAGNETOM Flash with a total circulation of 20,000 copies is sent free of charge to Siemens MR customers, qualified physicians, technologists, physicists and radiology departments throughout the world. It includes reports in the English language on magnetic resonance: diagnostic and therapeutic methods and their application as well as results and experience gained with corresponding systems and solutions. It introduces from case to case new principles and procedures and discusses their clinical potential.
The statements and views of the authors in the individual contributions do not necessarily reflect the opinion of the publisher.
The information presented in these articles and case reports is for illustration only and is not intended to be relied upon by the reader for instruction as to the practice of medicine. Any health care practitioner reading this information is reminded that they must use their own learning, training and expertise in dealing with their individual patients. This material does not substitute for that duty and is not intended by Siemens Medical Solutions to be used for any purpose in that regard. The drugs and doses mentioned herein are consistent with the approval labeling for uses and/or indications of the drug. The treating physician bears the sole responsibility for the diagnosis and treatment of patients, including drugs and doses prescribed in connection with such use. The Operating Instructions must always be strictly followed when operating the MR system. The sources for the technical data are the corresponding data sheets. Results may vary.
Partial reproduction in printed form of individual contributions is permitted, provided the customary bibliographical data such as author's name and title of the contribution as well as year, issue number and pages of MAGNETOM Flash are named, but the editors request that two copies be sent to them. The written consent of the authors and publisher is required for the complete reprinting of an article.
We welcome your questions and comments about the editorial content of MAGNETOM Flash. Please contact us at magnetomworld.med@siemens.com. Manuscripts as well as suggestions, proposals and information are always welcome; they are carefully examined and submitted to the editorial board for attention. MAGNETOM Flash is not responsible for loss, damage, or any other injury to unsolicited manuscripts or other materials. We reserve the right to edit for clarity, accuracy, and space. Include your name, address, and phone number and send to the editors, address above.

MAGNETOM Flash

The Magazine of MR

SIEMENS

Issue Number 4/2010
Special Edition for the USA

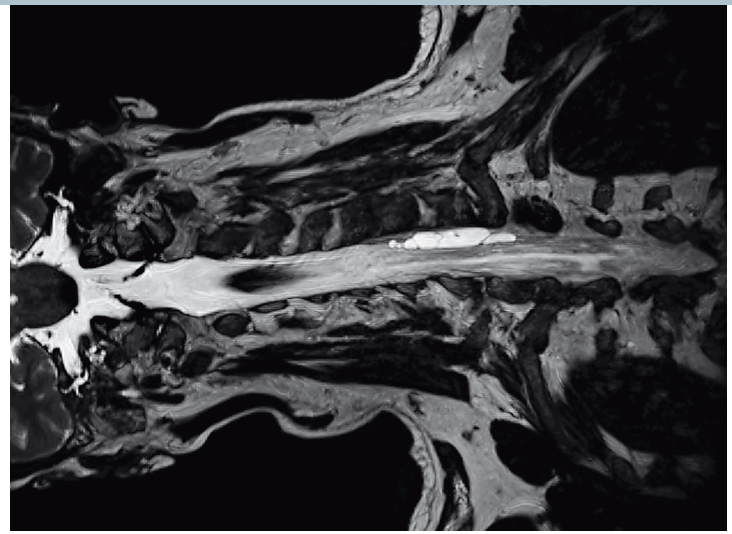

USA

Subscription

Please enter your business address

Institution

Department

Function

Title

Name

Street

Postal Code

City

State

Country

MR system used

Please include me in your mailing list for the following Siemens Healthcare customer magazine(s):

- ☐ Medical Solutions
- ☐ MAGNETOM Flash
- ☐ SOMATOM Sessions
- ☐ AXIOM Innovations

Stay up to date with the latest information Register for:

- ☐ the monthly e-Newsletter

E-mail

- ☐ Yes, I consent to the above information being used for future contact regarding product updates and other important news from Siemens.
- ☐ unsubscribe from info service

Please print clearly!

MAGNETOM Flash

Siemens AG
Medical Solutions
Magnetic Resonance
Antje Hellwich - Marketing
P.O. Box 32 60
D-91050 Erlangen
Germany

→ Visit www.siemens.com/magnetom-world for case reports, clinical methods, application tips, talks and much more clinical information.

SUBSCRIBE NOW!

– and get your free copy of future MAGNETOM Flash! Interesting information from the world of magnetic resonance – gratis to your desk. Send us this postcard, or subscribe online at www.siemens.com/MAGNETOM-World

Global Siemens Headquarters

Siemens AG
Wittelsbacherplatz 2
80333 Muenchen
Germany

Global Siemens Healthcare Headquarters

Siemens AG
Healthcare Sector
Henkestr. 127
91052 Erlangen
Germany
Phone: +49 9131 84-0
www.siemens.com/healthcare

www.siemens.com/healthcare-magazine

Order No. A91MR-1000-76C-7600 | Printed in Germany | CC MR 01000 ZS 09104. | © 09.10, Siemens AG

On account of certain regional limitations of sales rights and service availability, we cannot guarantee that all products included in this brochure are available through the Siemens sales organization worldwide. Availability and packaging may vary by country and is subject to change without prior notice. Some/All of the features and products described herein may not be available in the United States.

The information in this document contains general technical descriptions of specifications and options as well as standard and optional features which do not always have to be present in individual cases.

Siemens reserves the right to modify the design, packaging, specifications and options described herein without prior notice.
Please contact your local Siemens sales representative for the most current information.

Note: Any technical data contained in this document may vary within defined tolerances. Original images always lose a certain amount of detail when reproduced.

Global Business Unit

Siemens AG
Medical Solutions
Magnetic Resonance
Henkestr. 127
DE-91052 Erlangen
Germany
Phone: +49 9131 84-0
www.siemens.com/healthcare

Local Contact Information

In Asia
Siemens Pte Ltd
The Siemens Center
60 MacPherson Road
Singapore 348615
Phone: +65 6490-8096

In Canada
Siemens Canada Limited
Medical Solutions
2185 Derry Road West
Mississauga ON L5N 7A6
Canada
Phone: +1 905 819-5800

Europe/Africa/Middle East
Siemens AG
Medical Solutions
Henkestr. 127
91052 Erlangen
Germany
Phone: +49 9131 84-0

Latin America
Siemens S.A.
Medical Solutions
Avenida de Pte. Julio A. Roca No 516,
Piso 7
C1067ABN Buenos Aires
Argentina
Phone: +54 11 4340-8400

USA:
Siemens Medical Solutions U.S.A., Inc.
51 Valley Stream Parkway
Malvern, PA 19355-1406
USA
Phone: +1-888-826-9702

MAGNETOM Flash
USA
Issue Number 4/2010
Special Edition for the USA
SIEMENS